MODELLING THE ENANTIOMERIZATION AND ATROPOSELECTIVITY IN THIOHYDANTOIN DERIVATIVES

by

İpek Azizoğlu

B.S., Chemistry, Boğaziçi University, 2019

Submitted to the Institute for Graduate Studies in
Science and Engineering in partial fulfillment of
the requirements for the degree of
Master of Science

Graduate Program in Chemistry
Boğaziçi University

2022

ACKNOWLEDGEMENTS

This project would not have been possible without the support of many people. First of all I would like to express my sincere gratitude to my advisor İlknur Doğan for her support and guidance. Prof. Doğan was always willing and enthusiastic to assist in any way she could throughout this research project. I would also like to thank my co-supervisor Prof. Viktorya Aviyente, I am extremely grateful for her guidance, immense knowledge, patience, and continuous support throughout this study.

I would like to acknowledge the invaluable presence of Pınar Haşlak, who has been a great support with her experience during this journey. Furthermore, I wish to thank the CCBU research members for their friendship and helpful suggestions. Special thanks to my closest friends Gökçe Kantarcı and Beyza Yılmaz, for their constant support and companionship. I feel fortunate to spend these years with them, our Kare Blok coffee breaks and endless but joyful study nights are memories that made my graduate years unforgettable. I would like to extend my sincere thanks to my friend Maya Özyiğit, for being there every step of the way with her unique friendship.

I gratefully acknowledge my thesis committee members: Prof. Şaron Çatak and Assist. Prof. Semin Funda Oğuz for their insightful comments and advices on this thesis.

And finally, thanks to my parents, especially my mother Didem Azizoğlu who endured this long process with me, always offering support and love. I dedicate this thesis to my mother.

This thesis has been supported by the and TÜBİTAK Domestic Graduate Scholarship Program 2020/1 (BİDEB 2210-A). Computing resources used in this work were provided by the National Center for High Performance Computing of Turkey (UHeM) under grant number 1007542020.

ABSTRACT

MODELLING THE ENANTIOMERIZATION AND ATROPOSELECTIVITY IN THIOHYDANTOIN DERIVATIVES

Thiohydantoins have a wide range of pharmacological and biological properties. In the previous studies, nonracemic axially chiral thiohydantoins were synthesized and computational investigations have rationalized the synthesis mechanism of the products. Two kinds of isomerism are studied; atropisomerism due to hindered rotation around a chiral axis and central chirality. Selective synthesis of one enantiomeric form is important during drug synthesis because of the different pharmacological properties of enantiomers and diastereomers. Enantiopure products have less complex and more selective pharmacodynamic profile compared to racemic mixtures. In order to shed light on the factors determining the selectivity on the reactions of thiohydantoin molecules, DFT methods have been used to investigate the substituent and solvent effect on the kinetics of the reactions and the thermal stabilities of thiohydantoin stereoisomers SP, SM, RP and RM. This study consists of four parts, with different reaction conditions and mechanisms. In the first part, the substituent effect on the rotational barriers has been investigated and the results have been compared with the experimental data. In the second part, the solvent assisted racemization and rotation reactions have been modelled and their activation energies were calculated to establish the most plausable mechanism. After determination of the racemization mechanism in ethanol, the substituent effect on racemization has been modelled and the results have been compared with the experimental data. In the third part, we proposed an approach to calculate the product distributions of thiohydantoin stereoisomers by the Boltzmann distribution. In the last part, we have modeled the aldol formation reactions and explored the face selectivity of the enolate due to the bulky *ortho*-aryl substituent.

ÖZET

TİYOHİDANTOİN TÜREVLERİNDE ENANTİYOMERİZASYON VE ATROPOSEÇİCİLİĞİN MODELLEMESİ

Tiyohidantoinler çok çeşitli farmakolojik ve biyolojik özelliklere sahiptir. Daha önceki deneysel çalışmalarda rasemik olmayan eksenel kiral tiyohidantoinler sentezlenmiştir ve hesapsal araştırmalar ürünlerin sentez mekanizmalarına açıklık getirerek rasemizasyonun siklizasyondan sonra meydana geldiğini göstermiştir. Bu çalışmada iki tür izomerizm incelenmiştir; kiral bir eksen etrafında engellenmiş rotasyon nedeniyle oluşan atropizomerizm ve heterohalkada bulunan kiral merkez. İlaç sentezindeki önemli konulardan biri, bir enantiyomerik formun diğerine göre seçici sentezidir. Önemi enantiyomerlerin ve diastereomerlerin farklı farmakolojik özelliklerinden kaynaklanmaktadır. Enantiyomerik olarak saf ürünler, rasemik karışımlara kıyasla daha az karmaşık ve daha seçici farmakodinamik profile sahiptir. Tiyohidantoin moleküllerinin reaksiyonlarında seçiciliği belirleyen sübstitüent ve solvent etkilerine ışık tutmak için, DFT yöntemleri tiyohidantoin steroizomerlerinin (SP, SM, RP ve RM) reaksiyon kinetiği ve termal kararlılıkları araştırmak amacıyla kullanılmıştır. Bu çalışma, farklı reaksiyon koşulları ve mekanizmaları içeren dört bölümden oluşmaktadır. Birinci bölümde, sübstitüentlerin dönme bariyerlerine etkisi araştırılmış ve sonuçlar önceki deneysel verilerle karşılaştırılmıştır. İkinci bölümde, etanol varlığındaki rasemizasyon mekanizması modellenmiş ve aynı ortamdaki dönme reaksiyonlarının aktivasyon enerjileriyle en olası mekanizmayı belirlemek amacıyla karşılaştırılmıştır. Üçüncü bölümde, Boltzmann dağılımı kullanılarak tiyohidantoin steroizomerleri SP, SM, RP ve RM'nin ürün dağılımlarını hesaplamak için bir yaklaşım önerilmiştir. Çalışmanın son bölümünde, aldol oluşum reaksiyonları modellenmiş tiyohidantoin türevlerinin *orto*-sübstitüentinin enolatın yüzey seçiciliğine etkisi araştırılmıştır.

TABLE OF CONTENTS

LIST OF FIGURES

LIST OF TABLES

LIST OF SYMBOLS

°C	Celsius
$\hat{H}$	Hamiltonian Operator
K	Kelvin
T	Temperature
Å	Angstrom
ε	Dielectric Constant
$\Delta G^{\neq}$	Gibbs Free Energy of Activation
Ψ	Wave Function

LIST OF ACRONYMS/ABBREVIATIONS

2D	Two Dimensional
3D	Three Dimensional
B3LYP	Becke, 3-Parameter, Lee–Yang–Parr Functional
Bn	Benzyl Group
CM5	Charge Model 5
DFT	Density Functional Theory
DCM	Dichloromethane
IEFPCM	Integral Equation Formalism Polarizable Continuum Model
IRC	Intrinsic Reaction Coordinate
LDA	Lithium Diisopropylamide
M06-2X	Hybrid Meta Exchange-correlation Functional
PM3	Parameterization Method 3
TEA	Triethyl Amine
THF	Tetrahydrofuran
TS	Transition State

1. INTRODUCTION

1.1. Thiohydantoins

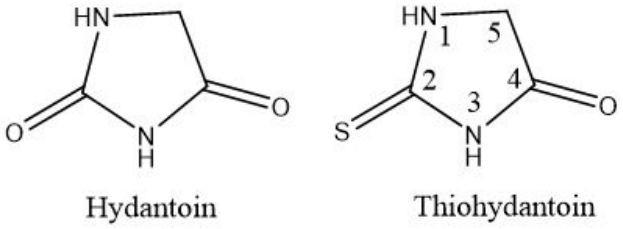

Figure 1.1. Hydantoin and thiohydantoin structures.

Hydantoin is a five-membered heterocycle and one of the oxidized forms of imidazolidine with a cyclic urea core. The term "hydantoin" refers to specific groups of compounds; containing the hydantoin sub-structure as a scaffold. 2-Thiohydantoin and 2-selenohydantoin are isosteric analogs of hydantoin [1]. Thiohydantoins are closely related analogues of hydantoins (Figure 1.1.) , they may have one or both of the carbonyl groups replaced by the thiocarbonyl groups [2]. Despite the small size of hydantoin, it provides four derivatizable positions and four hydrogen donors/acceptors [1].

Hydantoin derivatives possess a wide range of important biochemical effects and pharmacological properties [3]. They exhibit anticancer, anti-inflammatory, antidiabetic, antimicrobial [4], antidepressant, antiviral [5] and anti-HIV activities [6]. Besides their therapeutic activities, they possess a broad range of industrial applications. 2-Thiohydantoins are known as herbicides and fungicides; they are also used in textile printing, in the production of resins and plastics, and catalysts for polymerizations [7].

Examples of other areas of usage are listed in Figure 1.2.

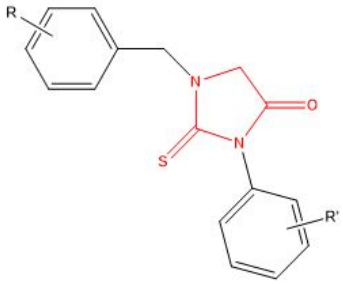

Anti-parasites: Anti-trypanosoma brucei agent.

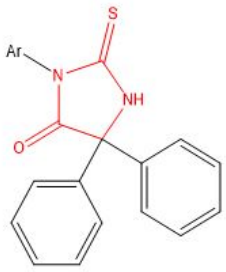

Anticonvulsant.

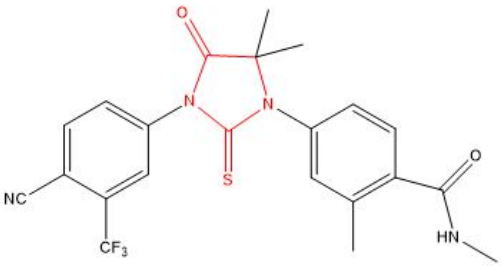

Androgen receptor antagonists that keeps prostate cancer cells from growing.

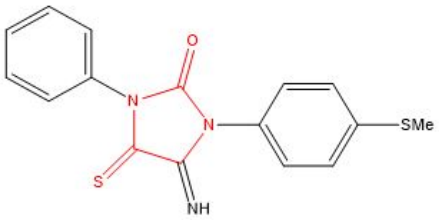

Antibacterial .

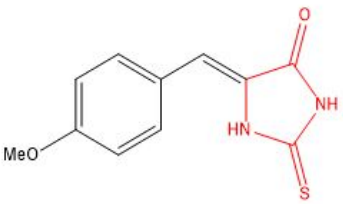

Cosmetic: It is used to ameliorate hyperpigmentation-related skin conditions.

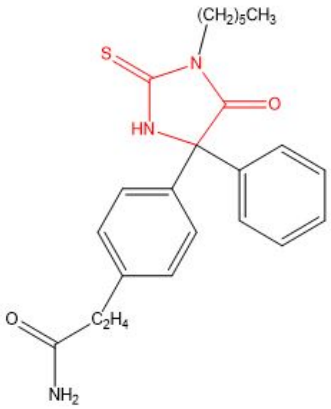

Inhibitor of a fatty acid amide hydrolase (FAAH) .

Figure 1.2. Various applications of thiohydantoin derivatives [1,7].

1.2. Atropisomerism

Axially chiral C-C and C-N-bonded atropisomers containing five-membered rings which exist in nature, consist of one or two five-membered rings from the indole, carbazole, or pyrrole series. The first synthesis of an axially chiral five-membered-ring compound was that of C-N bonded arylpyrrole, reported back in 1931, followed by a series of studies dealing with the preparation of the arylcarbazole and the dipyrryl biphenyl [8].

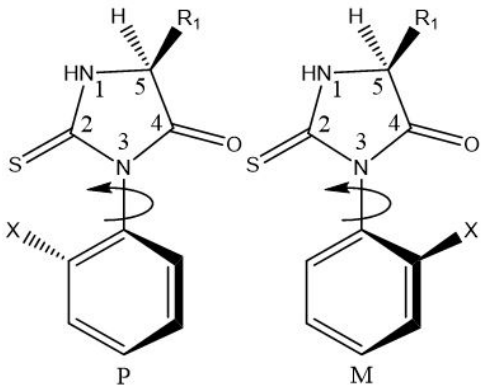

Figure 1.3. 3-Aryl thiohydantoin derivatives.

In this study 3-aryl thiohydantoin derivatives will be investigated shown in Figure 1.3. Due to the steric interference between the *ortho*-substituents on the N-aryl group and the exocyclic oxygen or sulfur on the heterocyclic ring, the aryl group in the ground state of the molecules is orthogonal (or nearly orthogonal) to the heterocyclic thiohydantoin backbone [9]. Atropisomerism is a fundamental property of molecules featuring a hindered rotation around a chemical bond, in our case the single bond between $N_{sp2} - C_{aryl}$ (aryl) [10]. Atropisomerism arises due to hindered rotation about a single bond, energy differences because of the steric strain create a barrier to rotation that is high enough to allow isolation of individual conformers. In the case of atropisomerism, racemization can occur spontaneously via bond rotation, rather than the process of bond breaking and bond making needed for the racemization of other cases of chirality [11]. Atropisomers interconvert with a half-life of at least 1000 seconds at a given temperature, corresponding to an energy barrier of 22 kcal/mol at 300 K [12].

In general, there are two crucial conditions for axial chirality in biaryl molecules; a rotationally stable axis and the presence of different substituents on both sides of the axis meaning A ≠ B and A' ≠ B' as shown in Figure 1.4. [13].

Determining the axial stereochemistry of biaryl atropisomers can be accomplished through the use of a Newman projection along the axis of hindered rotation. Substituents around the chiral axis are first assigned by priority based on Cahn-Ingold-Prelog priority rules: starting with the substituent of highest priority in the closest ring and moving along the shortest path to the substituent of highest priority in the other ring. The conformation is assigned P for clockwise and M for counterclockwise [13]. One example is given for one of thiohydantoin derivatives in Figure 1.4. (where R_1 and X substituents are -CH_3, abbreviated as M1 in this study) below. The rotation around carbon-carbon single bond is restricted due to the presence of an *ortho*-substituent at the aryl group. Therefore, rings remain orthogonal to each other [14].

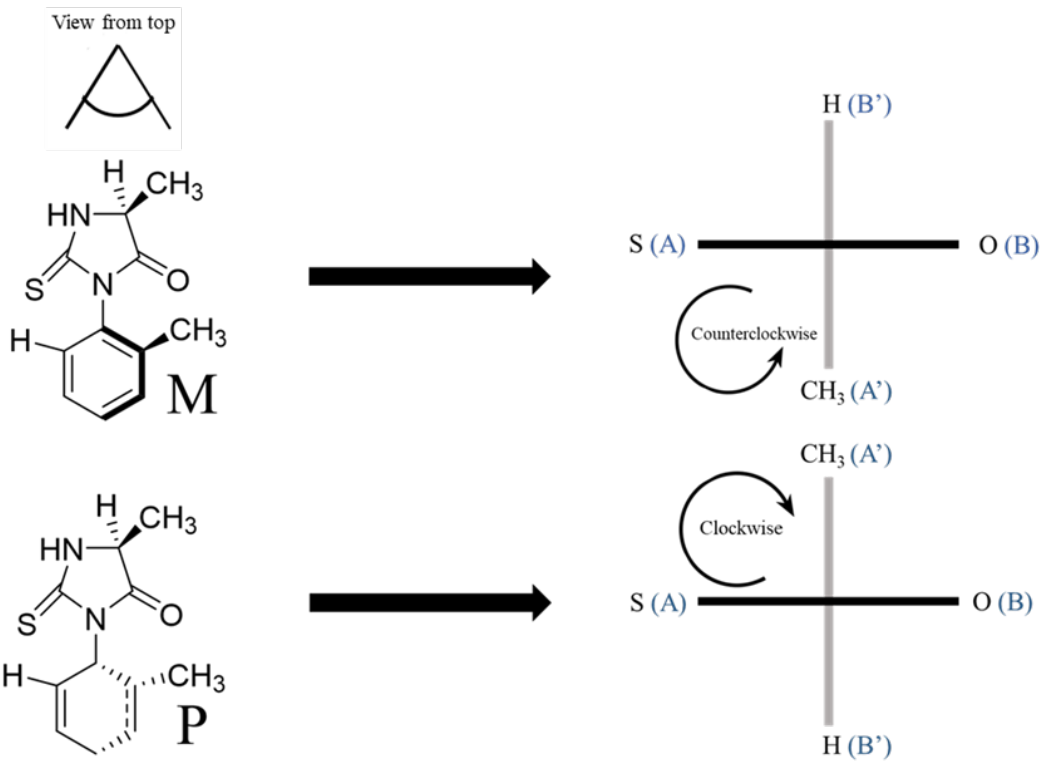

Figure 1.4. Determination of axial chirality.

Enantioselective and distereoselective synthesis of six or five membered carbocyclic and heterocyclic atropisomers constitute a central topic of research resulting in the development of many elegant synthetic approaches to be potentially useful as pharmacophores for drug discovery [15, 16]. However, atropisomeric species displaying one five-membered ring connected either by a C-N or C-C bond have been largely overlooked due to the increased distance between *ortho*-substituents next to the axis responsible of lower barriers to rotation hampering the conformational stability [13,17].

1.3. Central Chirality

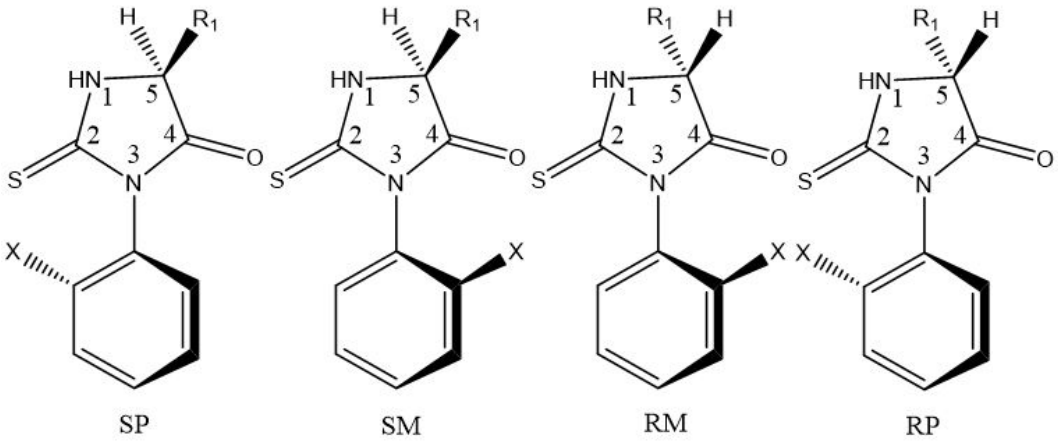

Figure 1.5. SP, SM, RM and RP isomeric forms of thiohydantoin derivatives

In this study we focused on atropisomerism and central chirality at C_5, shown in Figure 1.5.

Molecular chirality has an important role in organic chemistry. Most of the molecules of interest to the organic chemist are chiral, so, over the course of the years, a great amount of experimental work has been devoted to the selective formation of molecules with a given chirality, the so-called asymmetric synthesis [18]. This is a useful approach to synthesize selective stereoisomeric products for pharmaceutical applications because different enantiomers of molecules are known to have different biological activities and metabolism and pharmacokinetics are also influenced by chirality. Enantiomerization or racemization between enantiomers can also be undesirable and can cause a safe drug to be converted into toxic or ineffective form [19].

Racemization is an irreversible process in which an enantiopure quantity of compound is transformed into the opposing enantiomer. Enantiomerization is also related to racemization but it is a reversible conversion of one molecule of an enantiomer into its mirror image shown in Figure 1.6. Consequently, configurational stability of chiral drugs is an important concern in drug synthesis.

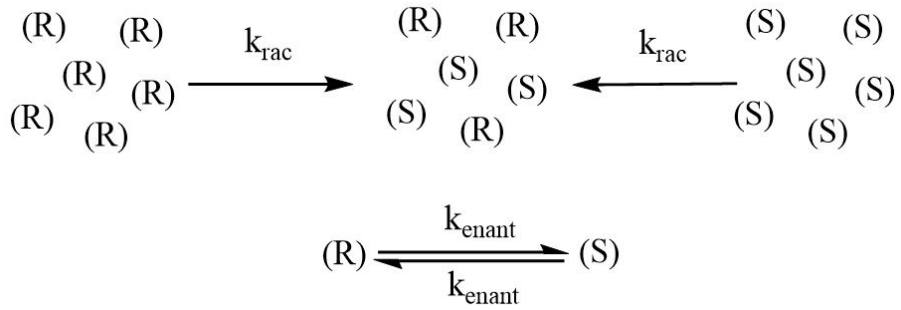

Figure 1.6. Difference between enantiomerization and racemization.

A molecule is referred to as chiral if it is not superimposable to its mirror image. An atom that has a capability to form four bonds such as carbon, forms a tetrahedral structure with four different groups attached to them. Chiral molecules having central chirality have stereogenic centers and it is refered as C_5 in this study. For example, SM and RP isomers have an identical chemical formula and they are enantiomers since their mirror images are not superimposible to each other.

When the enantiomers are present in a symmetric environment, they have identical chemical and physical properties however they have different properties in an asymetric environment. They are also called optically active, due to their difference in their ability to rotate plane-polarized light by equal amounts but in opposite directions [20].

1.4. Experimental Background

The experimental determination of steric barriers in atropisomers containing five-membered rings is a central research area of the previous experimental studies and it was facilitated by the development of chiral liquid chromatography, allowing efficient separations of atropisomers [8].

Nonracemic axially chiral thiohydantoins were synthesized [21] atroposelectively by the reaction of the corresponding *o*-aryl isothiocyanate with S or R amino acid ester HCl salts in the presence of triethylamine (Et_3N) and CH_2Cl_2 under reflux for 1 h shown in Figure 1.7. At the end of the reaction, extraction of crude product was done with distilled water and saturated brine solution, the solution was dried over with $MgSO_4$ and filtered and the solvent was removed immediately. The crude products were recrystallized from ethyl acetate/hexane, ethyl acetate, or methanol/water [22]. Although the synthesis started with an optically pure amino acid ester, the products were found to get racemized at C_5 during the reactions [14]. When X:H, we can not talk about a chiral axis and a racemic product was obtained. However when X is different than hydrogen, there is an *ortho*-substituent at an aryl ring and the axial chirality is present. The axially chiral products may exist in SP, RM, SM, and RP isomeric forms shown in Figure 1.4. SP/RM is transoid, whereas SM/RP is cisoid with respect to the substituent at C_5 and the *o*-aryl substituent and a high prevalence of the P isomers over the M isomers have been obtained when starting amino acid ester salt has a S configuration [22].

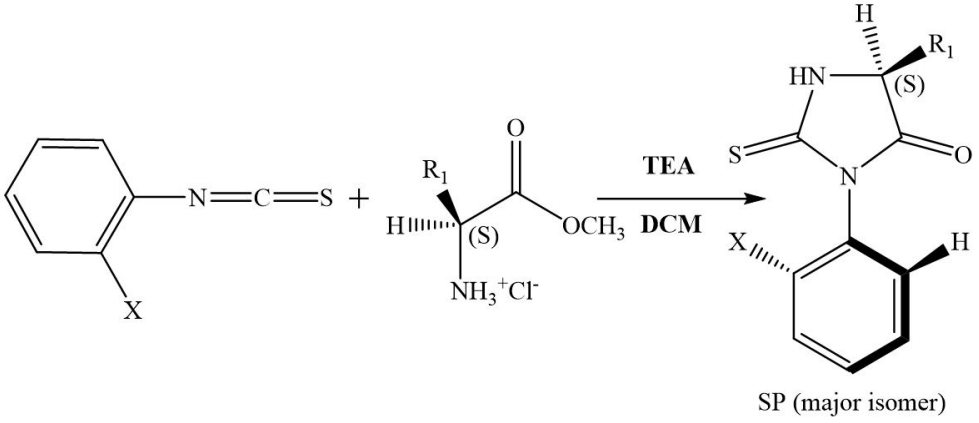

Figure 1.7. Synthesis of thiohydantoin molecules.

In the previous work of Doğan [22] the chirality transfer issue from the amino acid to the thiohydantoin ring has been addressed. It has been found that bulky *o*-aryl substituents at N_3 were found to suppress the C_5 racemization and in this way enabled the transfer of chirality from the α-amino acid to the products [22].

1.5. Aldol Reactions

Aldol reactions are very important, well known and widely studied C-C bond forming reactions in modern organic synthesis. Although the enantioselective and diastereoselective aldol reactions have been developed significantly [11, 23], atroposelective aldol reactions which rely on control originating from an element of axial chirality, especially non-biaryl types, are rare [24].

Asymmetric aldol reactions are used as a tool for the synthesis of complex and multifunctionalized molecules with significant biological activities such as the heart disease drug Lipitor [25] (Figure 1.8.) and steroidal antiandrogen Cyproterone [23] (Figure 1.9.) for the treatment of prostate cancer.

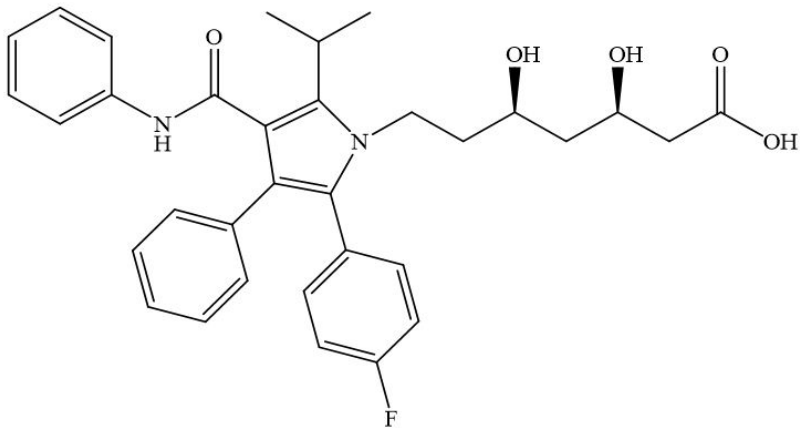

Figure 1.8. Molecular structure of Atorvastatin (Lipitor).

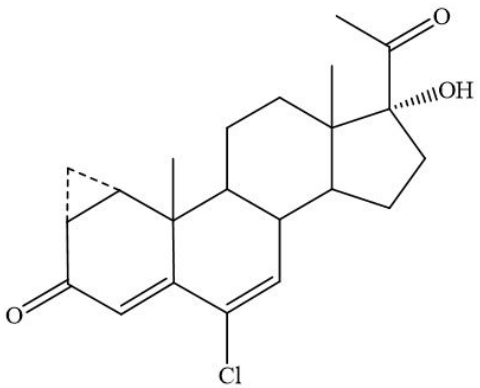

Figure 1.9. Molecular structure of Cyproterone.

Aldol reactions consist of two carbonyl compounds, one as electrophile and the other as nucleophile. A new carbon-carbon single bond is formed and a new β-hydroxy carbonyl compound is produced in the presence of an acid or a base (a strong base, LDA is used in this study) with the attack of the enolate to the benzaldehyde.

Diasteroselective synthesis can be explained from the anti-transition state structure in the work of Khatik [23]. The most stable conformation is when the phenyl and methyl groups are in a diequatorial conformation and this is possible only if they are trans to each other. This leads to an anti diastereoselectivity in the product formation shown in Figure 1.10.

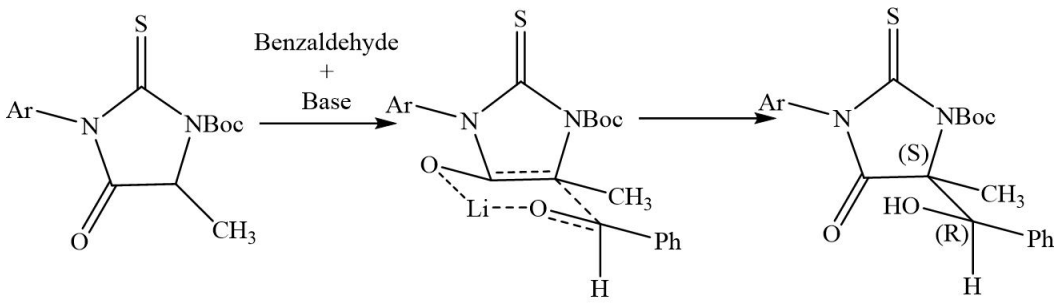

Figure 1.10. Anti-diastereoselectivity in the formation of aldol product.

Because of their ability to construct larger molecules from smaller ones, often with control of stereochemistry, reactions are a mainstay of organic synthesis. They are also common in metabolism, where aldolase, citrate synthase, and other enzymes catalyze aldol reactions and aldol condensations, or their reverse, leading to the suggestion that they reflect primordial metabolism [26].

1.6. Computational Background

Using computational tools to model the reaction mechanisms is important for understanding the details of the racemization steps in order to synthesize enantiomerically pure products. In the previous computational study, the aim was to rationalize the atroposelectivity observed in the synthesis of the axially chiral 2-thiohydantoin derivatives [27].

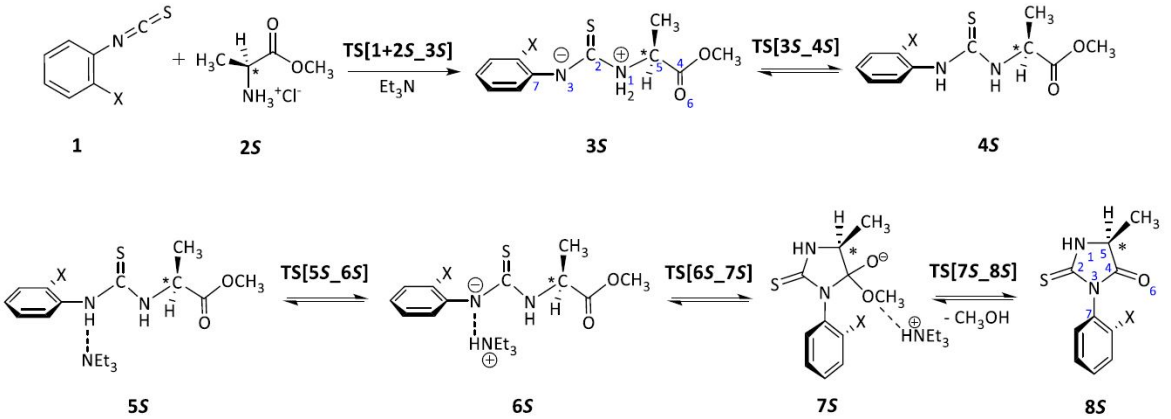

Figure 1.11. Synthesis of thiohydantoin [27].

In the work of Haşlak, the following question was answered: Does racemization occur before or after cyclization? The synthesis started with the nucleophilic addition of the amino acid to the *o*-aryl isothiocyanate yielding intermediate called 3S shown in Figure 1.10. Proton transfer from the positively charged N_1 to the negatively charged N_3 occured due to charge seperation in the structure 3S, yielding structure 4S. After the formation of 4S, there are three possible sites of deprotonation by TEA: N_1, N_3 or C_5. It was found that deprotonation from N_3 forms the most stable anion compared to other positions due to the resonance stabilization between 5S and 6S structures through N_3-aryl ring. For the cyclization of 6S, the protonated TEA in 6S formed a complex with methoxy oxygen. Then, N_3-C_4 bond formation occurs by the nucleophilic attack of negatively charged nitrogen (N_3) to the partially positive carbonyl carbon (C_4) and double bond between C_4 and O_6 opens. Finally, negative charge on O_6 closes back and methanol releases by the hydrogen transfer from protonated TEA.

After clarifying the synthesis mechanism of thiohydantoins, the aim was to rationalize the racemization mechanism of the thiohydantoin derivatives: did it occur before or after the cyclization? Different pathways for various molecules were modelled and their Gibbs energy barriers have been evaluated and shown in Figure 1.12. M06-2X/6-311+G(d,p) level of theory were used for all of the calculations, 6-311++G(3df,3pd) basis set is used only for Br for its heavy atom properties.

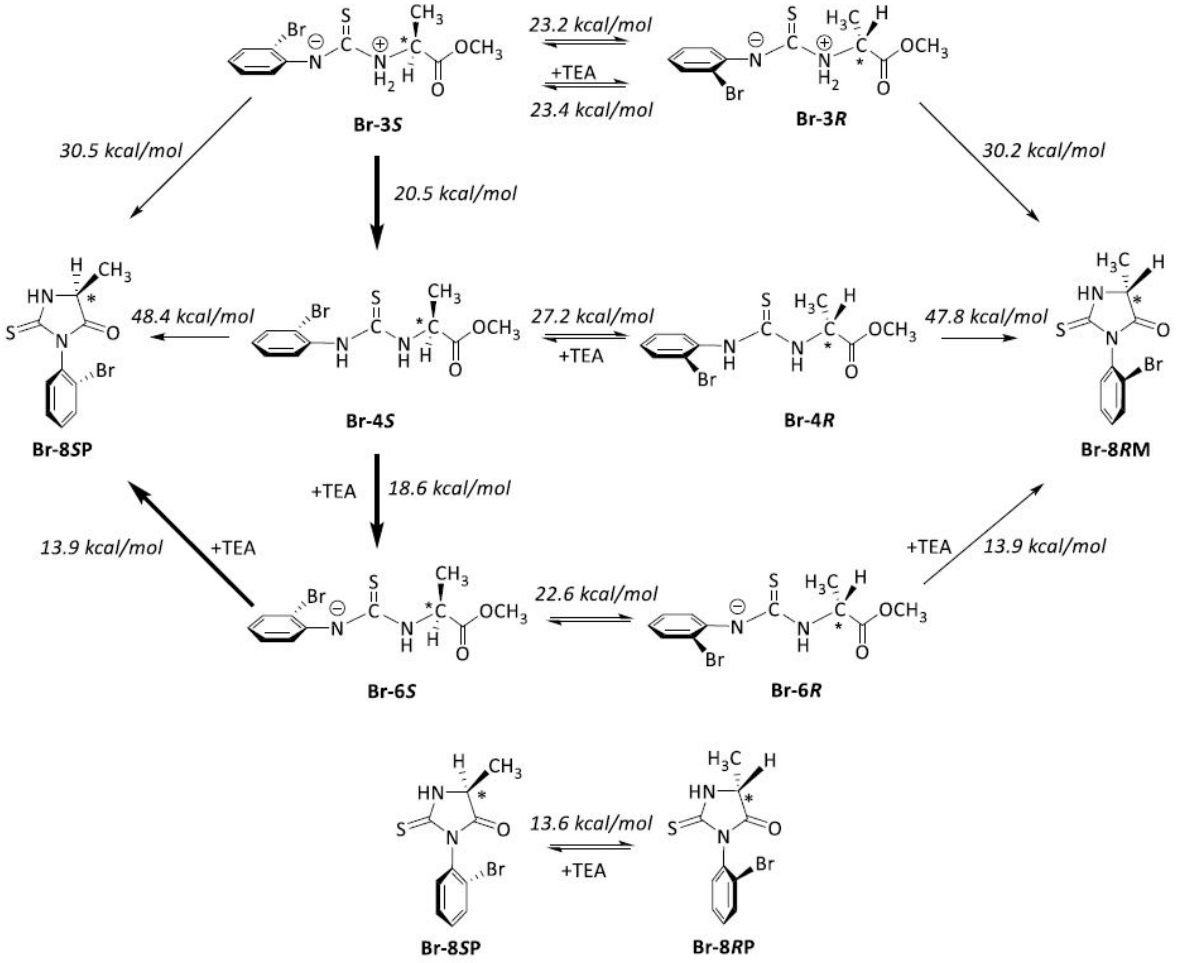

Figure 1.12. Different pathways for the cyclization mechanism of thiohydantoin [27].

Pathway with bold arrows gave the most probable route since these reactions had the lowest activation barriers, concluding that racemization occurs after the cyclization. The rotation of the bromoaryl ring (in this study abbreviated as M4), the transformation of SP to SM, had an experimentally determined barrier of 27.8 kcal/mol [27], and this relatively high barrier explains the fact that SP had %83 abundance whereas SM was only %3.

Calculations had shown that after racemization occured at C_5 of SP, RP was formed and the rotation of the bromo-aryl ring required 27.5 kcal/mol to give RM isomer [27]. At the end of these processes four different isomers can be observed in the reaction media.

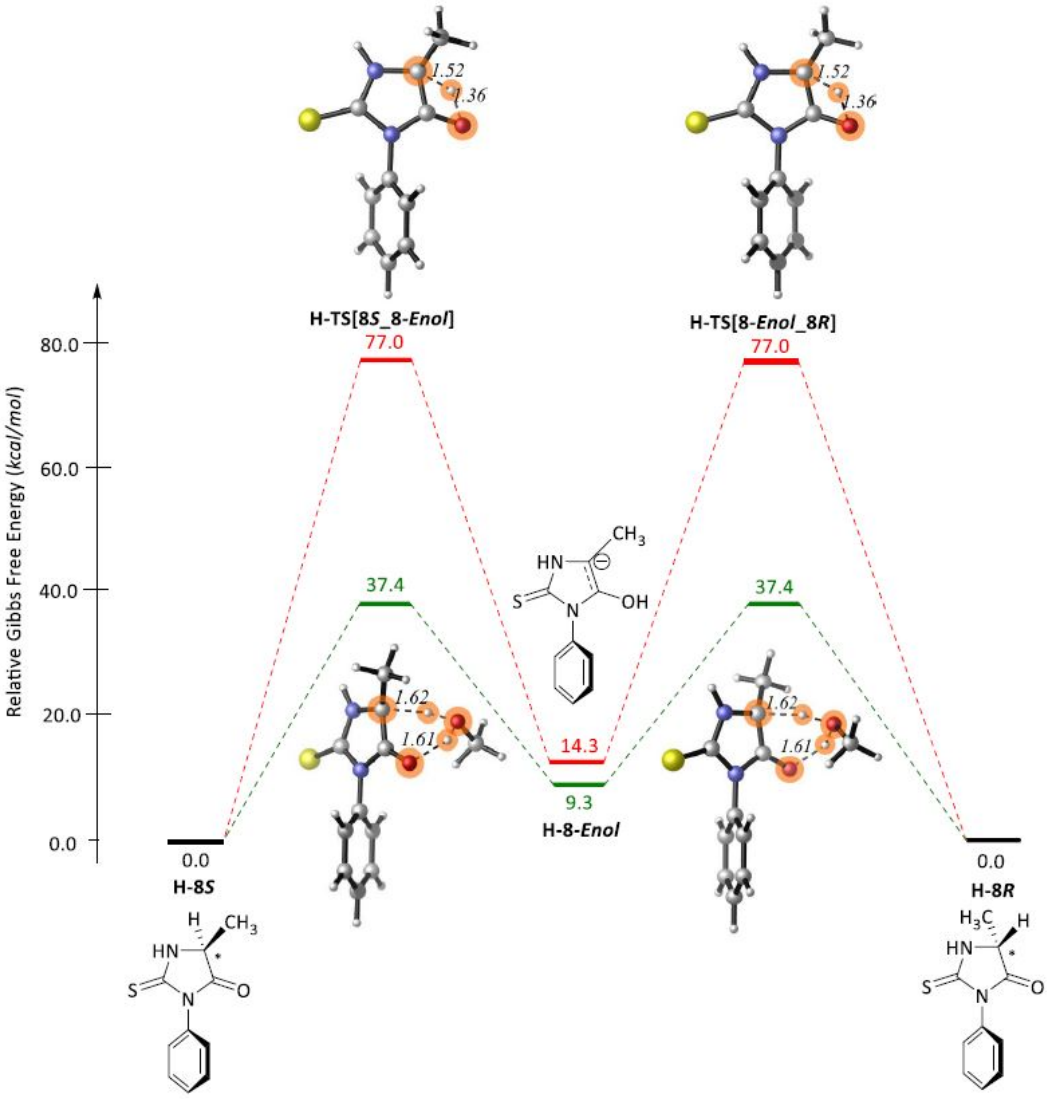

Figure 1.13. Racemization mechanism with and without a base catalyst [27].

The second question answered during the work of Haşlak was: Does racemization occur via the assistance of triethyl amine which is present in the reaction medium, methanol which is a side product or through unassisted keto-enol tautomerization? In order to rationalize the racemization process after the cyclization, three different mechanisms were proposed by Haşlak. The first two mechanism are shown in Figure 1.13., intramolecular proton transfer from C_5 to O_6 with and without a base catalyst.

The upper path (red line) shows that keto-enol tautomerization without a catalyst that was not possible kinetically due to very high activation barrier which is 77.0 kcal/mol. Since one mole of methanol is released during the cyclization step, it can abstract the hydrogen atom from the stereocenter (C_5) by transferring its -OH hydrogen to O_6 yielding the enolate in Figure 1.13.

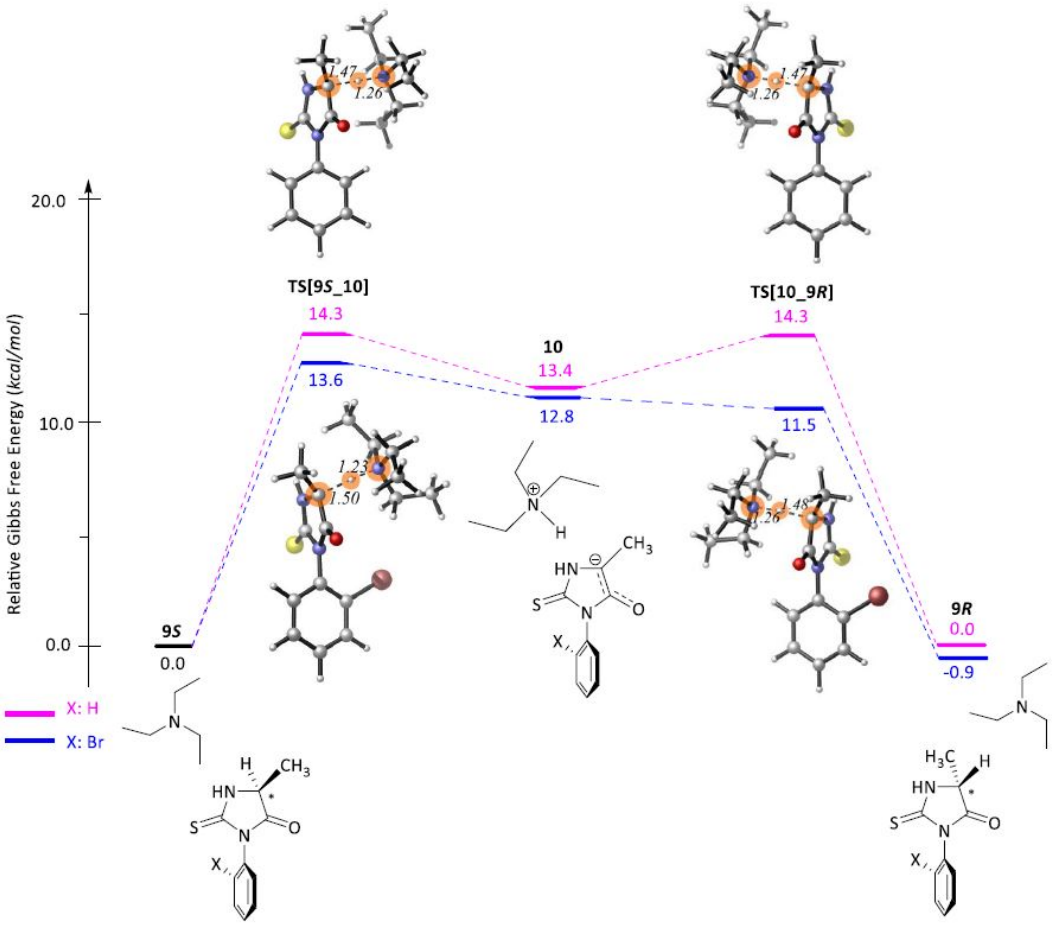

Figure 1.14. Racemization mechanism in the presence of TEA [27].

Since triethylamine mediated racemization at C_5 required the lowest activation barriers compared to other two mechanisms, it was considered to be the main racemization mechanism as shown in Figure 1.14.

2. AIM OF THE STUDY

Asymmetric synthesis is the selective synthesis of one enantiomeric form of a desired optically active molecule. The different enantiomers or diastereomers of a molecule often show different biological activities. Their liability to racemization is an important information [28]. Important properties of enantiomers arise when they are in an asymmetric environment, when they react with other enantiomers. Stereoisomers can have different pharmacokinetic and pharmacodynamic properties and these can be related to the drug-receptor interactions, the rate of metabolic conversions, the differences in transport processes, or even uptake and storage in particular tissues [29]. Isomerism can lead to different therapeutic uses and adverse drug reactions or two stereoisomers can compete for binding the receptors, one isomer can act as a competitive antagonist of the other, then the efficiency of a drug can be lowered [20]. For example for some barbiturates, the L-isomer is a depressant and the d-isomer is a convulsant. Determining the amount of racemization and racemization mechanisms are important steps during the drug synthesis [30]. Racemization can cause compounds to become toxic, lose their efficacy and ignoring racemization leads to wasted material and human resources [31].

It is important to yield pure compounds with few impurities as possible because single enantiomers (enantiopure products) have less complex and more selective pharmacodynamic profile, also they have less adverse drug reactions, improved therapeutic profile, less chances of drug interactions compared to racemic mixtures. Single enantiomers seem to be more advantageous over racemic mixtures and patients are exposed to less amount of drug so the body is exposed to the lesser metabolic, renal and hepatic load of drug, there is easier therapeutic drug monitoring of the pure active enantiomers [20]. Non-racemic axially chiral systems are considered as central elements for many scientific areas with numerous applications in catalyst design, drug discovery and material sciences [10].

Determining the factors of enantioselectivity and atroposelectivity of axially chiral thiohydantoin derivatives and reactions by using DFT calculations is the main aim of this study. This study consists of four parts:

In PART I: The aim is to rationalize the role of substituents, the size and the character of the R_1 and the *ortho*-substituent, on the rotational barriers through $N_{sp2}-C_{aryl}$ chiral axis and compare the results with the previous experimental data.

In PART II: The solvent assisted racemization is analyzed with the purpose of verifying computationally that the racemization reactions require lower barriers compared to rotation in ethanol, racemization is the most probable route for the thiohydantoin derivatives. In this part various possibilities for the racemization mechanisms of thiohydantoin derivatives have been modelled.

In PART III: We propose an approach to calculate the product distributions of thiohydantoin molecules SP, SM, RP and RM through Boltzmann distribution. In this part the aim is to demonstrate that the relative Gibbs Free Energies (kcal/mol) of uncyclized products (6S) before the cyclization step contribute to the final product distributions (thermodynamic control) of the isomers by giving the P/M ratios. Since these uncyclized products give cyclized SP, SM, RP and RM isomers after the ring closure and the chiral center was formed, relative stabilities of these thiohydantoin isomers also contribute to the final distribution by giving the S/R ratios.

In PART IV: The asymmetric aldol reaction has attracted the attention of synthetic organic chemists and is frequently seen as a major step of enantioselective C–C bond formation [25]. With the guidance of experimental results [32], we used quantum chemical calculations to seek further verification of the atroposelectivity of aldol formation reactions of thiohydantoin derivatives with benzaldehyde and further verify that the selectivity depends on the bulky *ortho*-substituents -CF_3 and -Cl.

Derivatives of 2-thiohydantoin molecules used in this study are given in Figure 2.1.

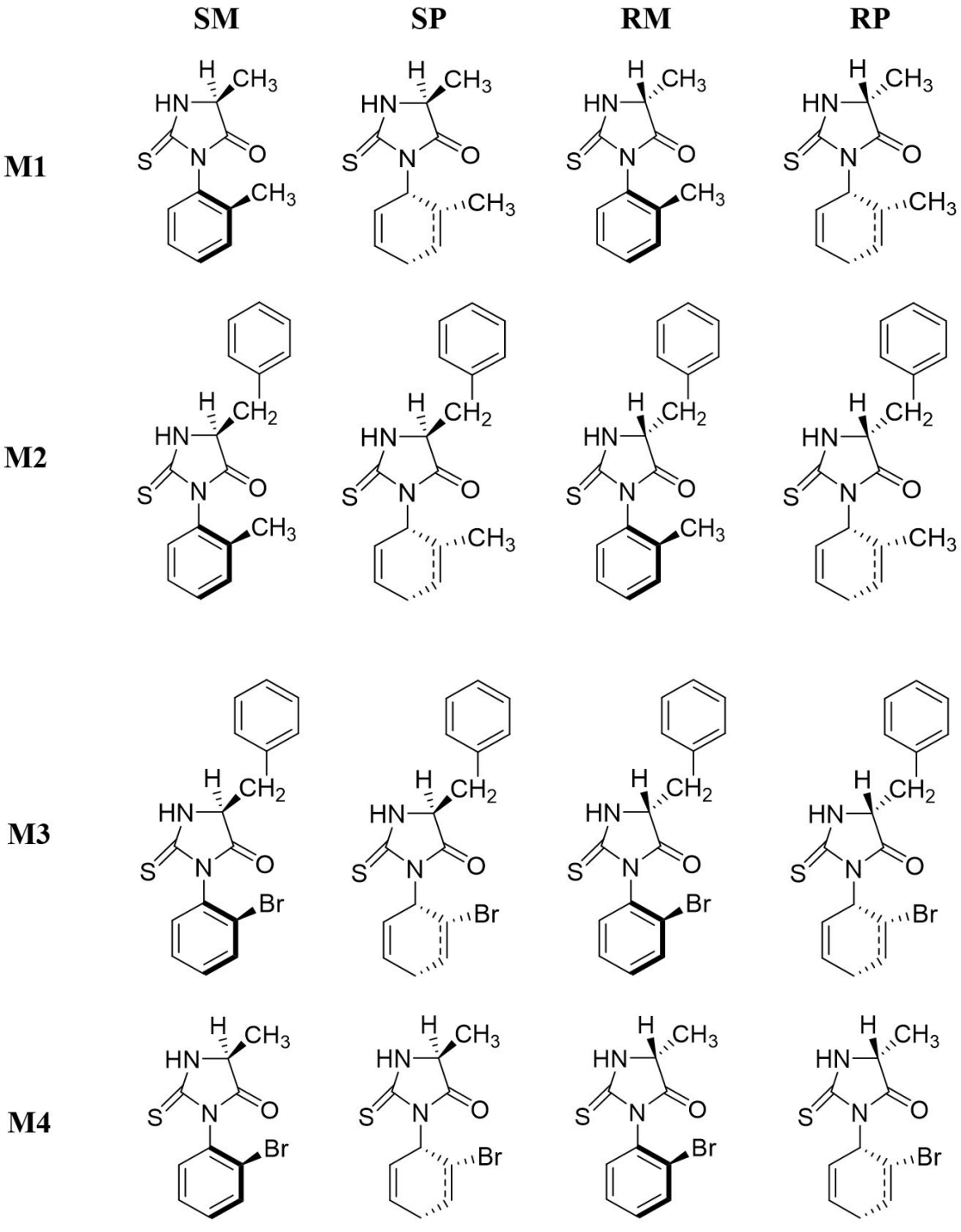

Figure 2.1. Thiohydantoin derivatives modelled in this study.

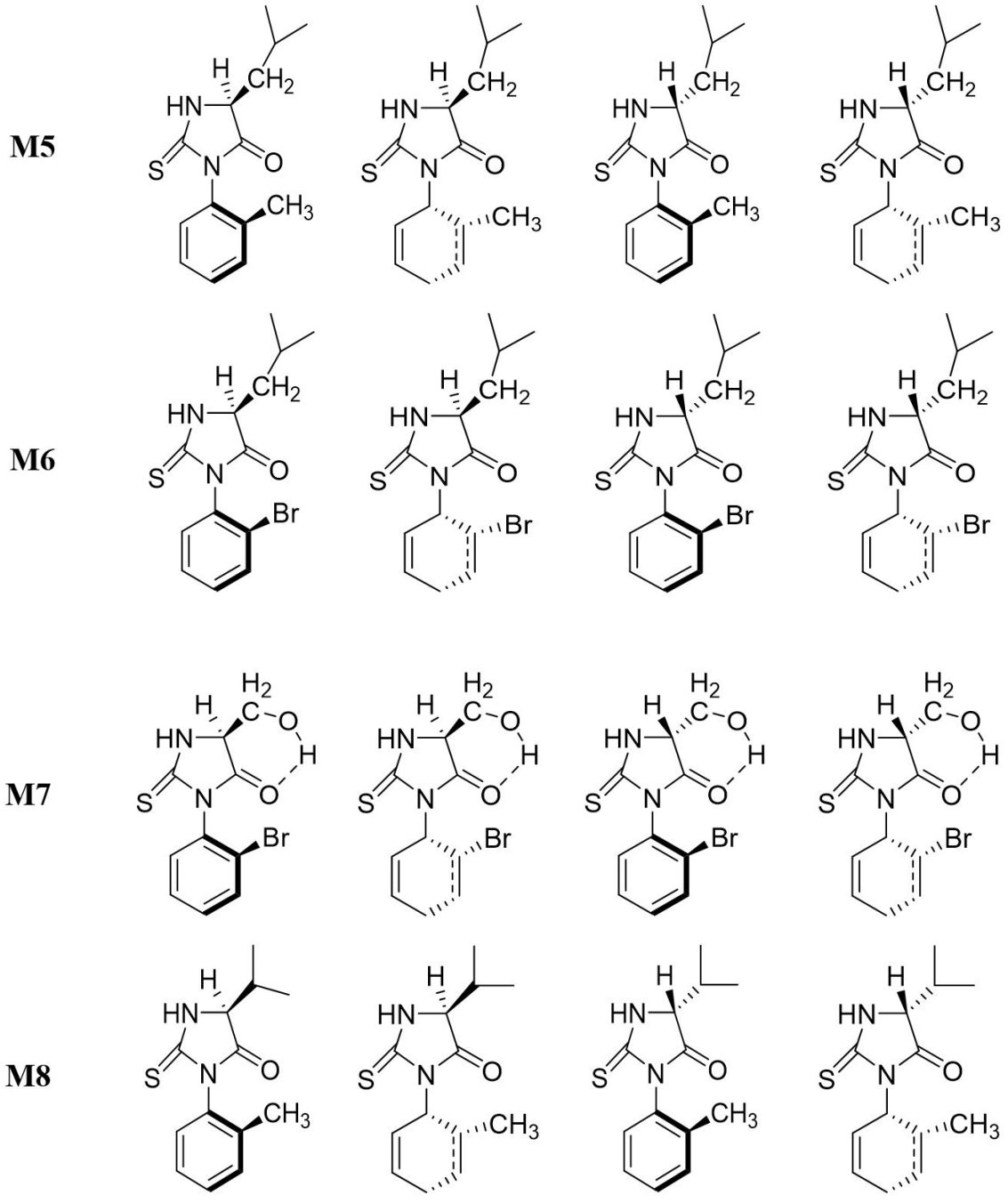

Figure 2.1. Thiohydantoin derivatives modelled in this study. (cont.)

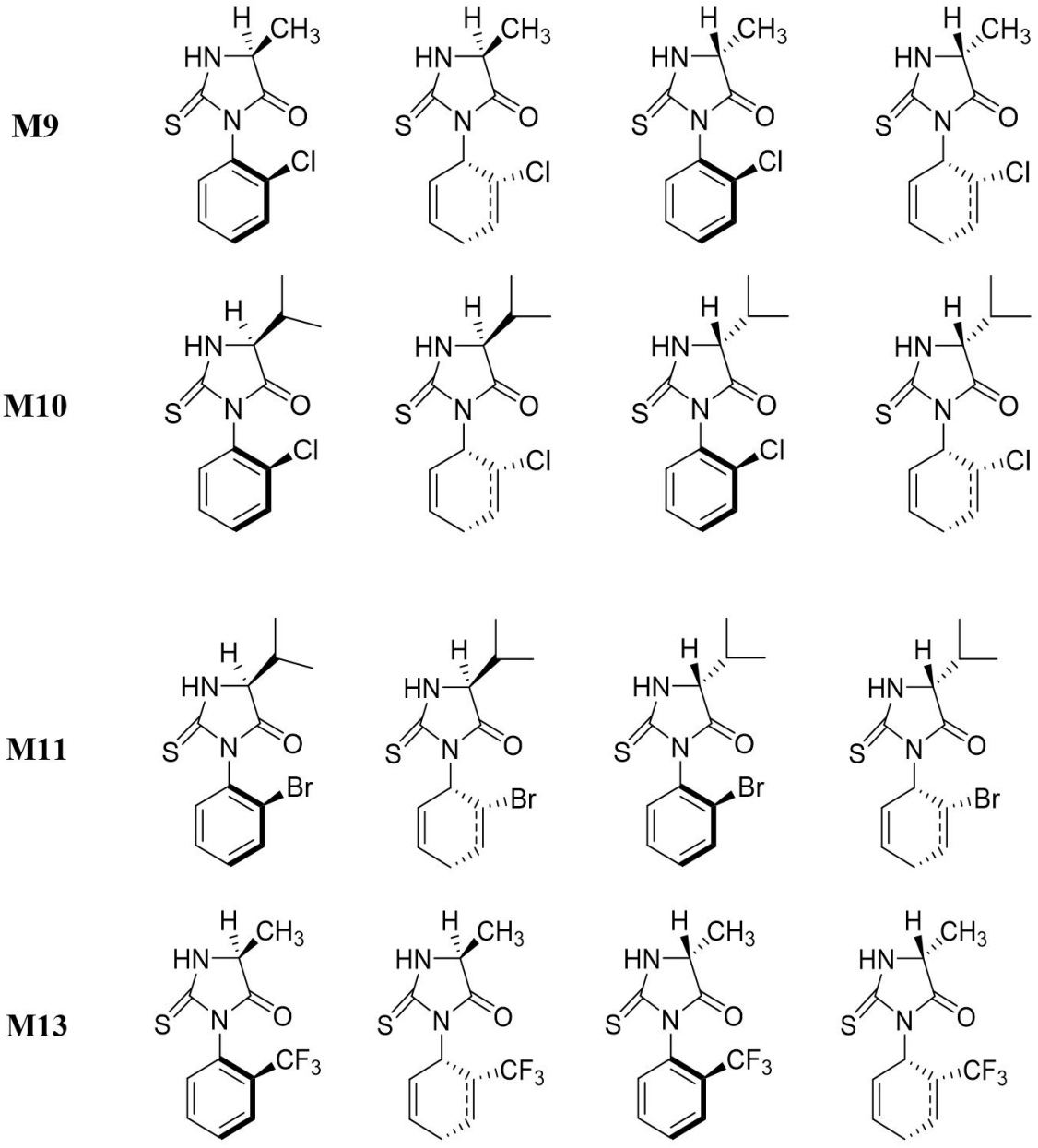

Figure 2.1. Thiohydantoin derivatives modelled in this study. (cont.)

3. METHODOLOGY

3.1. Density Functional Theory

Density Functional Theory (DFT) is the method of choice for the quantum mechanical simulations of many-body systems. DFT deals directly with the wave function and it is based on the electron density [33]. According to the Born–Oppenheimer approximation, the ground-state electronic structure and the nuclear repulsion in a molecule determine its ground-state geometry, potential energy surface, thermochemistry, rate constants, and other physical and chemical properties. DFT states that the electron density can be defined by the spatial coordinates (x,y,z) and given as;

$$\rho(r) = N \int ... \int |\Psi(r_1, r_2, ...r_n)|^2 \mathrm{d}r_1 \mathrm{d}r_2 ... \mathrm{d}r_n. \tag{3.1}$$

Current DFT uses the Kohn-Sham formalism, a system of independent non-interacting electrons in a common, one-body potential. Energy functional is divided into specific components in order to facilitate the analysis and given as;

$$E[\rho(r)] = V(r)\rho(r)\mathrm{d}r + T_{ni}[\rho(r)] + J[\rho(r)] + E_{XC}[\rho(r)]. \tag{3.2}$$

The term $T_{ni}[\rho(r)]$ refers to the kinetic energy of the non-interacting electrons where N is the number of electrons and it can be written as;

$$T_{ni}[\rho(r)] = \sum_{i}^{N} \int \psi_i(r) - \frac{\nabla^2}{2}\psi_i(r)\mathrm{d}r. \tag{3.3}$$

The term $J[\rho(r)]$ is the electron-electron Coulombic energy that does not consider the correlation between motions of electrons where M is the total number of nuclei and Z_A is the nuclear charge and it is written as;

$$J[\rho(r)] = -\sum_{A=1}^{M} \int \frac{z_A}{|r - R_A|}\rho(r)\mathrm{d}r + \int \frac{\rho_1(r)\rho_2(r)}{|r_1 - r_2|}\mathrm{d}r_1\mathrm{d}r_2. \tag{3.4}$$

The last term is and it accounts for the remaining electronic energy not included in the non-interacting kinetic and electrostatic terms, typically referred to as the exchange-correlation energy. It is defined as the difference between the exact total energy of a system and the classical Hartree energy and the quality of a DFT calculation is determined by how close the approximate exchange and correlation comes to the exact value. Exchange correlation energy can be expressed as;

$$E_{XC}[\rho(r)] = \int \rho(r)\varepsilon_{XC}\rho(r)\mathrm{d}r. \tag{3.5}$$

The derivative of Equation (3.5) with respect to electron density gives the following equation;

$$V_{XC}[\rho(r)] = \rho(r)\frac{\mathrm{d}\epsilon_{XC}\rho(r)}{\mathrm{d}\rho(r)} + \epsilon_{XC}\rho(r). \tag{3.6}$$

The Kohn-Sham orbitals (ψ_i) can be determined by solving the Kohn-Sham equations;

$$h_i^{KS}\psi_i = \varepsilon_i\psi_i. \tag{3.7}$$

The Kohn-Sham Hamiltonian operator can be expressed as;

$$h_i^{KS} = -\frac{\nabla^2}{2} - \sum_{A=1}^{N} + \frac{z_A}{|r - R_A|} + \int \frac{\rho_1(r)\rho_2(r)}{|(r_1 - r_2)\mathrm{d}r_1\mathrm{d}r_2|}V_{XC}[\rho(r)]. \tag{3.8}$$

The exchange-correlation potential is shown in Equation (3.6) and the exact density can be formed through the Kohn-Sham orbitals and the equation is given as;

$$\rho(r) = \sum_{i=1}^{N} |\psi_i|^2. \tag{3.9}$$

One setback is, the exact form of exchange-correlation functional is not known. For this purpose, DFT functionals are used to represent the approximations to solve the exchange-correlation functional.

3.2. DFT Functionals

In order to obtain the exact form of exchange-correlation functional, different approximations have been used. Local Density Approximation (LDA) is the one of the approximation to form the base of the exchange-correlation functionals [34]. LDA states that the electron density of a system is uniform and the electrostatic energy of the positivity, $\mathbf{E}_b$ is added to make the system neutral by the following equation:

$$E[\rho] = T_{ni}[\rho] + \int \rho(r)v(r)\mathrm{r} + J[\rho] + E_{xc}[\rho] + E_b. \tag{3.10}$$

Then the equation is simplified to the following form since the electron density and positive charge density are equal to each other. Also the exchange and the correlation functionals are expressed into separate terms:

$$E[\rho] = T_{ni}[\rho] + E_x[\rho] + E_c[\rho]. \tag{3.11}$$

$T_{ni}[\rho]$ is the kinetic energy functional, where C_F is a constant equal to 2.8712, and it can be written as:

$$T_{ni}[\rho] = C_F \int \rho^{5/3}\mathrm{d}r. \tag{3.12}$$

The following equation is used for the determination of the exchange functional and the term C_X equals to a contant of 0.7386:

$$E_x[\rho] = -C_x \int \rho(r)^{4/3}\mathrm{d}r. \tag{3.13}$$

However the electron density in a molecular system is rather far from uniformity and this is the limitation of the LDA approach. One way of improving the correlation functional is to make it depend not only on the local value of the density, but on the extent to which the density is locally changing meaning the gradient of the density. Including a gradient correction defines the second generation of density functionals called the generalized gradient approximation (GGA).

Most gradient corrected functionals are constructed with the correction being a term added to the LDA functional such as:

$$E_{XC}^{GGA}[n] = \int n(r)\varepsilon_{XC}(n(r), |\nabla n(r)|)\mathrm{d}r. \tag{3.14}$$

In third-generation functionals, the spin kinetic energy densities are included in the functional form and they are called meta-GGAs. Functionals combining local GGA functionals with non-local Hartree-Fock (HF) exchange are called hybrid functionals, and they are often more accurate than local functionals for main group thermochemistry.

M06-2X hybrid meta GGA functional is used in this study due to its improved performance for main-group thermochemistry, barrier heights, and noncovalent interactions. M06-2X is known to perform well in organic reaction systems by including the contribution of dispersive effects, it has shown results that are consistent with the experimental findings [35]. B3LYP meta functional is also used during the calculation of rotational barriers and gave slightly better results compared to M06-2X but not used in the other parts of the study where the dispersive interactions are signficant. B3LYP functional has some shortcomings: it underestimates the reaction barrier heights and it is inaccurate for long range interactions, such as van der Waals attraction, hydrogen-bonded systems and aromatic-aromatic stacking.

3.3. Basis Sets

A basis set is a set of functions which are combined in linear combination of atomic orbitals to extend the molecular orbitals [36] and it is given as;

$$\Psi_i = \sum_j c_{ij}\psi_j. \tag{3.15}$$

To describe the electronic states of molecules we construct wavefunctions, which are the approximate solutions to the Schrodinger equation, for the electronic states by using molecular orbitals. Ψ_i is the molecular orbitals, ψ_j represents an atomic orbital and c_{ij} is the coefficient. Major types of atomic orbitals are Gaussian-type orbitals (GTO) and Slater type orbitals (STO). Slater type of orbitals are used in the case when molecules consists of hydrogen-like atoms since hydrogenic orbitals describe atoms exactly if the electron-electron interactions are neglected, and they can describe the electron density around the nucleus. One drawback of the Slater type of orbitals is the high computational cost, because of this approximated types of STOs, Gaussian-type orbitals, are used for their better computational efficiency [37].

In split valence basis sets method, the number of basis functions used for core and valence electrons differ in order to reduce to computational cost, and more flexibility is given to valence basis functions since valence electrons are more active in chemical bonding. In order to get better approximation to the exact electronic energy, basis sets are modified by utilizing two functions, which are polarization and diffuse functions.

Polarization functions are used to describe the polarization of the electron density of the atom in molecules. This is very important for modeling chemical bonding because the bonds are often polarized. Polarization functions give higher angular momentum orbital to heavy atoms symbolized by an asterisk (*) or (d) and for the lighter atoms like hydrogen a second asteriks or (d,p) are added.

Diffuse functions give flexibility to the "tail" portion of the atomic orbitals, far away from the nucleus. Diffuse basis functions are important for describing anions or dipole moments, but they can also be important for accurate modelling of intramolecular and intermolecular bonding. Diffuse functions allow orbitals to occupy larger spaces and they are represented as plus signs, one plus sign "+" implies the diffuse function addition for heavy atoms and two plus signs "++" indicates that diffuse functions are used for hydrogen atoms.

A larger basis set provides more variable parameters to produce a better approximate wavefunctions, hence increases the accuracy of the calculations, however computational cost increases due to higher computational time. Therefore, selection of basis set should take into account the properties and the behavior of the system to be modeled.

3.4. Methodology Used in This Study

Conformations of the molecules are determined firstly with the semi-empirical PM3 method using the SPARTAN software and re-optimized by a higher level of theory DFT (Density Functional Theory) with the Gaussian09 program package. Geometry optimizations of ground and transition state structures are performed using M06-2X functional and 6-311+G** basis set for rotation, racemization and aldol reactions. B3LYP functional is tested for the rotational barriers and compared with the M06-2X functional and the experimental results. For the other parts of the study, due to the inability of B3LYP [38] to describe van der Waals complexes bound by medium-range interactions, we performed our calculations with Minnesota functionals. M06-2X has improved performance for main-group thermochemistry, conformational energies, barrier heights [39], and noncovalent interactions [40] as compared to B3LYP functionals in organic reactions.

Accurate prediction of chemical reaction barrier heights is important since comparison with the experimental results will be conducted in this work. Due to their partially stretched bonds, transition states are harder to model than equilibrium structures [41]. According to the work of Zhao [41], M06-2X is the best functional for the determination of barrier heights. The nature of the corresponding reactants and products is verified by intrinsic reaction coordinate (IRC) calculations on the transition state structures. Implicit solvation is used for various solvents except for racemization mechanism where the explicit solvent model is used by ethanol using the integral equation formalism polarizable continuum model (IEFPCM). The relative energies reported throughout the study are the Gibbs Free Energies (kcal/mol).

4. RESULTS AND DISCUSSIONS

4.1. PART I: Role of Substituents on the Internal Rotation of Thiohydantoin Derivatives

In the previous experimental studies [14, 22], thiohydantoin derivatives were synthesized by the process as follows:

- The appropriate ester salt was refluxed for some time with selected arylisothiocyanate with triethylamine in dichloromethane.
- To eliminate the remaining TEA used in the synthesis, extraction with distilled water was done.
- After evaporation of the dichloromethane, the crude product was crystalised using ethyl acetate and hexane mixture.
- After separation, stereoisomers were dissolved either in toluene (only rotation was observed, PART I) or ethanol (both racemization and rotation were observed for some derivatives, however racemization requires lower barriers, shown in PART II) .

In this study, rotational barriers of hindered rotation around the $N_{sp2} - C_{aryl}$ chiral axis have been calculated in toluene and compared with the experimental results and predictions about the determination of rotational barriers before the experimental procedures have been carried out. In the previous study of Arıca [14], no racemization was observed even the temperature was 110°C in toluene. Also in the work of Sarıgül [42] in order to see which interconversion that exists between the isomers, rotation around the chiral axis or racemization at C_5, SP was kept in toluene at a constant temperature bath and injected to HPLC at certain time intervals for analysis. It was found that SP converted to SM with time without formation of any other isomer shown in Figure 4.1. The reason for not observing any racemization in toluene is there is no environment to capture a proton from synthesized 2-thiohydantoins for racemization.

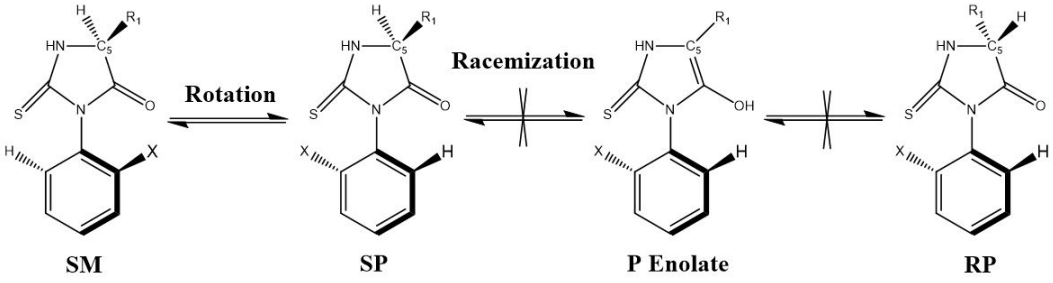

Figure 4.1. Possible interconversions for the SP isomer in toluene.

In previous experimental studies, experimental activation barriers of rotation is determined and they are shown in Table 4.1. Our aim is to rationalize these results with the computational tools.

Table 4.1. Experimental activation barriers (kcal/mol) in toluene at various temperatures.

Molecule Name	**SP to SM**	**SM to SP**	**RP to RM**	**RM to RP**
M1(303K) [22]	24.0	24.3	24.4	24.2
M2(313K) [14]	24.6	24.7	25.2	25.0
M3(383K) [14]	-	-	28.4	28.4
M4(333K) [22]	27.8	27.5	27.5	27.8
M5(313K) [14]	-	-	24.7	24.8
M6(383K) [14]	28.3	28.2	-	-
M8(303K) [22]	24.7	24.7	24.7	24.7
M9(333K) [22]	26.3	26.1	26.1	26.2
M10(333K) [42]	25.7	25.6	25.6	25.7
M11(333K) [22]	27.7	27.7	27.7	27.7
M13(333K) [32]	28.0	28.0	28.0	28.0

In the process of a reaction, transition state of a chemical reaction is a particular configuration corresponding to the highest potential energy along the reaction coordinate. In our case, it corresponds to the geometry where two rings lie in the same plane [43] where *ortho*-substituent X and the exo-cyclic groups O or S are too bulky that rotation is hindered as illustrated in Figure 4.2. R_1 represents substitution on C_5 which can be methyl, benzyl, isopropyl, isobutyl and phenyl and X represents *o*-aryl substituent on aromatic group which can be methyl, bromide, chloride and trifluoromethyl.

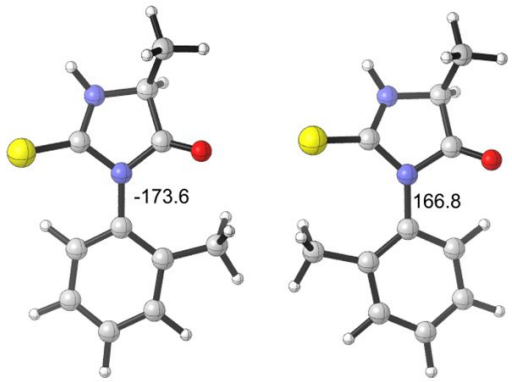

Figure 4.2. Rotational transition state structures for M1 in two different directions.

Table 4.2. Activation barriers (kcal/mol) of rotation in toluene for M1 (-R_1 and -X are -CH_3) where rotation occurs via two different directions.

	O-side (B3LYP/ 6-311+G)**	**O-side (M06-2X/6-311+G**)**	**S-side (B3LYP/6-311+G**)**	**S-side (M06-2X/6-311+G**)**
SM to SP	27.3	27.6	32.1	32.3
SP to SM	27.4	27.6	32.2	32.2
RM to RP	27.4	27.6	32.2	32.3
RP to RM	27.3	27.6	32.1	32.2

There are two ways in which rotation can occur around the chiral axis as shown for M1 in Figure 4.2. We observed that when exo-cyclic sulfur and *o*-aryl groups are on same plane the larger size of sulfur introduces larger steric hinderance compared to oxygen as shown in Table 4.2. Therefore, we continue with our calculations taking into consideration the fact that rotation happens on the site of oxygen instead of sulfur.

Table 4.3. Experimental and calculated activation barriers (kcal/mol) of rotation for SM to SP conversion of the molecules. Values in paranthesis display the SP to SM rotations.

	Experimental	**B3LYP/6-311+G****	**M06-2X/6-311+G****
M1(303K)	24.3 (24.0)	27.3 (27.3)	27.6 (27.6)
M2(313K)	24.7 (24.6)	27.6 (27.4)	27.2 (27.8)
M3(383K)	-	31.2 (30.9)	31.8 (32.9)
M4(333K)	27.5 (27.8)	30.1 (30.2)	31.3 (31.6)
M5(313K)	-	27.7 (27.7)	28.5 (27.7)
M6(383K)	28.2 (28.3)	30.8 (30.5)	30.7 (31.9)
M7(333K)	-	30.1 (29.9)	30.9 (30.8)
M8(303K)	24.7 (24.7)	27.1 (27.4)	27.5 (28.0)
M9(333K)	26.1 (26.3)	28.8 (29.1)	30.2 (30.5)
M10(333K)	25.6 (25.7)	28.7 (29.0)	29.5 (31.1)
M11(333K)	27.7 (27.7)	30.1 (30.4)	30.8 (31.5)
M13(333K)	28.0 (28.0)	30.0 (30.1)	30.5 (30.0)

In order to see the effect of *ortho*-substituent on rotation, we have selected M1 (X: -CH_3), M9 (X: -Cl), M4 (X: -Br) and M13 (X: -CF_3) for further analysis. It has been calculated that activation barriers of rotation from SM to SP are 27.6, 30.2, 31.3 and 30.5 kcal/mol for M1, M9, M4 and M13 respectively.

In the work of Lunazzi [44], it states that the steric effect during rotation is essentially determined by the size of the atom X and thus increases with the Van der Waals radius. Also in the work of Belot [45] the relative size of the *ortho*-substituents are given as -CF_3 > -Br > -CH_3 > -Cl. Methyl is larger than chlorine, however in our results we observe a higher barrier for the chloride substituent. This outcome may be explained by:

(i) In the case where -CH_3 is in *o*-aryl position (M1), rotation has the lowest barrier since the methyl group interacts with carbonyl oxygen with favorable interactions and it stabilizes the transition state structure and lowers the activation barrier of rotation. Due to the position of the carbonyl oxygen, only one lone pair of oxygen can interact with methyl hydrogens, however we observe two hydrogens which are capable of making this interactions.

(ii) A repulsion between the lone pairs of oxygen and the lone pairs of halogen groups can be one of the reasons for observing higher barriers of rotation for the molecules that have halogen substituents such as M4 (X: -Br) and M9 (X: -Cl) compared to methyl *ortho*-substituent. Bigger Van der Waals radius size of bromide compared to methyl group is also the reason for observing higher barriers when the *ortho*-substituent is bromide shown in Table 4.3.

Comparing halogen substituents, bromide (M4) has a higher barrier of rotation compared to chlorine (M9). They both have lone pairs, so the reason is the larger of bromide. Bromide has a larger electron cloud, repulsion with the carbonyl oxygen is larger thus it increases the barrier of rotation. Also in the work of Sarıgül [41], it was observed that there is a linear relationship between the size of the *o*-halogen substituent and the rotational barrier around the chiral axis, the bigger the atomic radius, the larger the rotational barrier.

We also looked for the CM5 charges of halogen substituents shown in Figure 4.3. Chlorine is more negative than bromide but we still observed a higher barrier for the bromide group due to size of the substituent. This steric effect also distorts dihedral angle being around 168° and situated the bromide group further away from the carbonyl oxygen compared to chlorine shown in Figure 4.3.

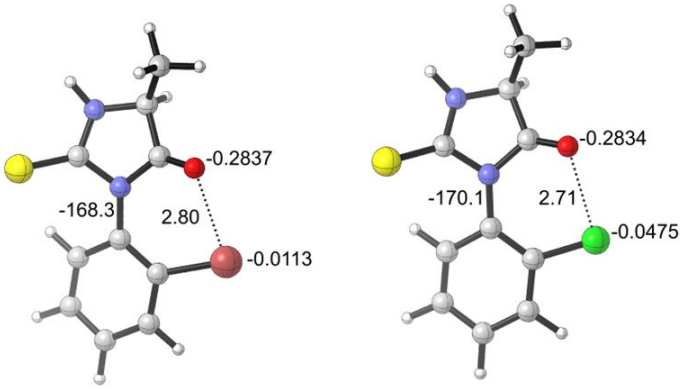

M4-TS-S (X: -Br)
SM to SP: 31.3 kcal/mol
SP to SM: 31.6 kcal/mol

M9-TS-S (X: -Cl)
SM to SP: 30.2 kcal/mol
SP to SM: 30.5 kcal/mol

Figure 4.3. Charges and distances between the carbonyl oxygen and the *ortho*-substituents.

When X_1 is -CF_3 (M13), different than the methyl group, hydrogens are replaced with fluorines therefore we no longer observe a favorable interaction with the carbonyl oxygen. Also, this group is sterically larger and F atoms possess a partial negative charge due to their electronegativity and the lone pairs. These effects further increase the repulsion between the carbonyl oxygen and in experimental results causes the largest barrier of rotation. However for the calculated results in this study, this barrier (X: -CF_3) is closer to the rotational barriers of M4 (X: -Br) where the bromide lone pairs having a repulsive effect with oxygen. These findings are also validated by comparing M8 (X: -CH_3), M10 (X: -Cl) and M11 (X: -Br) where the R_1 substituent is isopropyl as depicted in Figure 4.4. Also comparing molecules which have the same R_1 substituent and different X substituent such as M2 (X: -CH_3) - M3 (X: -Br) and M5 (X: -CH_3) - M6 (X: -Br), the same conclusion is obtained which is, the size of the *o*-aryl substituents and the lone pairs of halogen are the factors affecting the rotational trends.

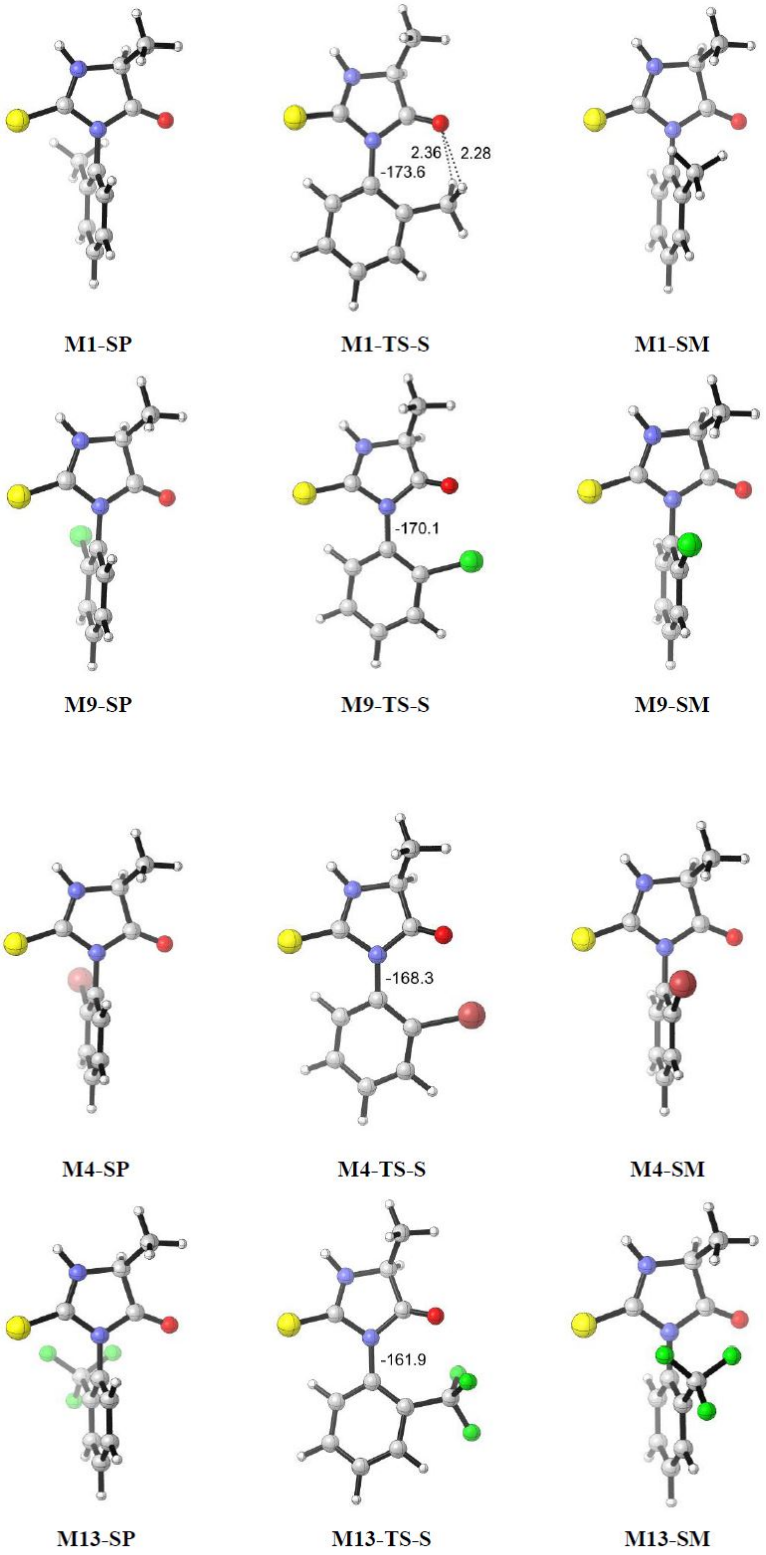

Figure 4.4. 3D structures of ground and transition states of M1 (R_1: -CH_3 and X: -CH_3) , M4 (R_1: -CH_3 and X: -Br), M9 (R_1: -CH_3 and X: -Cl), M8 (R_1: isopropyl and X: -CH_3), M10 (R_1: isopropyl and X: -Cl) and M11 (R_1: isopropyl and X: -Br).(M06-2X/6-311+G** / iefpcm / Solvent = Toluene)

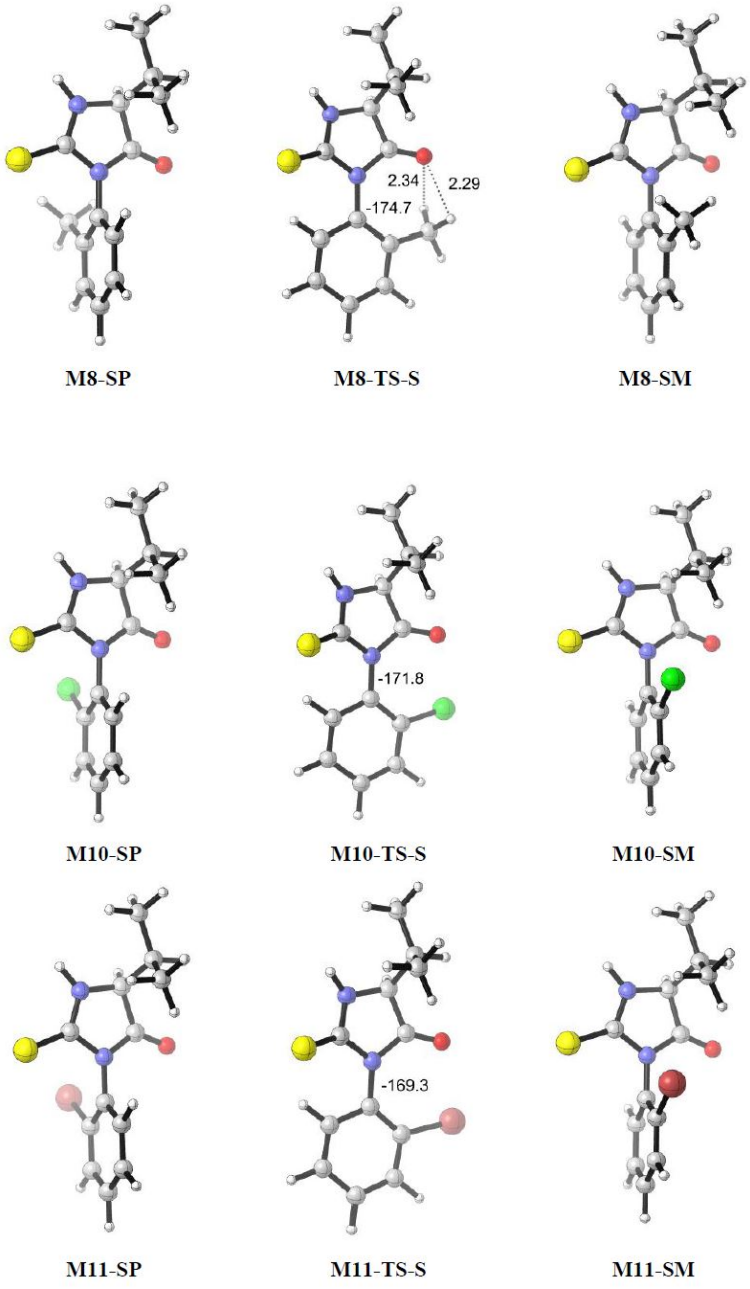

Figure 4.4. 3D structures of ground and transition states of M1 (R_1: -CH_3 and X: -CH_3) , M4 (R_1: -CH_3 and X: -Br), M9 (R_1: -CH_3 and X: -Cl), M8 (R_1: isopropyl and X: -CH_3), M10 (R_1: isopropyl and X: -Cl) and M11 (R_1: isopropyl and X: -Br).(M06-2X/6-311+G** / iefpcm / Solvent = Toluene) (cont.)

The effect of R_1 on rotation is further investigated by comparing M1, M2, M5 and M8 where *ortho*-substituent is methyl and each molecule has a different R_1 substituent. As shown in Table 4.3., having thiohydation derivatives with different functional groups such as simple alkanes (M1, M4, M8, M11, M5 and M6), alcohol (M7 and M12) and aromatic ring (M2 and M3) do not impose any effect on the rotational trends. We verified these findings by selecting X=Br in molecules such as M4, M3, M6, M7 and M11 as listed in Table 4.3.

The reason of this outcome can be explained in two ways, electronic and steric influence, because of the acceptor/donor capacity of functional groups attached on C_5 carbon, electron density on carbonyl oxygen could change. For example if R_1 substituent decreases the electron density on oxygen by being a electron withdrawing group, less repulsion could have occurred between oxygen and X_1 and it may decrease the rotational barrier. However there are three atoms (Figure 4.5.) between carbonyl oxygen and R, this distance does not impose any significant effect so we observe similar rotational barriers. Also because of the distance, R_1 group does not impose any steric effect on groups near the rotation site.

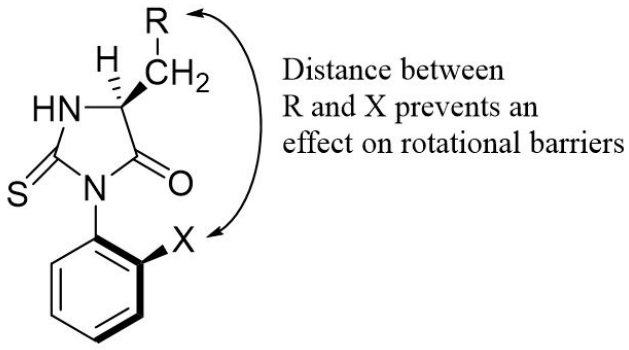

Figure 4.5. Distance between the functional group R and the carbonyl oxygen in thiohydantoin derivatives.

For M7 where R_1 is -CH_2OH, for the lowest energy conformers, -OH group interacts with carbonyl oxygen through favorable interactions. We predicted this interaction to lower the rotational barrier, however this stabilization happens for both ground state and transition state structures simultaneously, so the difference doesn't change remarkably as shown in Table 4.3.

When X_1 is methyl such as M1, M2, M5 and M8, the dihedral angle of chiral axis on TS structures is around 180^0. However, when X_1 is bromide such as M4, M3, M6, M11 and M7, the dihedral angle of chiral axis on TS structures is around 170^0 (Figure 4.4. and Figure 4.7.). To explain this outcome, we can predict that hydrogens on methyl group tend to make favorable interactions with the oxygen of the thiohydantoin ring. 5-Membered thiohydantoin ring and the aryl ring come close to each other in order to make this interaction thus, we observe more planar (closer to 180^0 dihedral angle) structure. For the case when X_1 is bromide, due to repulsion between carbonyl oxygen and -Br, two ring structures can't be on the same plane and this distorts dihedral angle being around 168^0. The relation between the rotational barriers and the deviation from the 180^0 is given in Figure 4.6.

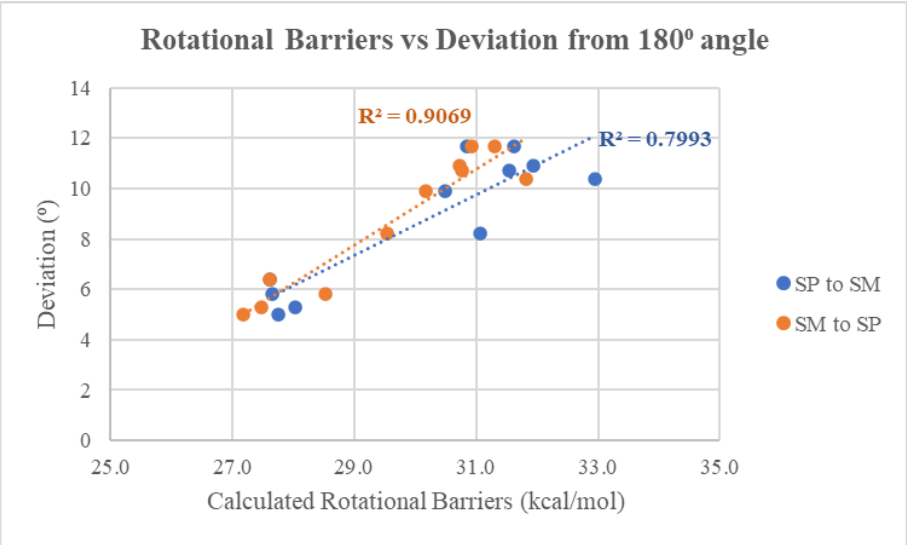

Figure 4.6. Rotational barriers vs. deviation from 180^0 for the SM to SP and SP to SM rotation.

M2 and M3, differ only in the identity of the *ortho*-substituent. In the lowest energy conformers of ground and transition states of M2, as shown in Figure 4.8. the benzyl group (R_1) interacts with H (SP) or -CH_3 (SM) attached to benzene. However, in the lowest energy conformers of ground and transition states of M3, this π interaction is not favored and benzyl group does not have any interaction with the aryl ring.

In the case of M2, despite of the steric effect, benzyl (R_1) interacts with *ortho*-methyl or hydrogen of the aryl group in the optimized and the transition structures of M2's lowest energy conformers through C-H$\cdots\pi$ interactions. Under the class of the weak H-bonds, the C-H$\cdots\pi$ systems form a separate class. Unlike conventional hydrogen bonded systems where the hydrogen is attached to an electronegative atom, here the hydrogen is attached to a carbon atom. Second, in conventional H-bonded systems, the proton acceptor is an electronegative atom or ion however, in the C-H$\cdots\pi$ systems, the proton acceptor is the π electron system [46].

Attraction between benzene and hydrocarbon molecules is considerably weaker than the hydrogen bond between waters. In the work of Tsuzuki [47] calculations indicate that dispersion interaction is mainly responsible for the attraction between benzene and hydrocarbon molecules. Electrostatic interaction is not essential for the attraction in benzene-methane complexes, which is considerably smaller than dispersion interaction. C-H bond prefers to point toward the benzene ring (Figure 4.7.) , this preference is not the result of unusual attraction between the C-H bond and the π system. The orientation of the C-H bond is controlled by relatively weak, but highly orientation dependent electrostatic interaction.

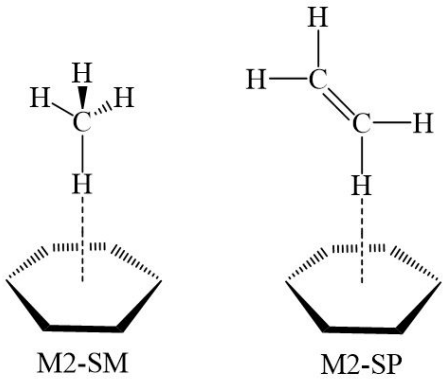

Figure 4.7. *o*-methyl$\cdots$phenyl and H$\cdots$phenyl interactions.

Note that, since there is no C-H$\cdots\pi$ systems for M3 conformers when X is bromide, electron cloud on bromide and delocalized π-electrons on benzene repel each other and benzyl gets further away from bromide.

This explains the geometry of lowest energy conformers of the M3 (X: -Br) and M2 (X: -CH_3) molecules being different from each other, the nature of the *ortho*-substituents effect the orientations of the R_1 substituents in such cases.

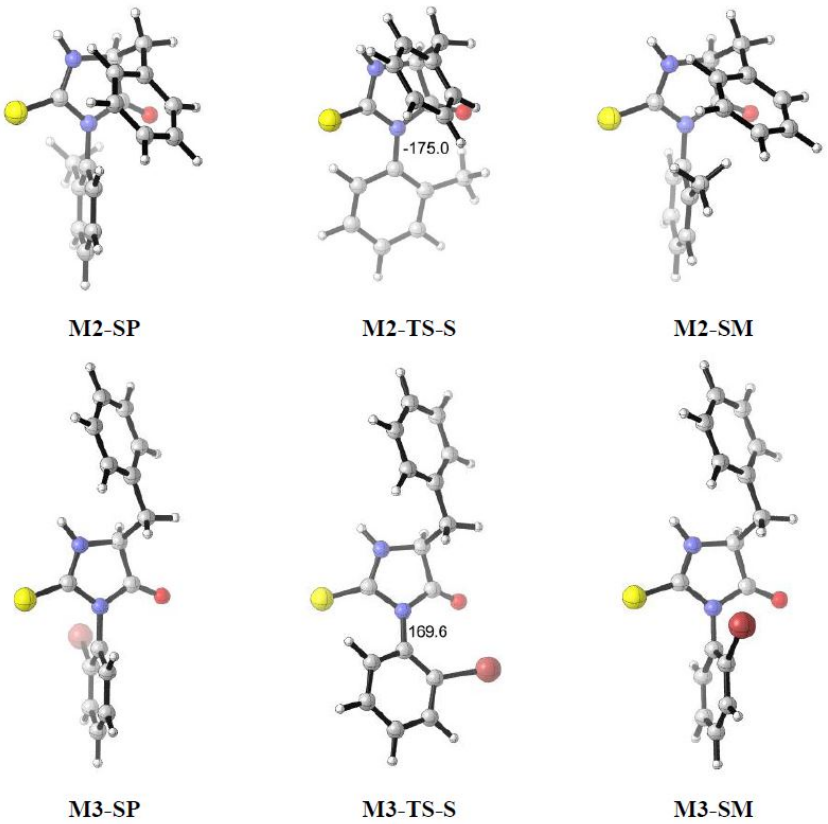

Figure 4.8. 3D structures of ground and transition states of M2 (R_1: benzyl and X: -CH_3), M3 (R_1: benzyl and X: -Br), M5 (R_1: isobutyl and X: -CH_3), M6 (R_1: isobutyl and X: -Br) and M7 (R_1: -CH_2OH and X: -CH_3). (M06-2X/6-311+G** / iefpcm / Solvent = Toluene)

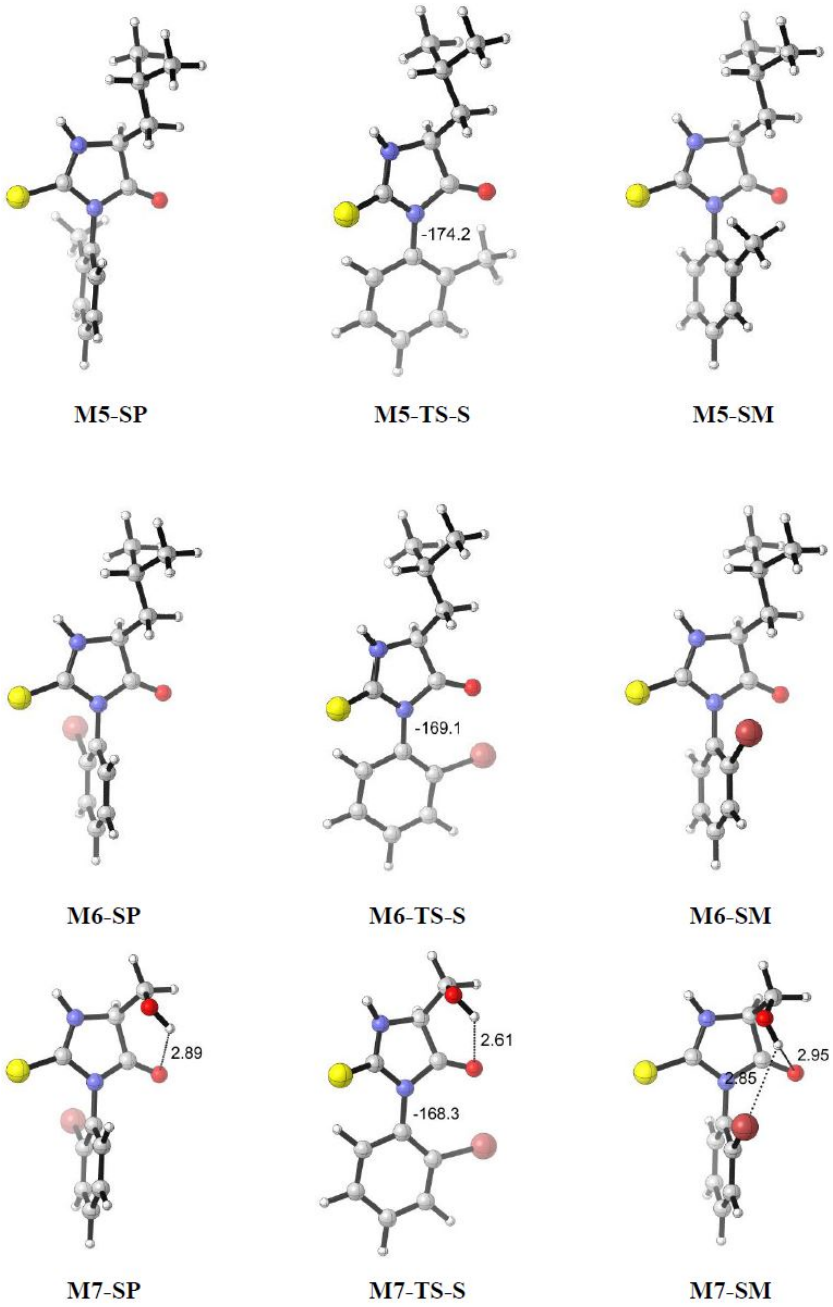

Figure 4.8. 3D structures of ground and transition states of M2 (R_1: benzyl and X: -CH_3), M3 (R_1: benzyl and X: -Br), M5 (R_1: isobutyl and X: -CH_3), M6 (R_1: isobutyl and X: -Br) and M7 (R_1: -CH_2OH and X: -CH_3). (M06-2X/6-311+G** / iefpcm / Solvent = Toluene) (cont.)

Experimental and calculated rotational barriers are not equal to each other as shown in Table 4.3. Generally, calculated results (B3LYP and M06-2X) are 3 kcal/mol higher than the experimental data. This may due to the limitations of DFT or the experimental results. However, there is a linear correlation between experimental and calculated values as shown in Figure 4.9. and Figure 4.10. and this relationship and methodology can be further used for the prediction of rotational barriers of thiohydantoin derivatives before the experimental procedure.

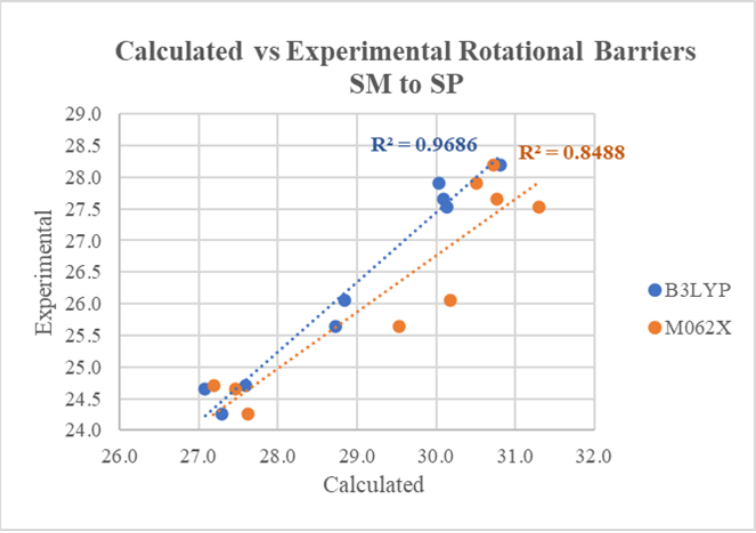

Figure 4.9. Experimental vs Calculated Rotational Barriers (kcal/mol) of thiohydantoin derivatives. (SM to SP)

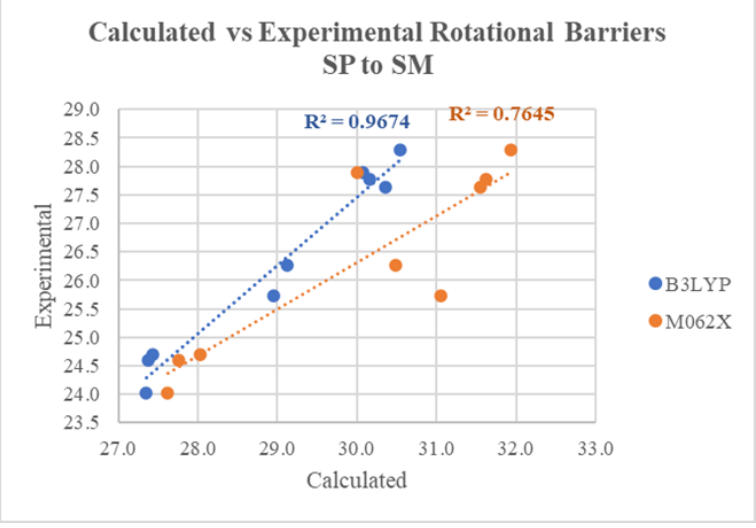

Figure 4.10. Experimental vs Calculated Rotational Barriers (kcal/mol) of thiohydantoin derivatives. (SP to SM)

4.2. PART II: Solvent Assisted Racemization of Thiohydantoin Derivatives

Molecular chirality has an important role in organic chemistry. Chiral molecules having central chirality have stereogenic centers. If two molecules with identical chemical formula are not superimposable, they are called enantiomers [18]. SM and RP isomers are enantiomers since they are not superimposible mirror images of each other.

Racemization (Figure 4.11.) is the process where a single enantiomer is converted into a mixture of both enantiomers. Racemization is a particular concern to drug discovery because the two enantiomers are highly likely to have different biological properties, particularly in vivo [48]. A process related to racemization is enantiomerization, which refers to one enantiomer being stereoselectively converted into the other and which can also lead towards a mixture of the two enantiomers [48].

In this text we refer to racemization where the central chirality that is the tetrahedral sp^3 hybridized C_5 atom of the heterocylic ring is converted from S to R or R to S.

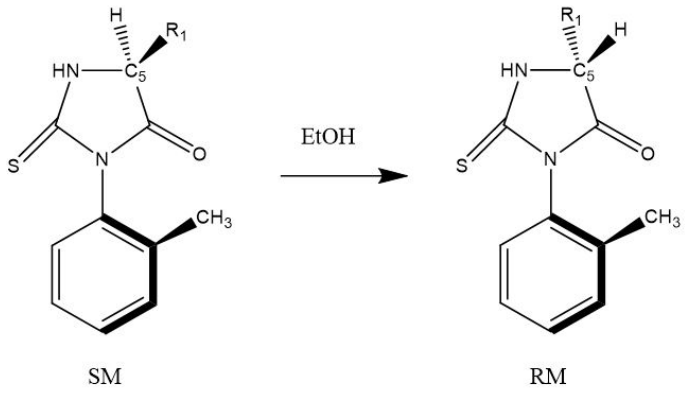

Figure 4.11. SM to RM racemization at C_5.

As an experimental data, we have barriers of racemization in the presence of ethanol. However, before we do our calculations we suggest a reaction mechanism in the presence of ethanol.

In order to do that, we model the reaction without the assistance of any ethanol, and with the assistance of one and two explicit EtOH for M3 (R_1: benzyl and X: -Br). Results are shown in Table 4.4. and 3D geometries are shown in Figure 4.12.

Table 4.4. Different racemization mechanisms and barriers (kcal/mol) of M3 (-R_1: benzyl and X: -Br) compared with the experimental data. (M06-2X/6-311+G**, 313 K, Solvent: Ethanol)

Conditions	**Experimental**	**M06-2X/6-311+G****
Self Tautomerization (M3-TS-Rac)	24.5	79.1
1EtOH (M3-1EtOH-TS)	24.5	36.5
2 EtOH (M3-2EtOH-TS1)	24.5	25.2

Based on the results coming from Table 4.4., for the mechanism of the reaction, racemization is observed with the assistance of two ethanol molecules which are abbreviated as EtOH-1 (in the vicinity of C_5 carbon) and EtOH-2 (in the vicinity of carbonyl oxygen) in Figure 4.13.

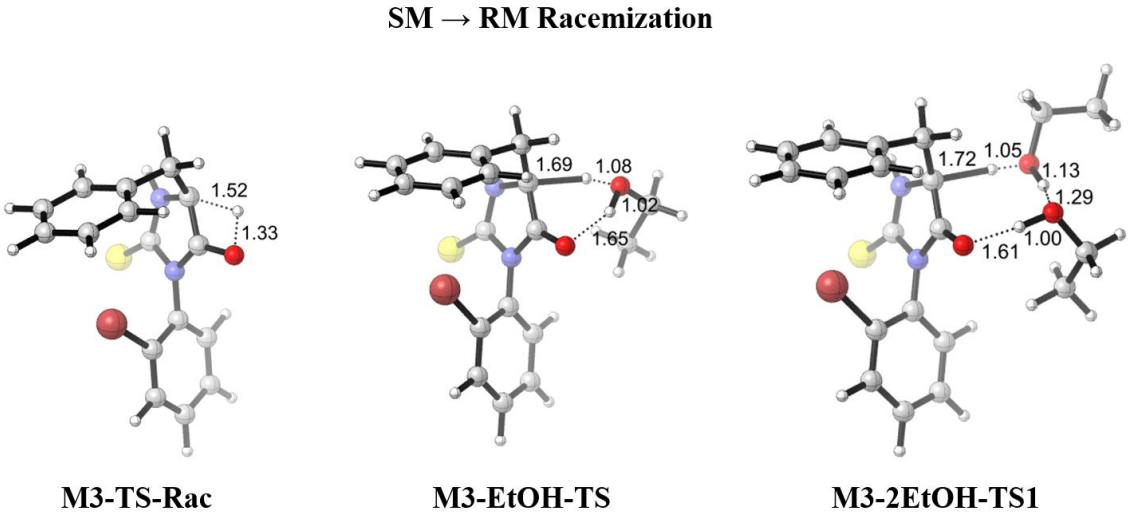

Figure 4.12. Self tautomerization (M3-TS-Rac), 1EtOH (M3-EtOH-TS) and 2EtOH (M3-2EtOH-TS1) assisted transition state structures. (M06-2X/6-311+G**, 313 K, Solvent: Ethanol)

In our calculations, we mainly focus on SM to RM racemization where we start modelling with the SM isomer. When SM isomer is the reactant, two ethanol molecules approach to C_5 and the carbonyl oxygen and we observe a transition state as shown in Figure 4.13. In the transition state the following steps take place in the order;

(i) Hydrogen attached to C_5 is captured by EtOH-1,
(ii) EtOH-1 gives its hydrogen to EtOH-2,
(iii) EtOH-2 gives its hydrogen to carbonyl oxygen,
(iv) C_4=C_5 double bond forms and we observe an enol intermediate as shown in Figure 4.13.

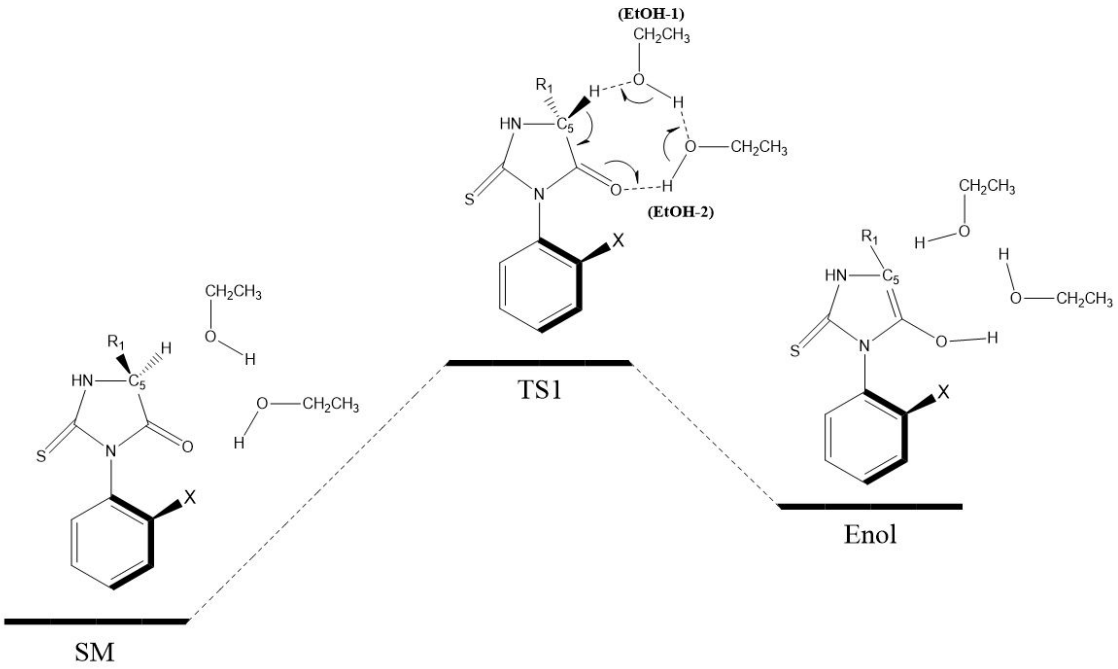

Figure 4.13. SM to enol formation mechanism in the presence of 2EtOH.

After enol is formed as an intermediate, chirality at C_5 is lost since now C_5 is no longer sp^3 hybridized and in the tetrahedral form. Since due to loss of chirality, direction of attachment of hydrogen to C_5 is significant. As observed in Figure 4.14., when the hydrogen of EtOH-1 approachs to from Re-face (same side as X substituent) chirality of the thiohydantoin molecule changes and we obtain RM isomer. After that, racemization process is completed.

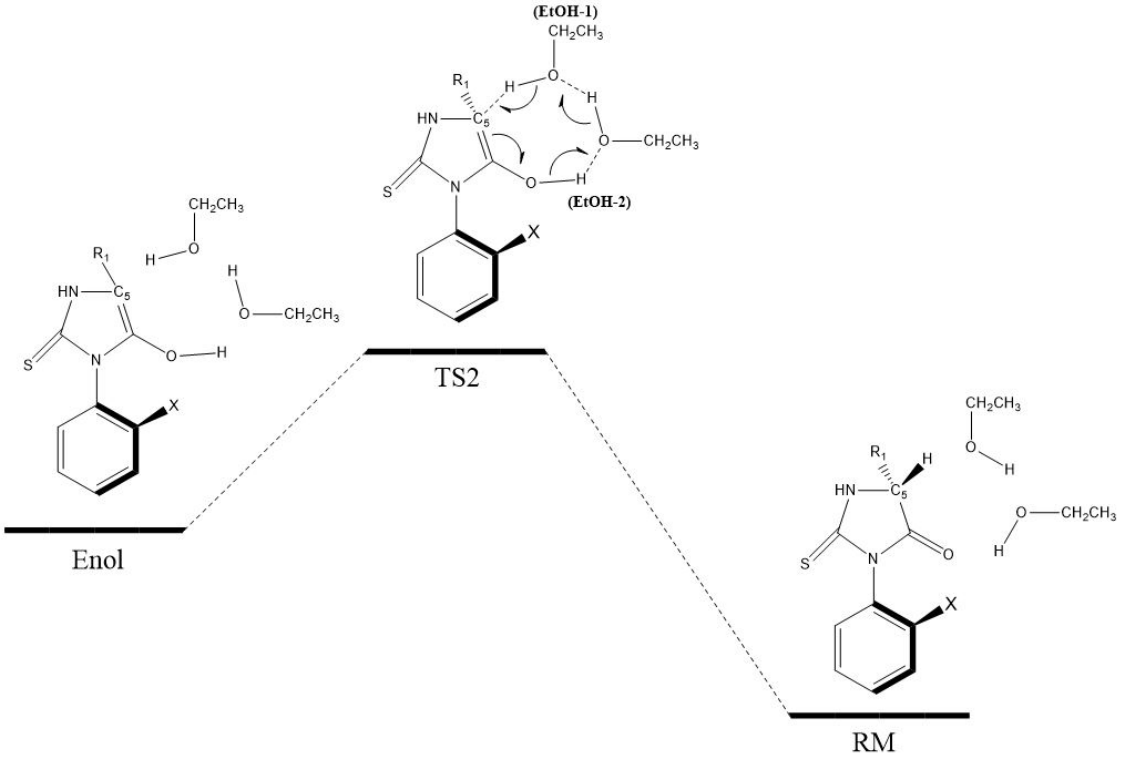

Figure 4.14. Enol to RM formation mechanism in the presence of 2EtOH.

In this study, racemization barriers of M2 (R_1: benzyl and X: -CH_3), M3 (R_1: benzyl and X: -Br), M5 (R_1: isobutyl and X: -CH_3) and M6 (R_1: isobutyl and X: -Br) are calculated and compared with the experimental data in the work of Arıca. Barriers of racemization are calculated to be close to experimental data and no remarkable difference is observed when R_1 or X is different as shown in Table 4.9.

In the previous study of Arıca [14], it has been found that although the stereoisomers converted to each other only by rotation in toluene, in ethanol racemization was accompanied with rotation depending on the temperature of the thermal interconversion experiment [49].

SM isomers were found to interconvert to SP isomers via rotation around the $N_{sp2} - C_{aryl}$ chiral axis in toluene, similarly RM rotated to give RP in toluene. However, when the solvent was changed to ethanol, that is, when the SM stereoisomers of compounds M2, M3, M5 and M6 were kept in ethanol instead of toluene, SM was found to convert to RM. Thus racemization at C_5 of the heteroring occurred in ethanol, in this solvent also RM converted to SM. Rotational barriers are calculated in ethanol and observed to be higher than ethanol assisted racemization in respective temperatures. In the work of Arıca for M2 (R_1: benzyl and X: -Br) in ethanol and at 40°C, both racemization and rotation reactions were observed. In order to decrease the rotation rate, calculations were done also at 25^0C (298 K) and at that temperature only racemization was observed. Calculated results also give the same outcome given in Table 4.5. and rotational transition state structures in ethanol are shown in Figure 4.15.

Table 4.5. Experimental and calculated rotation and racemization barriers (kcal/mol) of M2 (-R_1: benzyl and X: -CH_3) in ethanol at 298 K.

	Experimental	**M06-2X/6-311+G****
SM to SP (RM to RP)	-	29.4 (30.4)
SM to RM (RM to SM)	24.0 (24.0)	25.4 (25.7)

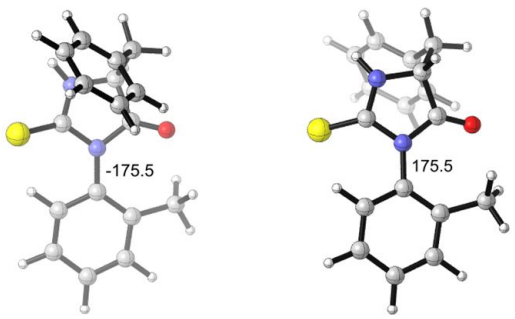

M2(S)-TS-Rot (SM to SP) **M2(R)-TS-Rot** (RM to RP)

Figure 4.15. Rotational transition state structures of M2 (R_1: benzyl and X: -CH_3) in ethanol.(M06-2X/6-311+G**, 313 K, Solvent: Ethanol)

Pathway for SM to RM and RM to SM two ethanol assisted racemization of M2 (R_1: benzyl and X: -CH_3) is shown in Figure 4.16.

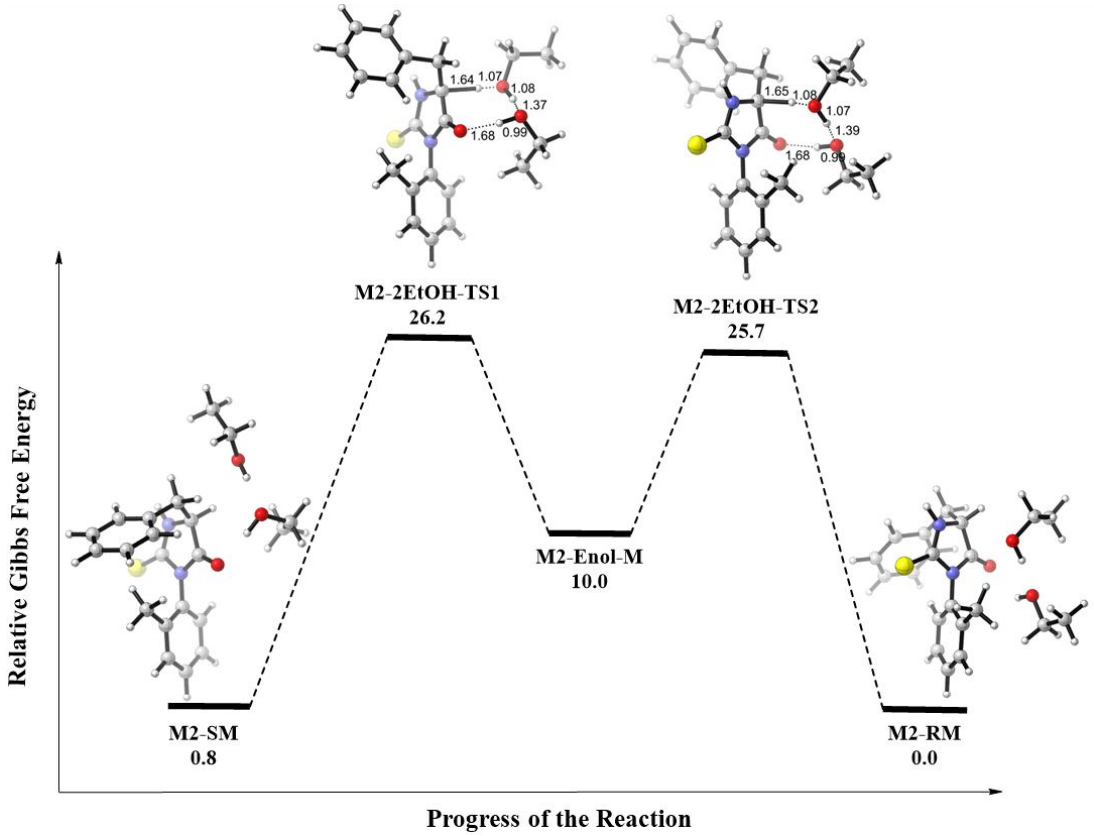

Figure 4.16. Energy profile (kcal/mol) of SM to RM / RM to SM ethanol assisted racemization for M2. (M06-2X/6-311+G** / Temperature = 298 K / Solvent = Ethanol)

In the work of Arıca for M3 (R_1: benzyl and X: -Br), at 298 K and 313 K in ethanol, only racemization was observed. In order to verify that the racemization requires lower barriers in ethanol and it is a more plausible mechanism, calculations were done in both of the temperatures.

Different types of approach were used for determining rotational barriers. One is the rotation of the aryl ring in the presence (explicit) of two ethanol molecules abbreviated as **, other one is the rotation without (implicit) the presence of any ethanol molecules abbreviated as *.

Both methods gave similar results, showing that rotation requires more energy compared to racemization in ethanol shown in Table 4.6.

Table 4.6. Experimental and calculated rotation and racemization barriers (kcal/mol) of M3 in ethanol. (*explicit ethanol / **implicit ethanol)

	Experimental	**M06-2X/6-311+G****
298K		
SM to RM*	24.5	25.1
SM to SP*	-	33.7
SM to SP**	-	32.9
313K		
SM to RM*	25.0	25.2
SM to SP*	-	33.8
SM to SP**	-	32.6
RM to RP**	-	32.8

3D geometries of explicit ethanols for M2 (R_1: benzyl and X: -CH_3) and M3 (R_1: benzyl and X: -Br) is as follows:

- Around the SM isomer, EtOH-1 displays the classic anti form as a conformer as expected. For EtOH-2, the anti form is disrupted. Methyl hydrogens of the ethanol molecule may interact with the carbonyl oxygen of the thiohydantoin heteroring by favorable interactions and as well as the aryl ring.
- After the course of the reaction when ethanol molecules come closer to the thiohydantoin molecule in order to form the transition state geometry, EtOH-1's methyl move away from the thiohydantoin because of the steric effect caused by the benzyl substituent. However EtOH-2's conformer is the same as in the reactant since the benzyl group is far from EtOH-2 to change the conformer.

Transition state structures of rotation and racemization for M3 are shown in Figure 4.17. Transition state structures of rotation and racemization for M5 are shown in Figure 4.18. Transition state structures of rotation and racemization for M6 are shown in Figure 4.19.

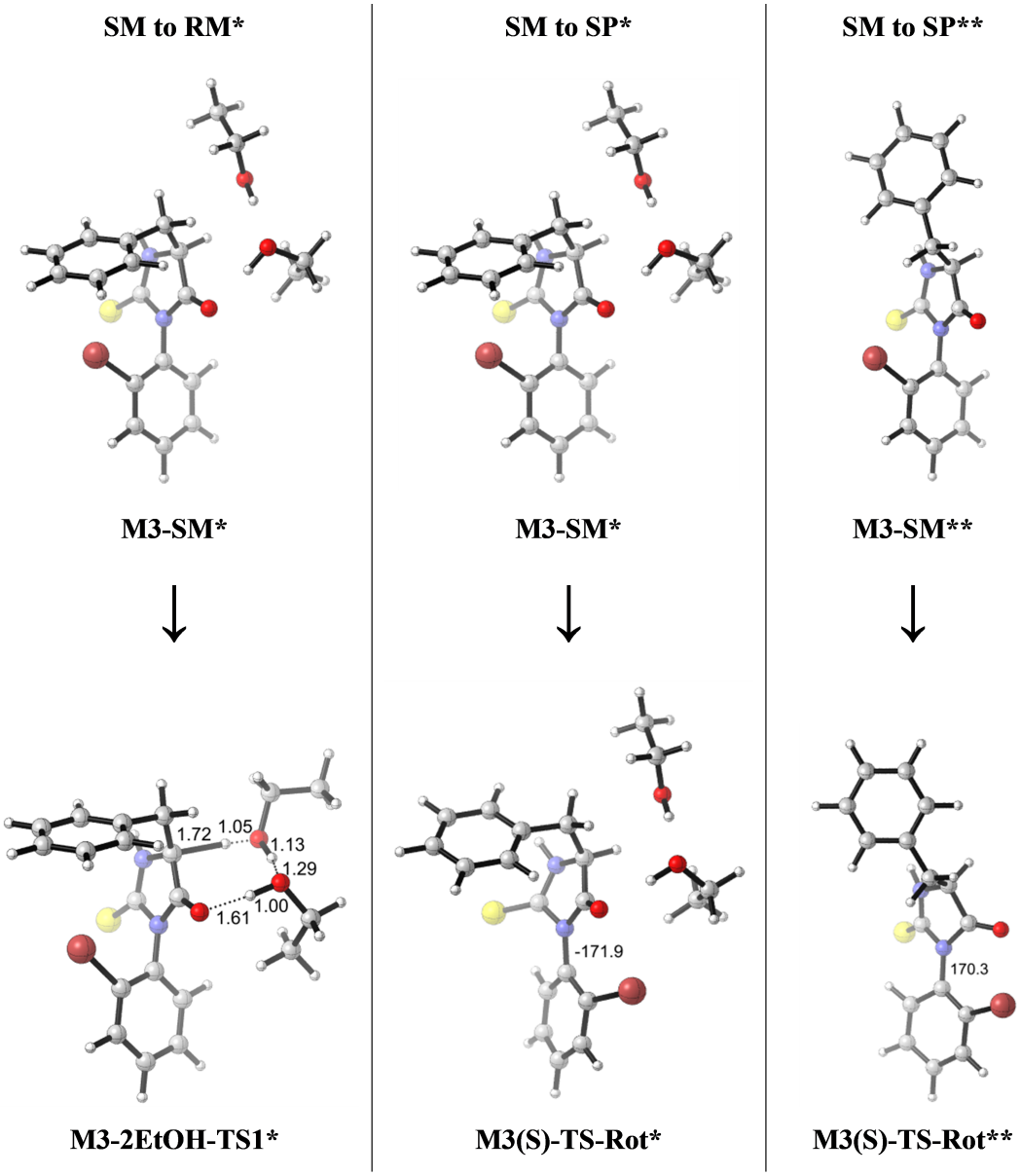

Figure 4.17. Racemization and rotation transition states and ground state structures of M3.

In the work of Arıca for M5 (R_1: isobutyl and X: -CH_3), after separation of RM, SM, RP and SP, each stereoisomer was dissolved in ethanol at 298 K. For all stereoisomers only racemization was observed with time until equilibrium in ethanol at 298 K, it was verified computationally and the results are shown in Table 4.7. At 313 K both racemization and rotation were observed in ethanol.

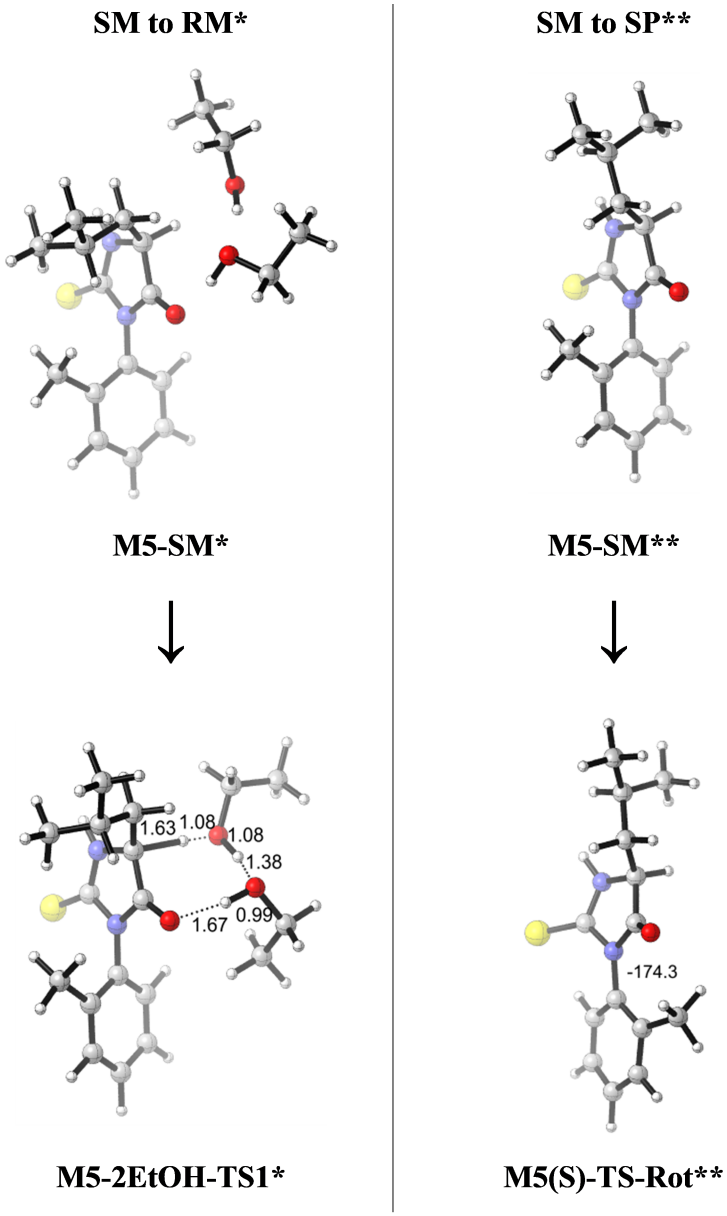

Figure 4.18. Racemization and rotation transition states and ground state structures of M5.

For the M6 (R_1: isobutyl and X: -Br) in the work of Arıca at 313 K in ethanol, only racemization was observed. At 313 K both racemization and rotation were observed in ethanol. In order to verify this result, we also calculated rotational barriers in that temperature. It was observed that rotation requires a higher barrier of rotation compared to racemization in these reaction conditions, results are given in Table 4.8.

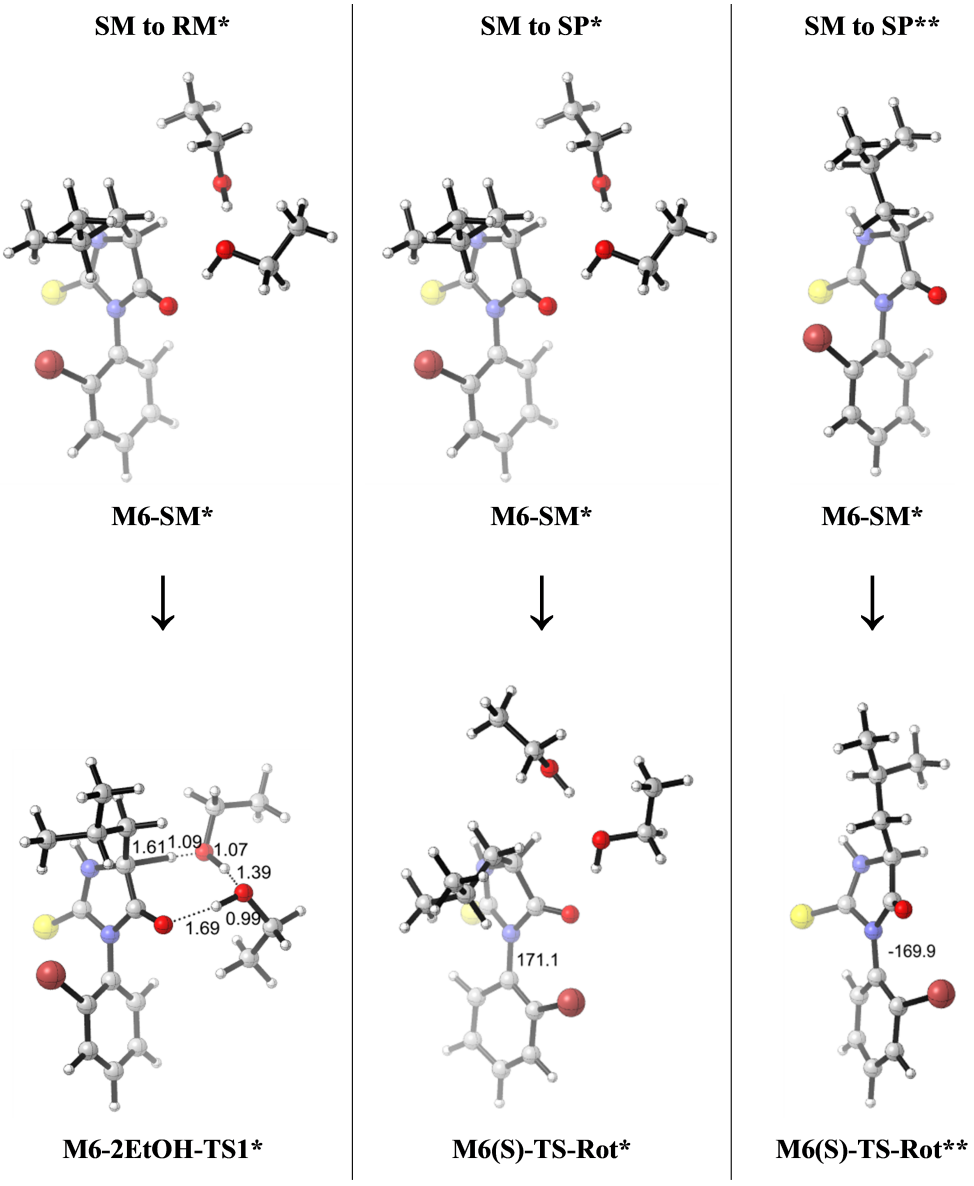

Figure 4.19. Racemization and rotation transition states and ground state structures of M6.

3D geometries of explicit ethanols for M5 (R_1: isobutyl and X: -CH_3) and M6 (R_1 : isobutyl and X: -Br) is as follows:

- Around the SM isomer for EtOH-1, methyl of the ethanol did not interact with thiohydantoin ring and anti form remained. In the case of EtOH-2, methyl of the ethanol did not interacted with the aryl ring and the carbonyl oxygen and the anti-form is remained as well because of the distance between these groups.
- When ethanol molecules come closer to the thiohydantoin molecule in order to form the transition state geometry, EtOH-1's methyl move away from the thiohydantoin ring because of the steric effect caused by the isobutyl substituent. EtOH-2's methyl changed its conformation and came closer to the carbonyl oxygen and the aryl group, because of the decreased distance between them. This allows the interaction between these groups and making the steric effect caused by the isobutyl group less significant.

Table 4.7. Experimental and calculated rotation and racemization barriers (kcal/mol) of M5 (-R_1: isobutyl and X:-CH_3) in 298 K. (*explicit ethanol / **implicit ethanol).

	Experimental	**M06-2X/6-311+G****
SM to SP**	-	29.8
RM to RP**	-	28.9
SM to RM*	24.0	23.7

Table 4.8. Experimental and calculated rotation and racemization barriers (kcal/mol) of M6 (-R_1: isobutyl and X: -Br) in 313 K. (*explicit ethanol / **implicit ethanol)

	Experimental	**M06-2X/6-311+G****
SM to SP	-	30.8
RM to RP	-	32.0
SM to RM	24.5	24.3

Computational results for the racemization barriers with the assistance of two ethanol molecules for the thiohydantoin derivatives M3, M5 and M6 are in a excellent agreement with experimental data. However for M2 (R_1: benzyl and X: -CH_3), activation barriers of racemization (SM to RM and RM to SM) are calculated to be slightly higher than expected. In conclusion, R_1 and X substituents do not effect the racemization activation barriers in ethanol at respective temperatures and racemization is a more plausible mechanism in ethanol compared to rotation shown in Table 4.9.

Table 4.9. Comparison of calculated and experimental racemization barriers (kcal/mol) of M2 (-R_1: benzyl and X: -CH_3), M3 (-R_1: benzyl and X: -Br), M5 (-R_1: isobutyl and X: -CH_3) and M6 (-R_1: isobutyl and X: -Br).

	T	**Transition**	**Exp.**	**M06-2X/6-311+G****
M2	298K	SM to RM (RM to SM)	24.0 (24.0)	25.4 (25.7)
M3	298K (313K)	SM to RM	24.5 (25.0)	25.1 (25.2)
M3	313K	SM to RM	25.0	25.2
M5	298K	SM to RM	24.0	23.7
M6	313K	SM to RM	24.5	24.3

4.3. PART III: Product Distribution of the Thiohydantoin Derivatives

Evolution of the product ratio is determined by two parameters: the rate coefficients (activation energies) and the thermodynamics [50]. Thermodynamic or kinetic reaction control in a chemical reaction can direct the composition in a reaction product when the reaction conditions influence the selectivity or stereoselectivity. One example is given in Figure 4.20. B is the kinetically controlled product, in the case when the product B forms faster than product A because the activation energy for product B is lower. While in other case A is the thermodynamic product since it is thermodynamically stable and favoured under thermodynamic control.

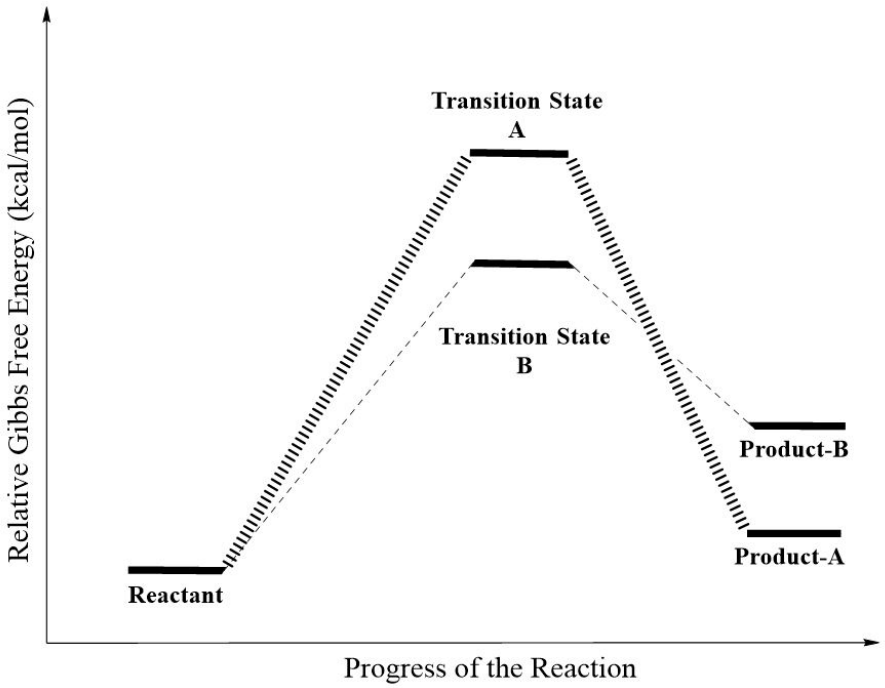

Figure 4.20. Reaction schematics of thermodynamic vs kinetic control.

As mentioned before, during the thiohydantoin ring formation four different types of isomers are formed such as SP, RP, SM and RM. In such circumstances, we need to consider the product distribution, the ratio of one product to another. How much of one product we get in relation to other products can be determined from energetic considerations. Their percentages after the synthesis is quite important due to determination of S to R racemization ratio, hence the stereoselectivity of the reaction.

In the previous studies the product distribution of S/R ratio of M4 (R_1: -CH_3 and X: -Br) is calculated to be 88/12 according to the Boltzmann distribution function, which is in very good agreement with the reported experimental ratio [27]. (S/R:86/14) In this study in addition to calculating S/R ratios, we determined the product distributions of four isomers (SP:RP:SM:RM) separately for M3 (R_1: benzyl and X: -Br) and M6 (R_1: isobutyl and X: -Br) and compared with the experimental data. The calculation consists of two steps.

According to the work of Haşlak [27] before the cyclization, an intermediate named 6S is formed and it is shown in Figure 1.11. 6S can be in two forms; 6S-1 and 6S-2, they can convert to each other via free rotation through N_{sp2}-C_{aryl} single bond and their only difference is the orientation of X (-Br) shown in Figure 4.21. After this step, cyclization occurs by the attack of negatively charged nitrogen to the carbonyl. 6S-1 gives P and 6S-2 gives M atropisomers based on the direction of Br. After the cyclization rotation through an axis is limited because of newly cyclized ring strain (hindered rotation), their barriers are calculated in Part I in this study.

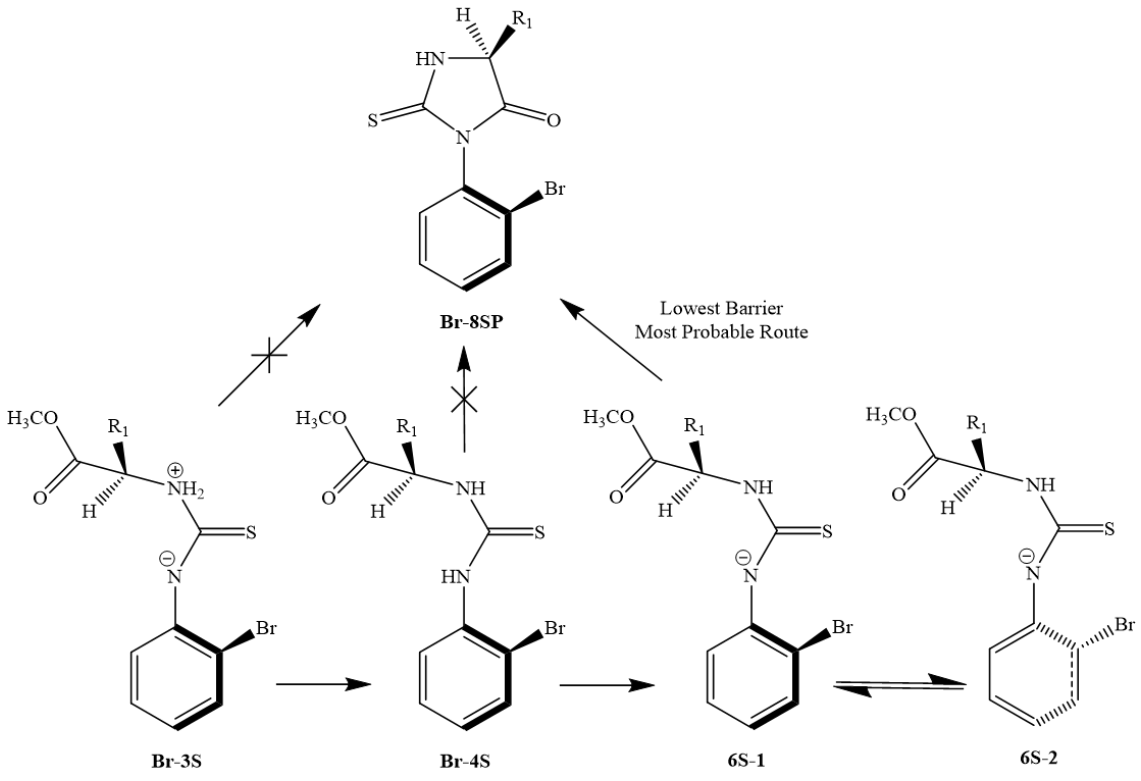

Figure 4.21. Cyclization route of the thiohydantoin molecule.

It is important to determine the percentages of 6S-1 and 6S-2 because their ratios will also determine the percentages of P and M isomers after the cyclization step.

We determine the percentages of the 6S-1 and the 6S-2 structures for M3 (R_1: benzyl and X: -Br) (Table 4.10.) and M6 (R_1: isobutyl and X: -Br). In order to demonstrate the calculation steps for M3, Boltzman equation (kT is 0.59 kcal/mol, M06-2X/6-311+G** / Temperature = 298 K / Solvent = DCM) is given as:

$$\begin{aligned} \%N_{M3-6S-2} &= \frac{e^{-\frac{\Delta G_{(2-1)}}{kT}}}{e^{-\frac{\Delta G_{(1-1)}}{kT}} + e^{-\frac{\Delta G_{(2-1)}}{kT}}} \times 100 \\ \%N_{M3-6S-2} &= \frac{e^{-\frac{0.37}{0.59}}}{1 + e^{-\frac{0.37}{0.59}}} \times 100 = 35 \\ \%N_{M3-6S-1} &= 100 - \%N_{M3-6S-2} = 65. \end{aligned} \tag{4.1}$$

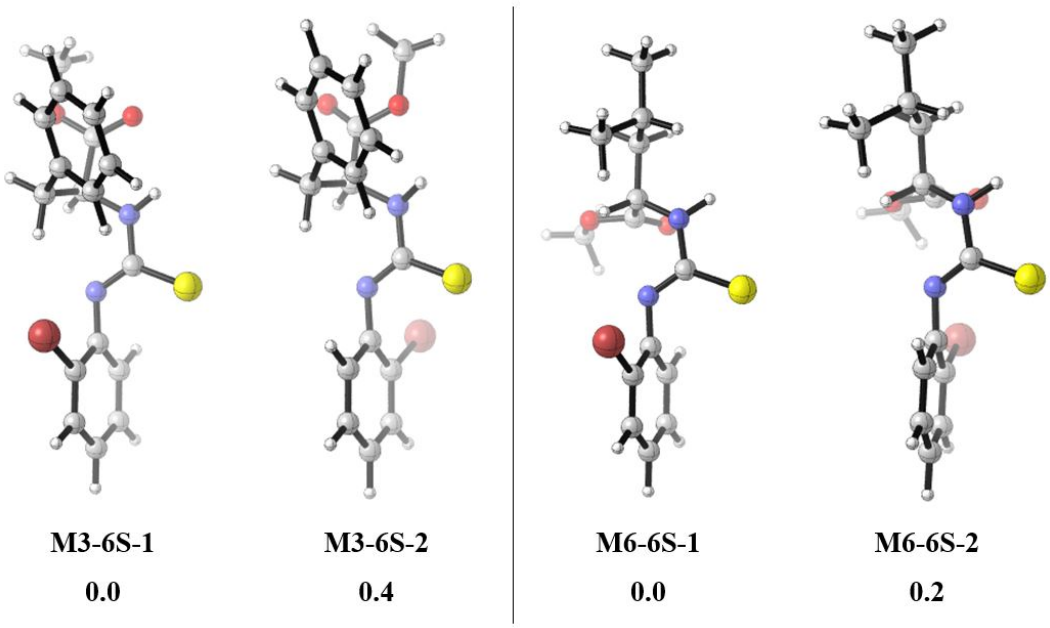

Figure 4.22. 3D structures of 6S-1 and 6S-2 conformers of M3 and M6. (M06-2X/6-311+G** / Temperature = 298 K / Solvent = DCM)

3D structures of 6S-1 and 6S-2 conformers of M3 (R_1: benzyl and X: -Br) and M6 (R_1: isobutyl and X: -Br), and their relative Gibbs Free Energies are shown in Figure 4.22.

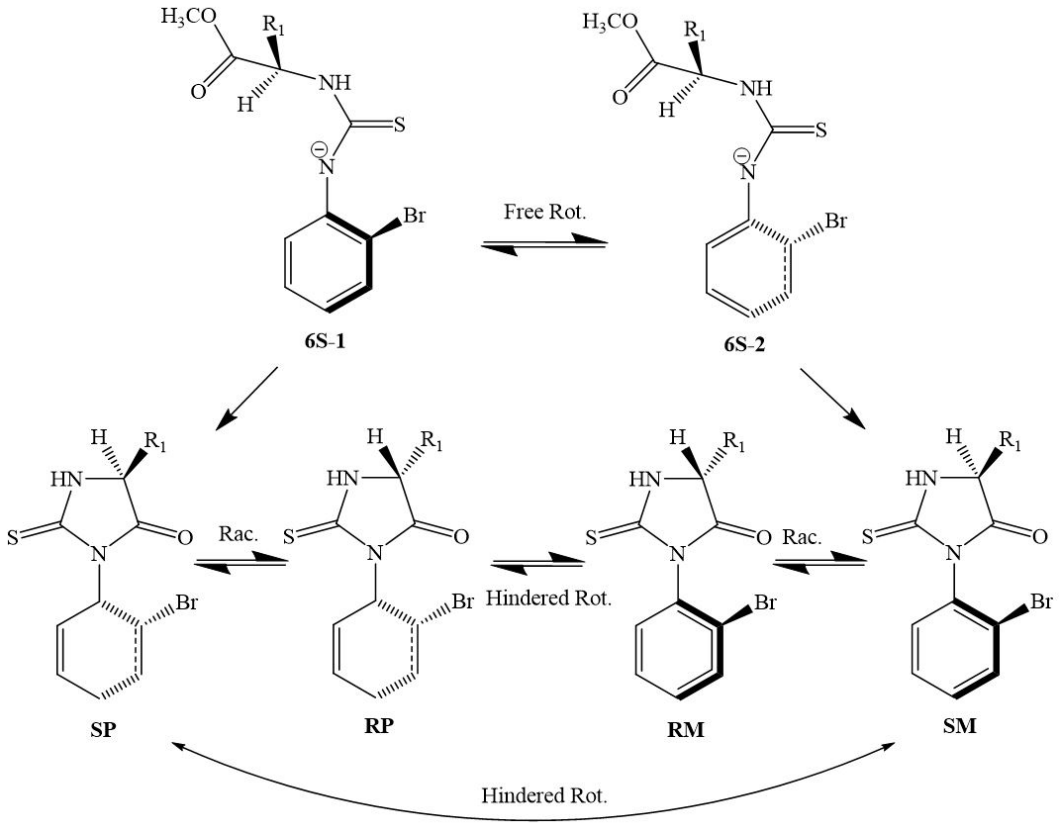

Figure 4.23. Possible reaction mechanisms during and after the thiohydantoin synthesis.

As seen in Figure 4.23. after the cyclization, four different types of cyclized thiohydantoin isomers are formed:

- 6S-1 gives SP isomer and racemization occurs to give RP in the presence of TEA with a low barrier at 298 K. (Figure 1.14.)
- 6S-2 gives SM isomer and racemization occurs to give RM in the presence of TEA at 298 K.

We rule out the possible interconversions of SP $\leftrightarrow$ SM and RP $\leftrightarrow$ RM because of the higher barriers of rotation determined in PART I.

3D structures of SP, RP, SM and RM for M3 and M6 are shown in Figure 4.24.

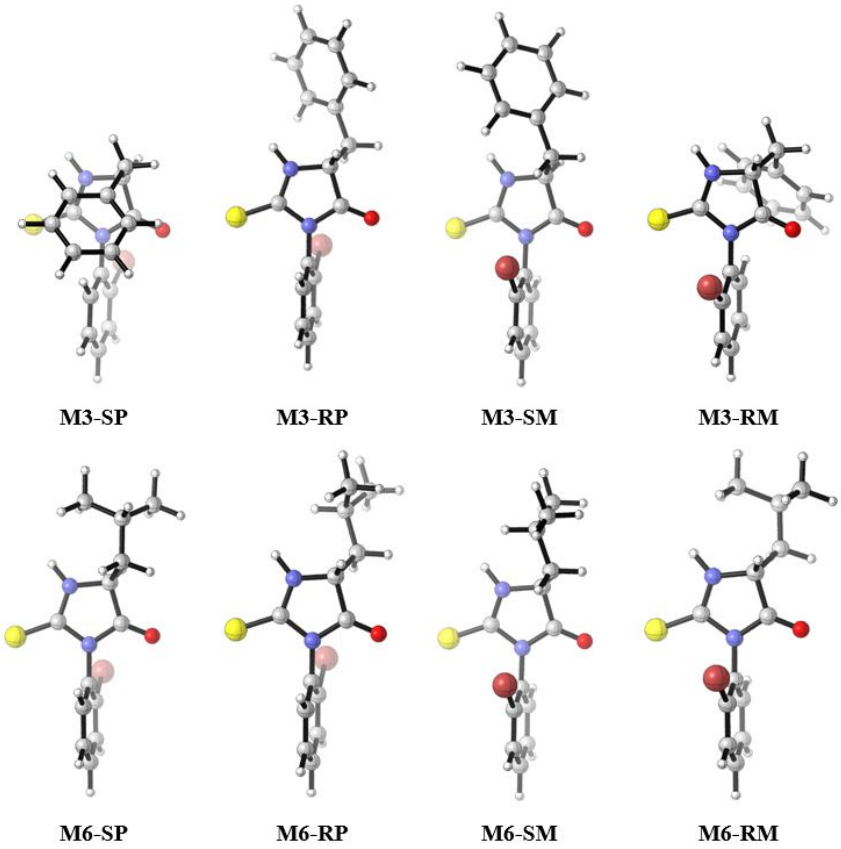

Figure 4.24. 3D structures of thiohydantoin isomers of M3 and M6.

Table 4.10. Calculated S/R percentages of thiohydantoin derviatives for M3. (M06-2X/6-311+G** / Temperature = 298 K / Solvent = DCM)

Molecule Name	**Relative Gibbs Free Energies (kcal/mol)**	**%**
M3-SP (M3-RM)	0.0	75
M3-RP (M3-SM)	0.7	25

Since P (M) atropisomers consist of SP (RM) and RP (SM), their percentages are determined by their relative Gibbs free energies (kcal/mol) shown in Table 4.10. Now, the last step is to combine all the results. For that purpose we multiply the result that comes from 6S product distributions and percentages of cyclized ring structures shown in Equation (4.2):

$$\begin{aligned} \%SP_{final} &= \%SP \times \frac{\%P}{100} = 49 \\ \%RP_{final} &= \%RP \times \frac{\%P}{100} = 16 \\ \%SM_{final} &= \%SM \times \frac{\%M}{100} = 9 \\ \%RM_{final} &= \%RM \times \frac{\%M}{100} = 26. \end{aligned} \tag{4.2}$$

The calculated results show that both for M3 and M6, the RM isomer is more stable than RP and gives higher product ratio compared to experimental data as shown in Table 4.11.

Table 4.11. Experimental vs calculated product distributions of M3 (R_1: benzyl and X: -Br) and M6 (R_1: benzyl and X: -Br). (M06-2X/6-311+G** / Temperature = 298 K / Solvent = DCM)

	Exp. (SP:RP:SM:RM) [14]	**Comp. (SP:RP:SM:RM)**
M3	51:41:2:6 (S:R → 53:47)	49:16:9:26 (S:R → 58:42)
M6	49:40:3:8 (S:R → 52:48)	37:21:15:27 (S:R → 52:48)

In RM, R_1 and X substituents are transoid to each other and this may decrease the steric effect and cause the stability compared to RP where these substituents are on the same side with each other. M3-RP is the most stable conformer, where the benzyl group does not prefer to interact with the bromide. Also in the case where R_1 is isobutyl, M6-RP is the most stable conformer, indicating that methyl groups tend to stay away from the bromide group. This shows that, steric effects are more significant than the electronic interaction between R_1 and X substituents. (π-π interaction between the benzyl and the aryl ring for M3, favorable interaction between the bromide and hydrogens of the methyl groups for M6)

According to our calculations, relative Gibbs free energies (kcal/mol) of the thiohydantoin isomers can be used for the determination of product distributions (thermodynamic control). If the reactions are controlled kinetically, barriers of rotation can be taken into consideration with the racemization barriers. Even though rotation is hindered, it can still occur and this interconversion between the isomers may effect the calculation of the percentages. Also the difference between the RM and RP ratios in experimental and calculated results can be explained by conducting calculations with the racemization barriers (kinetic control) for further studies.

4.4. PART IV: Sterically Controlled Aldol Reactions of Thiohydantoins with Benzaldehyde

In the work of Sarigul et al. [32] it was found that, after purification of the crude product by simple recrystallization, the R amino acid ester yields thiohydantoins having only M axial chirality since they are transoid to each other, on the other hand the S amino acid ester forms the P isomers solely with *ortho*-trifluoromethylphenyl isothiocyanate shown in Figure 4.25.

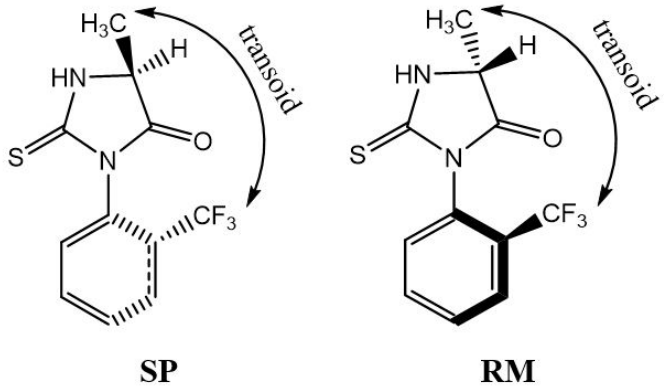

Figure 4.25. Transoid configurations of R_1 and X for thiohydantoin derivatives.

This result has encouraged them of performing sterically controlled aldol reactions starting from M and P thiohydantoin atropisomers, reactions of M13-M (R_1: -CH_3 and X: -CF_3) are shown in Figure 4.26. and 4.27.

The aldol reactions were performed with thiohydantoin derivatives of M13 (R_1: -CH_3 and X: -CF_3) or M9 (R_1: -CH_3 and X: -Cl) and benzaldehyde at -78^{0}C (195 K) with LDA as a strong base catalyst. In the first step referred to as reaction 1 in Figure 4.26., the hydrogen at C_5 is captured by lithium diisopropylamide (LDA) and Li attaches to carbonyl oxygen of the thiohydantoin ring to generate an enolate (M13-R1-Enolate-M). In the second step referred to as reaction 2, when the attack of the enolate to benzaldehyde occurs from the less hindered side (Re-face) by face shielding of the *ortho*-trifluoromethyl group of intermediate enolates, M13-RMR*-with Li and M13-RMS*-with Li stereoisomers can form as the major isomers.

For the minor isomers, M13-SMS* -with Li and M13-SMR* -with Li can form if the attack to benzaldehyde occurs from the more hindered side (Si-face).

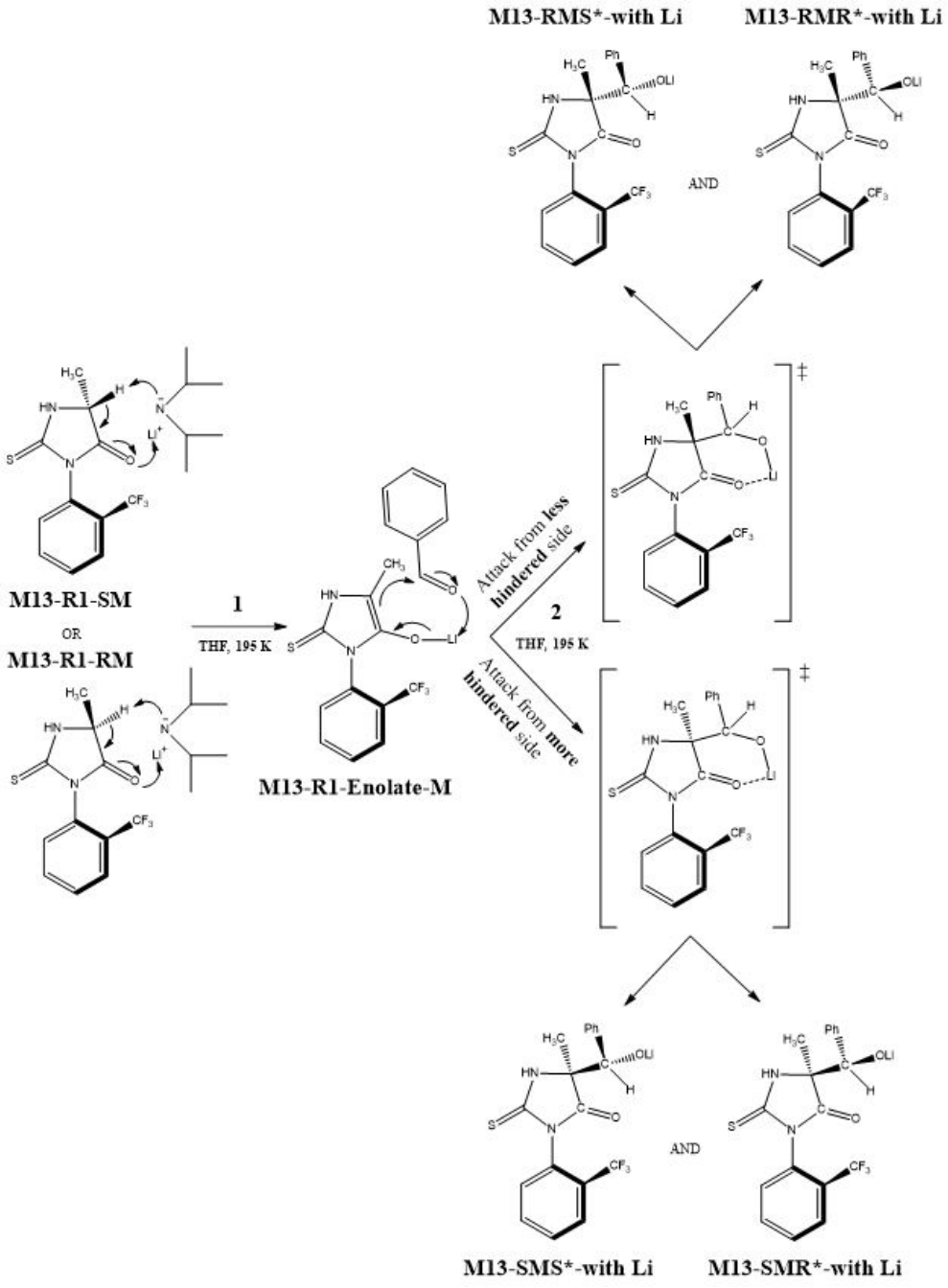

Figure 4.26. Enolization and aldol formation mechanisms.

In the last step referred to as reaction 3 in Figure 4.27.(M13-RMS*-with Li is used as an example), quenching mechanism, with the presence of NH_4Cl, leads to the formation of stable aldol isomers by the protonation of the product. Ammonium ion captures Li atom attached to the oxygen and gives hydrogen back to the same oxygen molecule and M13-RMS* is formed as the final product.

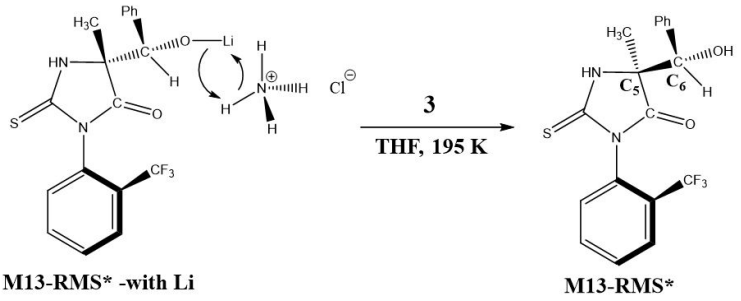

Figure 4.27. Quenching mechanism of the aldol product M13-RMS*.

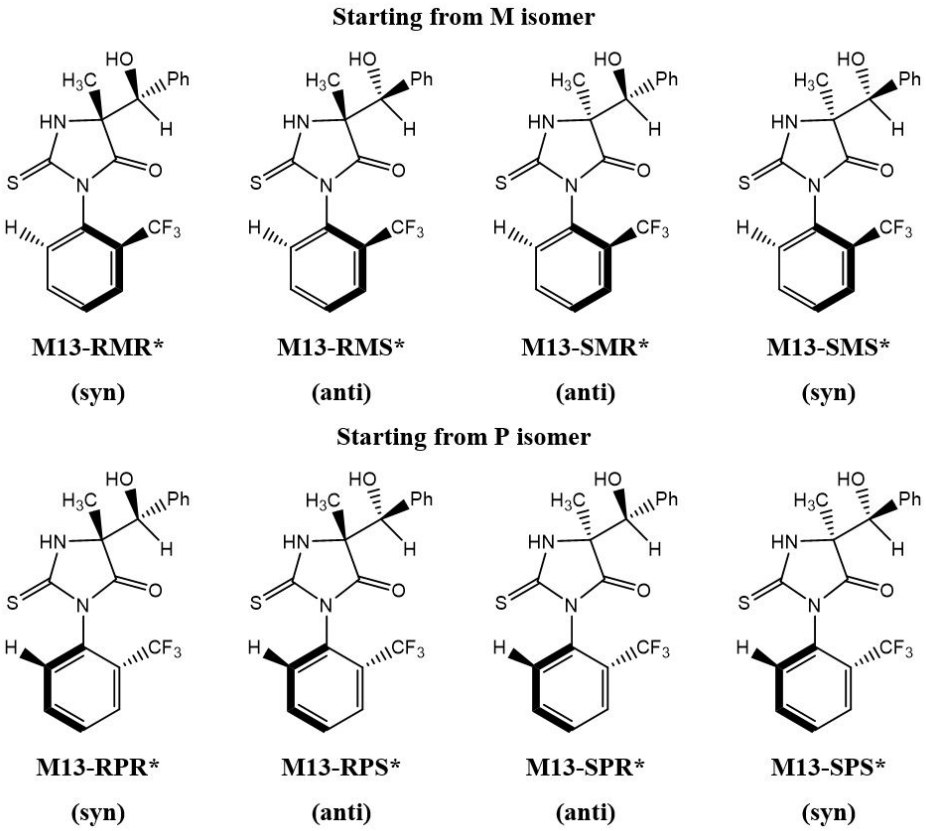

Figure 4.28. Eight different isomeric forms of M13 aldols.

As shown in Figure 4.26. aldol products have a chiral centre at C_5 of the heterocyclic ring, the chiral axis between $N_{sp2} - C_{aryl}$ bond, and the newly formed chiral centre at C_6 which is denoted by *.There can be 8 different isomeric forms of aldols: M13-RMR*, M13-RMS*, M13-SMS*, M13-SMR*, M13-RPR*, M13-RPS*, M13-SPS*, and M13-SPR* as shown in Figure 4.28.

M13-RMS* molecule as the final product, reaction 1 and reaction 2 mechanisms are modelled by DFT methods (M06-2X/6-311+G** / iefpcm / Temperature: 195 K / Solvent: THF) and the energy profile of the reactions are shown in Figure 4.29. and Figure 4.31.

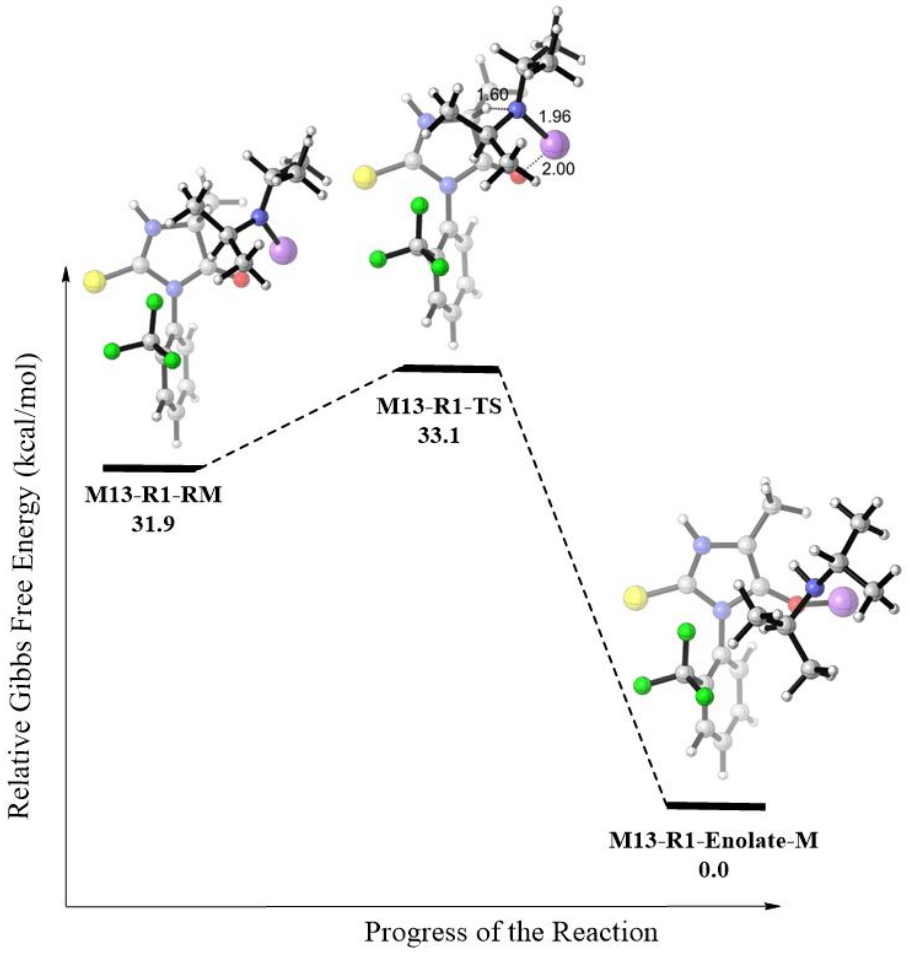

Figure 4.29. Energy profile enolate formation.

Calculated results for the reaction 1 show that, capturing hydrogen at C_5 requires a low barrier (1.2 kcal/mol) and the reaction leads to a stable enolate compound.

The axial chirality, starting with a mixture of RM and SM isomers (or SP and RP) would be equivalent to starting with 100 M (or P) isomer (no rotation is observed). This means that, reaction 1 does not contribute to the selectivity of the aldol reactions since reactants SM and RM both will give the enolate-M as the product. The S and R chiral centers are lost after the enolate formation and now the C_5 is planar, P and M axial chirality obtained from S and R alanine, respectively, will persist and control the face selectivity of enolate during the aldol reactions (reaction 2) by the presence of the *ortho*-substituent shown in Figure 4.31. [32].

The reason for choosing *ortho*-trifluoromethylphenyl and *ortho*-chlorophenyl thiohydantoin derivatives as a reactant in aldol reactions is their high rotational barriers even at high temperatures (333 K), as shown in Table 4.3. In order to further verify that the atropisomerism is conserved throughout the aldol reaction conditions, we calculated the rotation barriers of M13-M for SM, RM and enolate forms (Figure 4.30.) and the results are shown in Table 4.12.

Table 4.12. Rotational barriers (kcal/mol) of the thiohydantoin derivatives and the enolate molecule for M13-M in THF. (M06-2X/6-311+G** / Temperature = 195 K)

	Oxygen Side	**Sulfur Side**
M13-R1-SM to M13-R1-SP	29.9	37.3
M13-R1-Enolate-M to M13-R1 -Enolate-P	30.1	37.7
M13-R1-RM to M13-R1-RP	29.5	36.8

Rotation requires high barriers for SM, RM and enolate and it happens from the oxygen side rather than the sulfur side. This is due to oxygen's smaller size compared to sulfur, making the steric effect less significant and decreasing the barriers.

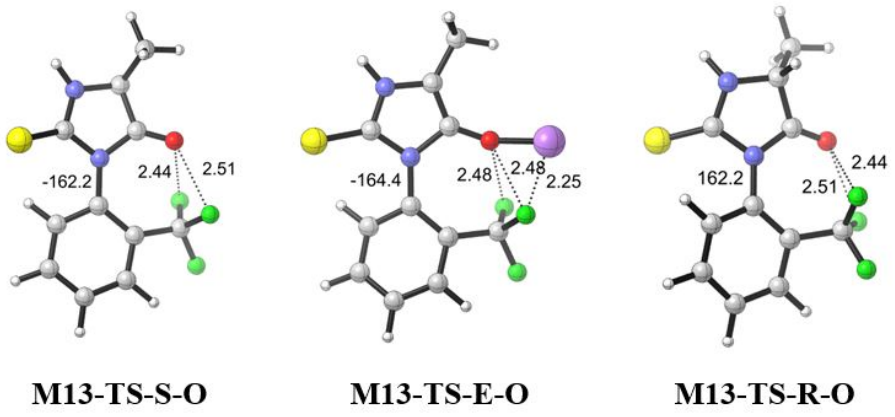

Figure 4.30. Rotational transition state structures of M13 enolate and thiohydantoin molecules.

In PART I (Table 4.2.) the difference between the O-side and the S-side barriers is around 5 kcal/mol and the *ortho*-substituent is -CH_3. In aldol reaction conditions where the *ortho*-substituent is -CF_3, the difference increased to 7 kcal/mol (Table 4.12.), the increase of size of the *ortho*-substituent further increased the difference between the O-side and the S-side barriers, favoring rotation via O.

For the enolate rotation, carbonyl oxygen is replaced with O-Li, however this change does not affect the barriers. As shown in Figure 4.30. , the distance between the carbonyl oxygen and F's does not change and this may the reason for similar rotation barriers of the thiohydantoin and the enolate molecules (Li does not affect the barrier).

Along the synthesis starting with R-alanine, SM and RM isomers will be formed but no rotation will occur, only the M enolate will be obtained. After that, also the M-enolate does not rotate through the $N_{sp2} - C_{aryl}$ rotation axis (3D structures of rotation in THF are in APPENDIX A). This is why with only one type of axially chiral form, four isomeric aldol products are obtained instead of eight as displayed in Figure 4.26.

The new C_5 chiral centre will be selectively formed by the nucleophilic attack of the enolate to the benzaldehyde (reaction 2), as shown in Figure 4.31. The stereoselectivity of the reaction depends on the shielding effect of the *ortho*-substituent (X: -CF_3 for M13 and X: -Cl for M9) of the enolate intermediate.

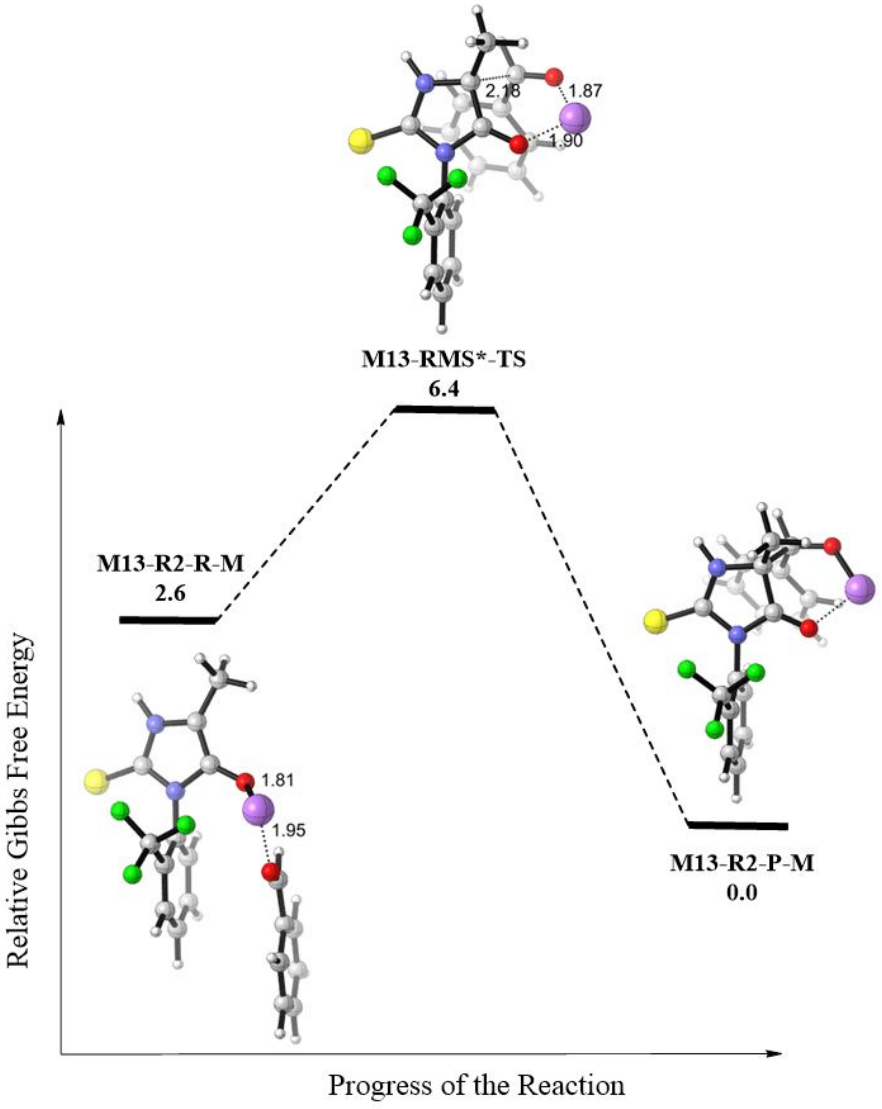

Figure 4.31. Energy profile (kcal/mol) of aldol formation.

In the experimental studies of aldol formation reactions, Sarıgül et al. come into conclusion that; for the M atropisomers the *ortho*-substituent shields the Si face of the intermediate enolate, the attack to benzaldehyde would occur mainly from the less hindered side which is the Re face of the intermediate enolate. Thus, two diastereomers RMR* and RMS* can be obtained from the M isomers substantially. Vice versa, in the case of P isomers SPR* and SPS* will be major products . Experimental S/R ratios are given in Table 4.13. For the experimental result, the ratio was obtained from the integration of the singlets observed for the hydrogen at the benzylic carbon around 5 ppm in 1H NMR spectrum taken in $CDCl_3$ after the reaction without any purification [32].

Table 4.13. Experimental S/R and syn:anti ratios of M9 and M13.

Molecule Name	**R_1**	**X**	**S:R**	**syn:anti**
M13-M	-CH_3	-CF_3	20:80	-
M13-P	-CH_3	-CF_3	63:37	-
M9-P	-CH_3	-Cl	77:23	10:90

In the last step referred to as reaction 3 in Figure 4.27. (M13-RMS-with Li is used as an example), the presence of NH_4Cl leads to the formation of stable aldol isomers by the protonation of the product and it is called quenching. At the end, four different forms of aldol isomers RMR*, RMS*, SMS* and SMR* are formed. This step has no influence of the selectivity of the aldol formation reactions as well, since only Li attached to oxygen at C_6 is replaced with H.

In order to verify the experimental product distributions of aldol isomers, aldol formation mechanism shown in Figure 4.26. (reaction 2) was modelled. These reactions may be thermodynamically or kinetically controlled, because of this reason calculations were done using two different strategies in order to determine final product distributions of aldol isomers and further verify the experimental data.

When the reaction is thermodynamically controlled, the relative stabilities of the products determines the final product distributions, in this case thermal stabilities of the four aldol isomers.

For this purpose, relative Gibbs Free energies (kcal/mol) of the products are determined and used to calculate the product ratios by the Boltzman Equation shown in Equation (4.3) (kT is 0.39 kcal/mol, at 195 K):

$$\begin{aligned} \%N_1 &= \frac{e^{-\frac{\Delta G_{(1-1)}}{kT}}}{N_1+N_2+N_3+N_4} \times 100 \qquad \%N_2 = \frac{e^{-\frac{\Delta G_{(2-1)}}{kT}}}{N_1+N_2+N_3+N_4} \times 100 \\ \%N_3 &= \frac{e^{-\frac{\Delta G_{(3-1)}}{kT}}}{N_1+N_2+N_3+N_4} \times 100 \qquad \%N_4 = \frac{e^{-\frac{\Delta G_{(4-1)}}{kT}}}{N_1+N_2+N_3+N_4} \times 100 \end{aligned} \tag{4.3}$$

where $N_1+N_2+N_3+N_4 = e^{-\frac{[\Delta G_{1-1}+\Delta G_{2-1}+\Delta G_{3-1}+\Delta G_{4-1}]}{kT}}$.

In order to determine the most accurate functional and solvent model, a benchmark calculation was done for M13-M (R_1: -CH_3 and X: -CF_3) and compared with the experimental results, shown in Table 4.14.

Reactions occur in THF and H-NMR measurements to determine the final product ratios were done in $CDCl_3$. No remarkable difference were observed in different conditions, M13-RMR* and M13-RMS* isomers formed as major products.

Table 4.14. Benchmark calculation for the comparison of experimental and calculated product ratios for M13 (R_1: -CH_3 and X: -CF_3) (thermodynamic control).

Methodology	**SMS*: SMR*: RMR*: RMS***	**syn : anti**
Experimental	20:80 (SMS*+SMR*):(RMR*+RMS*)	-
B3LYP/6- 311+G**		
iefpcm,THF	4 : 96 (3 : 1 : 3 : 93)	6 : 94
smd,THF	21 : 79 (19 : 2 : 12 : 67)	31 : 69
iefpcm,$CHCl_3$	9 : 91 (8 : 1 : 5 : 87)	13 : 88
smd,$CHCl_3$	11 : 89 (10 : 1 : 7 : 82)	17 : 83
M06-2X/6- 311+G**		
iefpcm,THF	1 : 99 (1 : 1 : 30 : 69)	31 : 70
smd,THF	13 : 87 (3 : 10 : 23 : 64)	26 : 74
iefpcm,$CHCl_3$	2 : 98 (1 : 1 : 30 : 67)	31 : 68
smd,$CHCl_3$	5:95 (2 : 3 : 12 : 83)	14 : 86

Since all the previous calculations were done with the M06-2X/6-311+G** methodology and the iefpcm solvent model, the same methodology was used for aldol reactions of other molecules (M13 (R_1: -CH_3 and X:-CF_3) and M9 (R_1: -CH_3 and X: -Cl), starting with P isomer) as shown in Table 4.15.

It was observed that experimental and calculated results are in a good agreement with each other. Different than the experimental data, for the calculated results we observed higher face selectivity by the *ortho*-substituents for the M (M13-M) and P (M13-P and M9-P) atropisomers.

Table 4.15. Experimental and calculated (thermodynamic control) product ratios of the aldol for M13 and M9.

M13-M (R_1: -CH_3 and X: -CF_3)		
	SMS*: SMR*: RMR*: RMS*	**syn : anti**
Experimental	20:80 (SMS*+SMR*):(RMR*+RMS*)	-
Calculated	1 : 99 (1 : 1 : 30 : 69)	31 : 70
M13-P (R_1: -CH_3 and X: -CF_3)		
Experimental	63 : 37 (SPS*+SPR*):(RPR*+RPS*)	-
Calculated	99 : 1 (30 : 69 : 1 : 1)	31 : 70
M9-P (R_1: -CH_3 and X: -Cl)		
Experimental	77 : 23 (SPS*+SPR*):(RPR*+RPS*)	10 : 90
Calculated	96 : 4 (21 : 75 : 3 : 1)	24 : 76

For all the cases, products formed by the attack of the enolate to benzaldehyde from the more hindered side have higher energies due to the steric hinderence between substituents at C_6 and the *ortho-* substituents. For M13-RMR*, the benzyl group interacts with the hydrogen at the aryl ring, and for the M9-RPR* benzyl group interacts with chloride *ortho*-substituent.

Because of the larger size of the -CF_3, the benzyl tends to be far from the aryl ring for the M13-RPR, and the interaction formed between the carbonyl oxygen and the -OH of the aldol lowers the energy and renders that conformer the most stable one. The same results were observed for M13-SMS*, M13-SPS* and M9-SPS*.

3D structures of aldol products and their relative Gibbs Free energies (kcal/mol) are given in Figure 4.32. (M06-2X/6-311+G** / iefpcm / Solvent = THF / Temperature = 195 K)

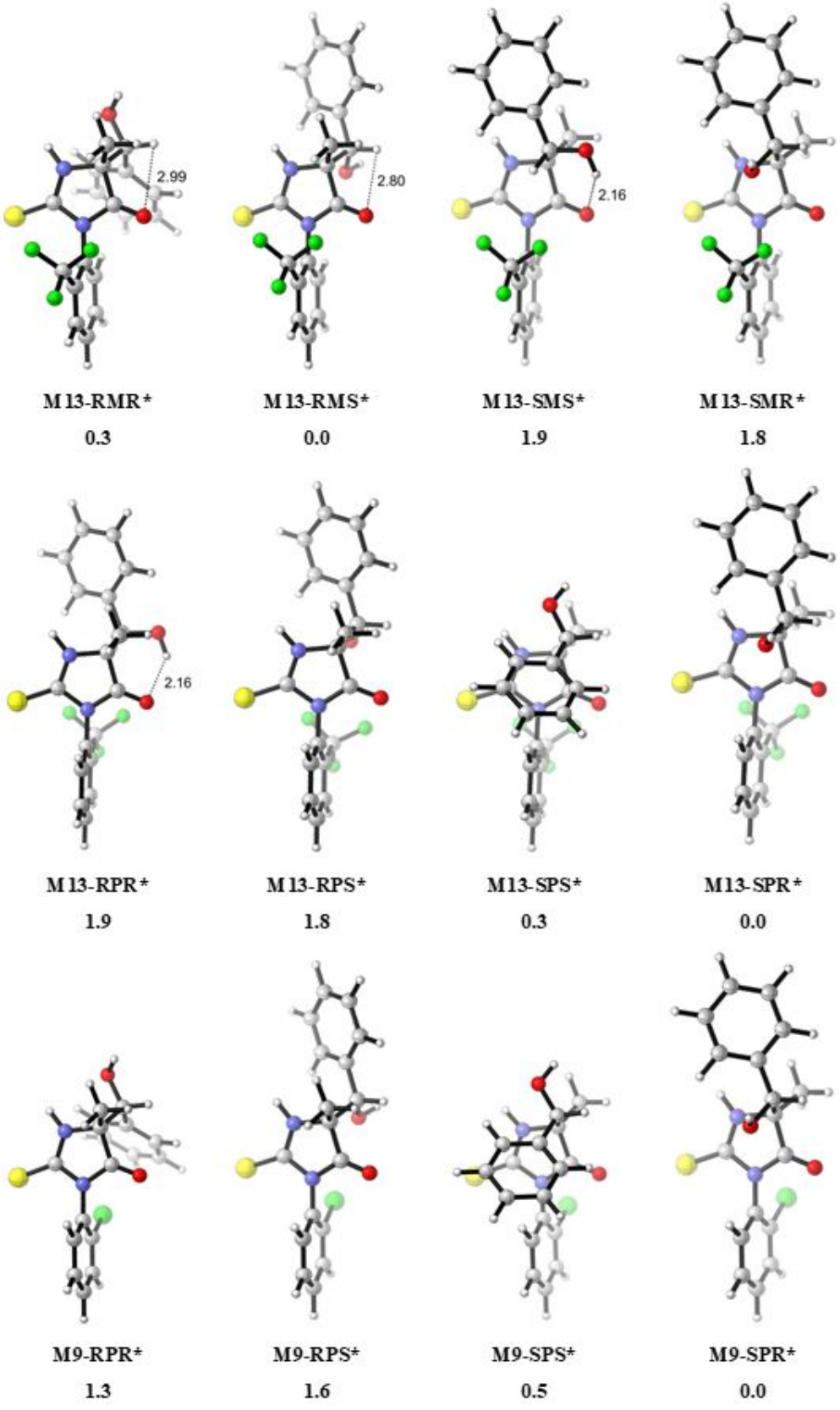

Figure 4.32. 3D Structures of the most stable conformers of aldol isomers and their relative Gibbs Free Energies (kcal/mol).

When the reaction is kinetically controlled, barriers of the reactions determine the final product distributions, in this case activation energies required for the formation of aldols by the reaction of thiohydantoins and benzaldehyde in a base catalyst (reaction 2). For this purpose, Boltzman Equation is again used the determine the product ratios and results are shown in Table 4.16. Different than the thermodynamic approach, activation barriers of reaction 2 are used instead of the thermal stabilities of the aldol producs for M13 (R_1: -CH_3 and X: -CF_3) and M9 (R_1: -CH_3 and X: -Cl).

Table 4.16. Experimental and calculated (kinetic control) product ratios of the aldol products. (M06-2X/6-311+G** / iefpcm / Temperature: 195 K / Solvent: THF)

M13-M (R_1: -CH_3 and X: -CF_3)		
	SMS*: SMR*: RMR*: RMS*	**syn : anti**
Experimental	20:80 (SMS*+SMR*):(RMR*+RMS*)	-
Calculated	40 : 60 (40 : 0 : 10 : 50)	50 : 50
M13-P (R_1: -CH_3 and X: -CF_3)		
Experimental	63 : 37 (SPS*+SPR*):(RPR*+RPS*)	-
Calculated	29 : 71 (5 : 24 : 71 : 0)	76 : 24
M9-P (R_1: -CH_3 and X: -Cl)		
Experimental	77 : 23 (SPS*+SPR*):(RPR*+RPS*)	10 : 90
Calculated	59 : 41 (3 : 56 : 41 : 0)	44 : 56

For the M13-M, attack of the enolate to the benzaldehyde (M13-M-R2-R) finally yields to four aldol products shown in Figure 4.32.

Activation energies required for the formation of these products and transition state structures are shown in Figure 4.33.(M06-2X/6-311+G** / iefpcm / Solvent = THF / Temperature=195 K)

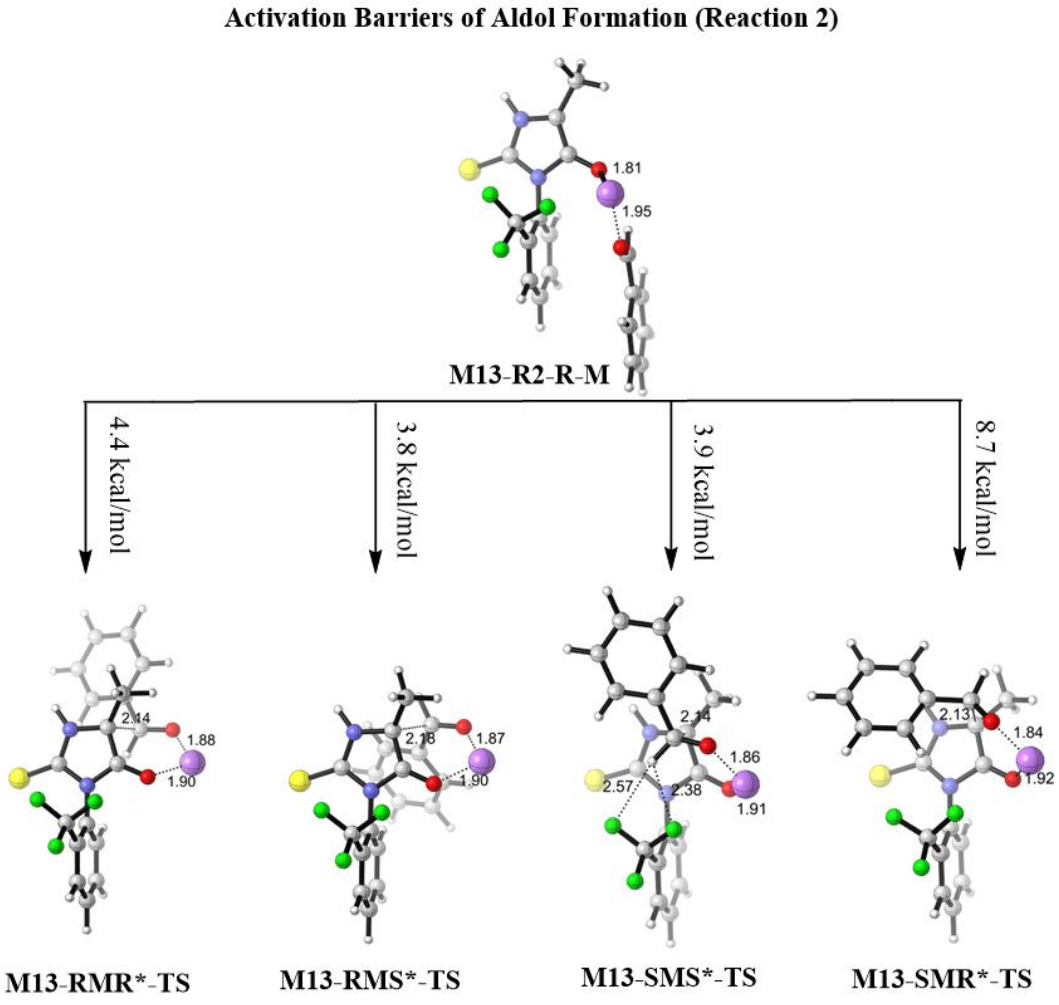

Figure 4.33. Transition state structures of aldol formation reactions for M13-M and their activation energies (kcal/mol). (M06-2X/6-311+G** / iefpcm / Temperature: 195 K / Solvent: THF)

For the transition state structures, we expected lower barriers during the formation of M13-RMR* and M13-RMS* products since substiuents at C_6 and X are transoid to each other referred as less hindered side. However in the case of M13-SMS*-TS, a more stable transition state structure was located as shown in Figure 4.33. and a higher product ratio was calculated for M13-SMS* isomer shown in Table 4.16.

This can be explained by the computational methodology (M06-2X) taking into consideration of the interaction between hydrogen attached to C_6 center and fluorides in -CF_3 group; making the transition state structure more stable than the others and lowering the barrier. Similar calculations have been carried out for the P atropisomeric form of M13 (R_1: -CH_3 and X: -CF_3) derivative given in Figure 4.34. (M06-2X/6-311+G** / iefpcm / Solvent = THF / Temperature=195 K)

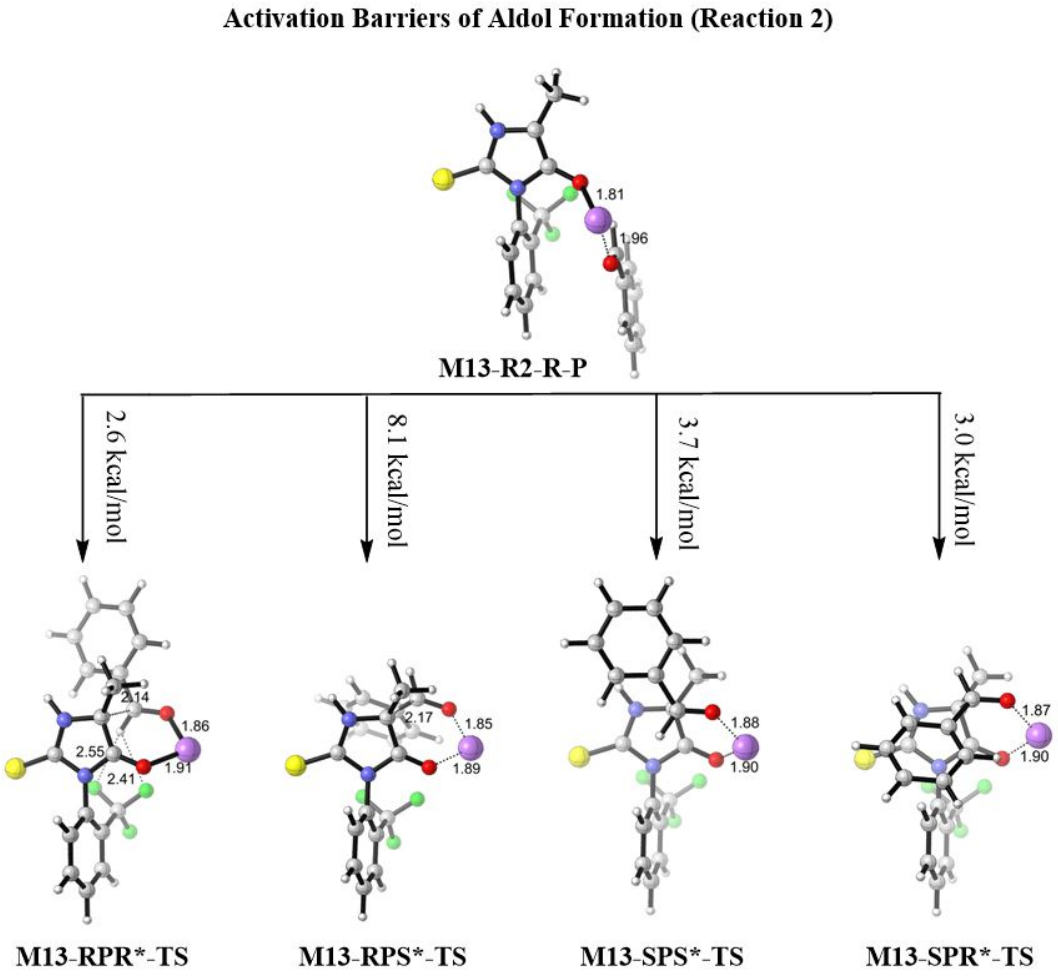

Figure 4.34. Transition state structures of aldol formation reactions for M13-P and their activation energies (kcal/mol). (M06-2X/6-311+G** / iefpcm / Temperature: 195 K / Solvent: THF)

For the transition state structures of M13-P, we expected lower barriers during the formation of M13-SPR* and M13-SPS* products since substituents at C_6 and X are transoid to each other referred as less hindered side.

However in the case of M13-RPR*-TS, a more stable transition state structure was located as shown in Figure 4.34. and a higher product ratio was calculated for M13-RPR* isomer shown in Table 4.16. This can be explained by the computational methodology (M06-2X) taking into consideration of the interaction between hydrogen attached to C_6 center and fluorides in -CF_3 group; making the transition state structure more stable than the others and lowering the barrier. For the final step, same calculations were done to P atropisomers of M9 (R_1: -CH_3 and X: -Cl) in order to observe the effect of the identity of the *ortho*-substituent on product distribution on aldol products. Barriers of aldol formation were similar to M13-P, eventhough the size of -CF_3 is larger than the chloride [45].

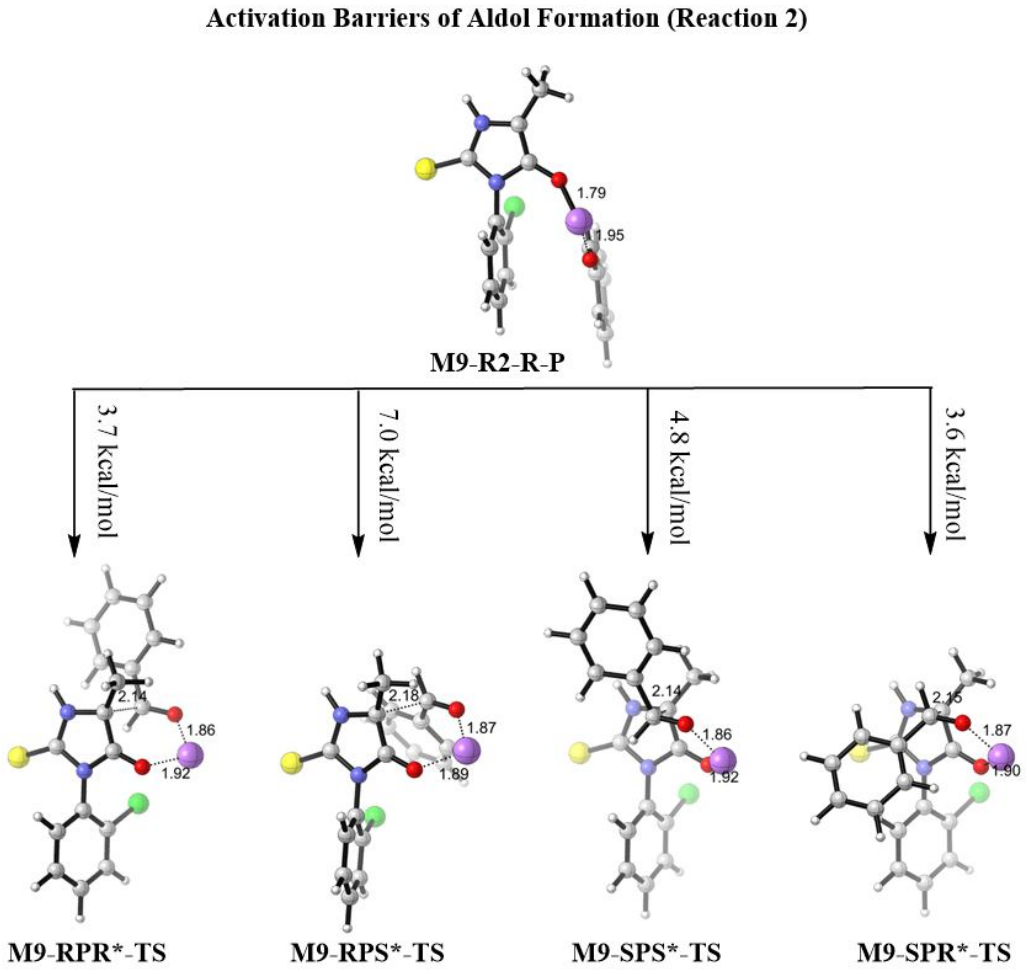

Figure 4.35. Transition state structures of aldol formation reactions for M9-P and their activation energies (kcal/mol). (M06-2X/6-311+G** / iefpcm / Temperature: 195 K / Solvent: THF)

This gives the conclusion that, the *ortho*-substituent on the aryl ring causes the face-selectivity during the aldol formation reactions regardless to the identity of the *ortho*-substituent which favores the less hindered side.

For the transition state structures, we expected low barriers during the formation of M9-SPR* and M9-SPS* products since substituents at C_6 and X are transoid to each other (less hindered side). However in the case of M9-RPR*-TS, a more stable transition state structure was located as shown in Figure 4.35. and a higher product ratio was calculated for M9-RPR* isomer shown in Table 4.16. This can be explained by the computational methodology (M06-2X) taking into consideration of the interaction between hydrogen attached to C_6 center and chlorine in *ortho*-aryl position; making the transition state structure more stable than the others and lowering the barrier. Different from the F—H interaction in M13-P (2.4 Å) , distance between H—Cl is longer (2.8 Å) and chloride is less electronegative than fluoride, because of these reasons this interaction is not very effective and does not lower the energy of M9-RPR*-TS structure as much as it lowers the energy of M13-RPR*-TS. Because of this reason M9-SPS*+M9-SPR* ratio is in a much better agreement with experimental data compared to computational results of M13-P (R_1: -CH_3 and X: -CF_3), confirming the assumption that starting with the P atropisomer gives the SPS* and the SPR* isomers as the major products.

In conclusion for this part, activation energies of aldol production (reaction 2) can not be used for the determination of final product distribution of aldol isomers. The barriers are low and do not effect the ratios significantly since they are highly achievable at 195 K. That is the reason why we do not observe similar results with experimental data when making the calculation with a kinetic approach.

5. CONCLUSION

In the first part of this study, it was determined that thiohydantoin isomers are converted to one another via rotation around the chiral axis, without racemization at C_5 in toluene, and the rotational barriers were determined by DFT methods (M06-2X/6-311+G**). It was observed that when the exo-cyclic sulfur and *o*-aryl groups are on same site, the larger size of sulfur introduces larger steric hinderance compared to oxygen, thus the aryl group tends to rotate from the carbonyl oxygen side. As observed experimentally, as the size of the *ortho*-substituent increases, higher barriers of rotation were observed. Having different functional groups at C_5 on the thiohydantoin ring such as simple alkyl (M1, M4, M8, M11, M5 and M6), alkoxy (M7) and aryl ring (M2 and M3) does not effect the rotational trends, as these groups are far from the rotation site which is the $N_{sp2} - C_{aryl}$ chiral axis.

Another outcome of this study is, when the *ortho*-substituent is a halogen, it causes repulsion between the carbonyl oxygen and the halogen atom because of the lone pairs around the halogen. Two ring structures can not be on the same plane and this distorts the dihedral angle being around 180^0. However, for the case when -CH_3 is the *ortho*-substituent, because of the favorable interaction of methyl hydrogens with the carbonyl oxygen, we observed dihedral angles closer to 180^0. The calculated activation barriers of rotation have been found to be around 3 kcal/mol higher than the experimental results for the M06-2X and B3LYP functional however, a linear correlation was obtained with the experimental data. Linear relation between the computational and experimental results gave the R^2 values of 0.85 for the SM to SP and 0.76 for the SP to SM conversion for the M06-2X functional. B3LYP functional gives better R^2 values of 0.96 for the SM to SP and SP to SM conversions and these correlations can be further used as a tool for predicting rotational barriers of thiohydantoin derivatives before the experimental procedures.

In the second part of this study, Gibbs free energies of racemization and rotation were calculated and it was found that racemization was a more probable mechanism compared to rotation due to the lower energy of activation in ethanol. Additionally, by comparing the experimental activation energies, it was confirmed that racemization occurred with the presence of two EtOH molecules instead of self tautemerization or one EtOH molecule assistance. The racemization barriers of M2, M3, M5 and M6 were in a good agreement with the experimental data, around 25 kcal/mol, and no remarkable effect was observed when R_1 or X is a different substituent.

In the third part of the study, the product ratios of thiohydantoin isomers after the synthesis were calculated in order to predict the percentages of the SP, SM, RP and RM isomers. The relative stabilies of 6S molecules (6S-1 giving P and 6S-2 giving M atropisomers), structures before the cyclization, were used to calculate the percentages of P and M isomers after the cyclization step. P atropisomers consist of SP and RP diastereomers and M atropisomers consist of SM and RM diastereomers, so their percentages were also determined by their relative Gibbs free energies (kcal/mol) with respect to each other, thermodynamic stabilities of SP-RP and SM-RM were taken into consideration to calculate S/R ratios in P and M atropisomers. The calculated results are in a good agreement with the experimental results in the case of total S/R ratios, however in the case of determination of four individual isomers, RM was found to be more stable than RP and gave higher product ratios.

In the last part of the study, in aldol reaction mechanisms, the calculations were done by M06-2X/6-311+G** methodology in THF and at 195 K, and were found to be in a good agreement with the experimental results. Atroposelectively controlled aldol reactions of the axially chiral thiohydantoin derivatives were carried out with benzaldehyde in the presence of LDA. Reactions started with only one type of axially chiral form, either M or P isomers, and the calculated rotational barriers have shown that rotation requires high barriers and atropisomerism does not change throughout the reaction. The chiral center is lost with the deprotonation by the base, and based on the high rotational barriers, axial chirality is conserved for the enolate form as well.

Due to presence of one kind of axialy chiral form, the reaction yielded four isomeric aldol products instead of eight. During the aldol reactions, the bulky *o*-trifluoromethyl and *o*-chloride groups protected one side of the molecule (refered as more hindered side) so the enolate attack to the aldehyde selectively took place from the less hindered side thus stereoselectivity was created by the bulky *ortho*-substituent. Because of the steric control of the bulky groups and face selectivity of the aldol reactions, P isomers yielded S configured aldol products as major products and for the M isomers R products were found to be in high majority. The diastereomeric ratios calculated using the thermodynamic stabilities of aldol products give better results compared to using the activation barriers for the determination of product distribution.

REFERENCES

1. Cho, S., S. H. Kim and D. Shin, "Recent Applications of Hydantoin and Thiohydantoin in Medicinal Chemistry", *European Journal of Medicinal Chemistry*, Vol. 164, pp. 517–545, 2019.

2. Ichitani, M., S. Kitoh, K. Tanaka, S. Fujinami, M. Suda, M. Honda, A. Kuwae, K. Hanai, K. Kunimoto *et al.*, "Synthesis and Crystal Structure of (S)-5-Isopropyl-5-methyl-2-thiohydantoin", *European Journal of Chemistry*, Vol. 4, pp. 350–352, 2013.

3. Kavitha, C., M. Nambiar, C. A. Kuma, B. Choudhary, K. Muniyappa, K. Rangappa and S. Raghavan, "Novel Derivatives of Spirohydantoin Induce Growth Inhibition Followed by Apoptosis in Leukemia Cells", *Biochemical Pharmacology*, Vol. 77(3), pp. 348–363, 2009.

4. Marton, J., J. Enisz, S. Hosztafi and T. Timar, "Preparation and Fungicidal Activity of 5-Substituted Hydantoins and their 2-Thio Analogs", *Journal of Agricultural and Food Chemistry*, Vol. 41(1), pp. 148–152, 1993.

5. El-Barbary, A. A., A. I. Khodair, E. B. Pedersen and C. Nielsen, "S-Glucosylated Hydantoins as New Antiviral Agents", *Journal of Medicinal Chemistry*, Vol. 37(1), pp. 73–77, 1994.

6. Metwally, M. A. and E. Abdel-Latif, "Thiohydantoins: Synthetic Strategies and Chemical Reactions", *Journal of Sulfur Chemistry*, Vol. 33(2), pp. 229–257, 2012.

7. Elhady, H., S. Mohamed, H. Al-Shareef and R. El-Mekawy, "Synthesis, Reactions, and Applications of 2-Thiohydantoin Derivatives", *Acta Poloniae Pharmaceutica*, Vol. 76, pp. 971–986, 2019.

8. Bonne, D. and J. Rodriguez, "A Bird's Eye View of Atropisomers Featuring a Five-

Membered Ring", *European Journal of Organic Chemistry*, Vol. 2018 (20-21), pp. 2417–2431, 2018.

9. Demir-Ordu, O. and I. Doğan, "Stereoselective Lithiation and Alkylation and Aldol Reactions of Chiral 5-Methyl-3-(*o*-aryl)-oxazolidinones", *Tetrahedron: Asymmetry*, Vol. 21(20), pp. 2455–2464, 2010.

10. Bonne, D. and J. Rodriguez, "Enantioselective Syntheses of Atropisomers Featuring a Five-membered Ring", *Chemical Communications*, Vol. 53(92), pp. 12385–12393, 2017.

11. Toenjes, S. T. and J. L. Gustafson, "Atropisomerism in Medicinal Chemistry: Challenges and Opportunities", *Future Medicinal Chemistry*, Vol. 10(4), pp. 409–422, 2018.

12. Oki, M., "Recent Advances in Atropisomerism", *Topics in Stereochemisty*, Vol. 14, pp. 1–81, 1983.

13. Bringmann, G., A. J. P. Mortimer, P. A. Keller, M. J. Gresser, J. Garner and M. Breuning, "Atroposelective Synthesis of Axially Chiral Biaryl Compounds", *Angewandte Chemie International Edition*, Vol. 44(33), pp. 5384—5427, 2005.

14. Arıca, O., 2016, *Hindered Rotation Versus Racemisation in Axially Chiral Thiohydantoin Derivatives*, Master's Thesis, Boğaziçi University.

15. Ding, W., P. Yu, Q. An, K. L. Bay, S. Xiang, S. Li, Y. Chen, K. Houk and B. Tan, "DFT-Guided Phosphoric-Acid-Catalyzed Atroposelective Arene Functionalization of Nitrosonaphthalene", *Chem*, Vol. 6(8), pp. 2046–2059, 2020.

16. Tampellini, N., P. Righi and G. Bencivenni, "Computational Investigation on the Origin of Atroposelectivity for the Cinchona Alkaloid Primary Amine-Catalyzed Vinylogous Desymmetrization of N-(2-*t*-Butylphenyl)maleimides", *The Journal of Organic Chemistry*, Vol. 86(17), pp. 11782—11793, 2021.

17. Shaaban, S., H. Li, F. Otte, C. Strohmann, A. P. Antonchick and H. Waldmann, "Enantioselective Synthesis of Five-Membered-Ring Atropisomers with a Chiral Rh(III) Complex", *Organic Letters*, Vol. 22(23), pp. 9199—9202, 2020.

18. Capozziello, S. and A. Lattanzi, "Geometrical Approach to Central Molecular Chirality: A Chirality Selection Rule", *Chirality*, Vol. 15(3), pp. 227—230, 2003.

19. Ballard, A., S. Narduolo, H. O. Ahmed, N. I. Keymer, N. Asaad, D. A. Cosgrove, N. J. Buurma and A. G. Leach, "Racemisation in Chemistry and Biology", *Chemistry*, Vol. 26(17), No. 17, pp. 3661—3687, 2020.

20. Chhabra, N., M. L. Aseri and D. Padmanabhan, "A Review of Drug Isomerism and its Significance", *International Journal of Applied and Basic Medical Research*, Vol. 3(1), pp. 16—18, 2013.

21. Wang, Z. D., S. O. Sheikh and Y. Zhang, "A Simple Synthesis of 2-Thiohydantoins", *Molecules*, Vol. 11(10), pp. 739—750, 2006.

22. Sarigul, S. and I. Dogan, "Atroposelective Synthesis of Axially Chiral Thiohydantoin Derivatives", *The Journal of Organic Chemistry*, Vol. 81(14), pp. 5895—5902, 2016.

23. Khatik, G. L., J. Kaur, V. Kumar, K. Tikoo, P. Venugopalan and V. A. Nair, "Aldol Derivatives of Thioxoimidazolidinones as Potential Anti-prostate Cancer Agents", *European Journal of Medicinal Chemistry*, Vol. 46(8), pp. 3291—3301, 2011.

24. Hughes, A. D., D. A. Price, O. Shishkin and N. S. Simpkins, "Diastereoselective Enolate Chemistry Using Atropisomeric Amides", *Tetrahedron Letters*, Vol. 37(42), pp. 7607—7610, 1996.

25. Heravi, M. M., V. Zadsirjan, M. Dehghani and N. Hosseintash, "Current Applications of Organocatalysts in Asymmetric Aldol Reactions: An Update", *Tetrahe-*

dron: Asymmetry, Vol. 28(5), pp. 587—707, 2017.

26. Perrin, C. L. and K. Chang, "The Complete Mechanism of an Aldol Condensation", *The Journal of Organic Chemistry*, Vol. 81(13), pp. 5631—5635, 2016.

27. Haslak, Z. P., S. A. Cinar, S. S. Ozbek, G. Monard, I. Dogan and V. Aviyente, "Elucidation of the Atroposelectivity in the Synthesis of Axially Chiral Thiohydantoin Derivatives", *Organic Biomolecular Chemistry*, Vol. 18(12), pp. 2233–2241, 2020.

28. Heravi, M. M., M. Dehghani and V. Zadsirjan, "Rh-catalyzed Asymmetric 1,4-Addition Reactions to a,b-Unsaturated Carbonyl and Related Compounds: An Update", *Tetrahedron: Asymmetry*, Vol. 27, pp. 513—588, 2016.

29. Ariens, E., "Special Article Stereochemistry , a Basis for Sophisticated Nonsense in Pharmacokinetics and Clinical Pharmacology", *European Journal of Clinical Pharmacology*, Vol. 26, p. 663–668, 1984.

30. Reist, M., B. Testa and P. A. Carrupt, 2003, *Drug Racemization and Its Significance in Pharmaceutical Research*, Springer, Berlin.

31. Ballard, A., H. O. Ahmad, S. Narduolo, L. Rosa, N. Chand, D. A. Cosgrove, P. Varkonyi, N. Asaad, S. Tomasi, N. J. Buurma and A. G. Leach, "A Quantitative Approach to Predicting Rate Constants for Aqueous Racemization Allows Pointless Stereoselective Syntheses to be Avoided", *Angewandte Chemie International Edition*, Vol. 57(4), pp. 982—985, 2017.

32. Ozbek, S. S., M. B. Erdik and I. Dogan, "Aldol Reactions of Conformationally Stable Axially Chiral Thiohydantoin Derivatives", *ACS Omega*, Vol. 6(42), pp. 27823—27832, 2021.

33. Jones, R. O., "Density Functional Theory: Its Origins, Rise to Prominence, and Future", *Reviews Of Modern Physics*, Vol. 87(3), pp. 897—923, 2015.

34. Burke, K., "Perspective on Density Functional Theory", *The Journal of Chemical Physics*, Vol. 136, p. 150901, 2012.

35. Yildirim, A., F. A. S. Konuklar, S. Catak, V. V. Speybroeck, M. Waroquier, I. Dogan and V. Aviyente, "Solvent-Catalyzed Ring–Chain–Ring Tautomerization in Axially Chiral Compounds", *Chemistry—A European Journal*, Vol. 18(40), pp. 12725—12732, 2012.

36. Sarangi, R., M. L. Vidal, S. Coriani and A. I. Krylov, "On the Basis Set Selection for Calculations of Core-level States: Different Strategies to Balance Cost and Accuracy", *Molecular Physics*, Vol. 118, 2020.

37. Jensen, F., "Atomic Orbital Basis Sets", *Wiley Interdisciplinary Reviews: Computational Molecular Science*, Vol. 3, 20132.

38. Wodrich, M. D., C. Corminboeuf and P. R. Schleyer, "Systematic Errors in Computed Alkane Energies Using B3LYP and Other Popular DFT Functionals", *Organic Letters*, Vol. 8(17), p. 3631–3634, 2006.

39. Cantillo, D. and C. O. Kappe, "A Unified Mechanistic View on the Morita-Baylis-Hillman Reaction: Computational and Experimental Investigations", *The Journal of Organic Chemistry*, Vol. 75(24), pp. 8615—8626, 2010.

40. Walker, M., A. J. A. Harvey, A. Sen and C. E. H. Dessent, "Performance of M06, M06-2X, and M06-HF Density Functionals for Conformationally Flexible Anionic Clusters: M06 Functionals Perform Better than B3LYP for a Model System with Dispersion and Ionic Hydrogen-Bonding Interactions", *The Journal of Physical Chemistry*, Vol. 117(47), pp. 12590—12600, 2013.

41. Zhao, Y. and D. G. Truhlar, "Density Functionals with Broad Applicability in Chemistry", *Accounts of Chemical Research*, Vol. 41(2), pp. 157—167, 2007.

42. Sarigul, S., 2017, *Atroposelective Synthesis and Reactions of Axially Chiral Thio-*

hydantoins, Ph.D. Thesis, Boğaziçi Üniversity.

43. Aydeniz, Y., F. Oğuz, A. Yaman, A. S. Konuklar, I. Doğan, V. Aviyente and R. A. Klein, "Barriers to Internal Rotation Around the C-N Bond in 3-(*o*-aryl)-5-methyl-rhodanines Using NMR Spectroscopy and Computational Studies. Electron Density Topological Analysis of the Transition States", *Organic and Biomolecular Chemistry*, Vol. 2, pp. 2426–2436, 2004.

44. Lunazzi, L., M. Mancinelli, A. Mazzanti, S. Lepri, R. Ruzziconi and M. Schlosser, "Rotational Barriers of Biphenyls Having Heavy Heteroatoms as *ortho*-substituents: Experimental and Theoretical Determination of Steric Effects", *Organic Biomolecular Chemistry*, Vol. 10(9), pp. 1847—1855, 2012.

45. Belot, V., D. Farran, M. Jean, M. Albalat, N. Vanthuyne and C. Roussel, "Steric Scale of Common Substituents from Rotational Barriers of N-(*o*-substituted aryl)thiazoline-2-thione Atropisomers", *The Journal of Organic Chemistry*, Vol. 82(19), p. 10188–10200, 2017.

46. Sundararajan, K., K. Sankaran, K. S. Viswanathan, A. D. Kulkarni and S. R. Gadre, "H- Complexes of Acetylene-Ethylene: A Matrix Isolation and Computational Study", *The Journal of Physical Chemistry A.*, Vol. 106(8), pp. 1504—1510, 2002.

47. Tsuzuki, S., K. Honda, T. Uchimaru, M. Mikami and K. Tanabe, "The Magnitude of the CH/ Interaction Between Benzene and Some Model Hydrocarbons", *Journal of the American Chemical Society*, Vol. 122(15), pp. 3746—3753, 2002.

48. Ballard, A., S. Narduolo, H. O. Ahmad, D. A. Cosgrove, A. G. Leach and N. J. Buurma, "The Problem of Racemization in Drug Discovery and Tools to Predict it", *Expert Opinion on Drug Discovery*, Vol. 14(6), pp. 1—13, 2019.

49. Roussel, C., M. Adjimi, A. Chemlal and A. Djafri, "Comparison of Racemization Processes in 1-Arylpyrimidine-2-thionaen and 3-Arylthiazoline-2-thione At-

ropisomers and Their Oxygen Analogues", *The Journal of Organic Chemistry*, Vol. 53(21), No. 21, pp. 5076—5080, 1988.

50. Lin, K., "Understanding Product Optimization", *Journal of Chemical Education*, Vol. 65(10), pp. 857—860, 1988.

APPENDIX A:

A.1. Rotational Barriers of Thiohydantoin Derivatives (RM to RP and RP to RM)

Table A.1. RM to RP and RP to RM Calculated and Experimental Rotational Barriers (kcal/mol).

	Experimental	**B3LYP/6-311+G****	**M06-2X/6-311+G****
M1(303K)	24.3 (24.0)	27.3 (27.3)	27.6 (27.6)
M2(313K)	24.7 (24.6)	27.6 (27.4)	27.2 (27.8)
M3(383K)	-	31.2 (30.9)	31.8 (32.9)
M4(333K)	27.5 (27.8)	30.1 (30.2)	31.3 (31.6)
M5(313K)	-	27.7 (27.7)	28.5 (27.7)
M6(383K)	28.2 (28.3)	30.8 (30.5)	30.7 (31.9)
M7(333K)	-	30.1 (29.9)	30.9 (30.8)
M8(303K)	24.7 (24.7)	27.1 (27.4)	27.5 (28.0)
M9(333K)	26.1 (26.3)	28.8 (29.1)	30.2 (30.5)
M10(333K)	25.6 (25.7)	28.7 (29.0)	29.5 (31.1)
M11(333K)	27.7 (27.7)	30.1 (30.4)	30.8 (31.5)
M13(333K)	28.0 (28.0)	30.0 (30.1)	30.5 (30.0)

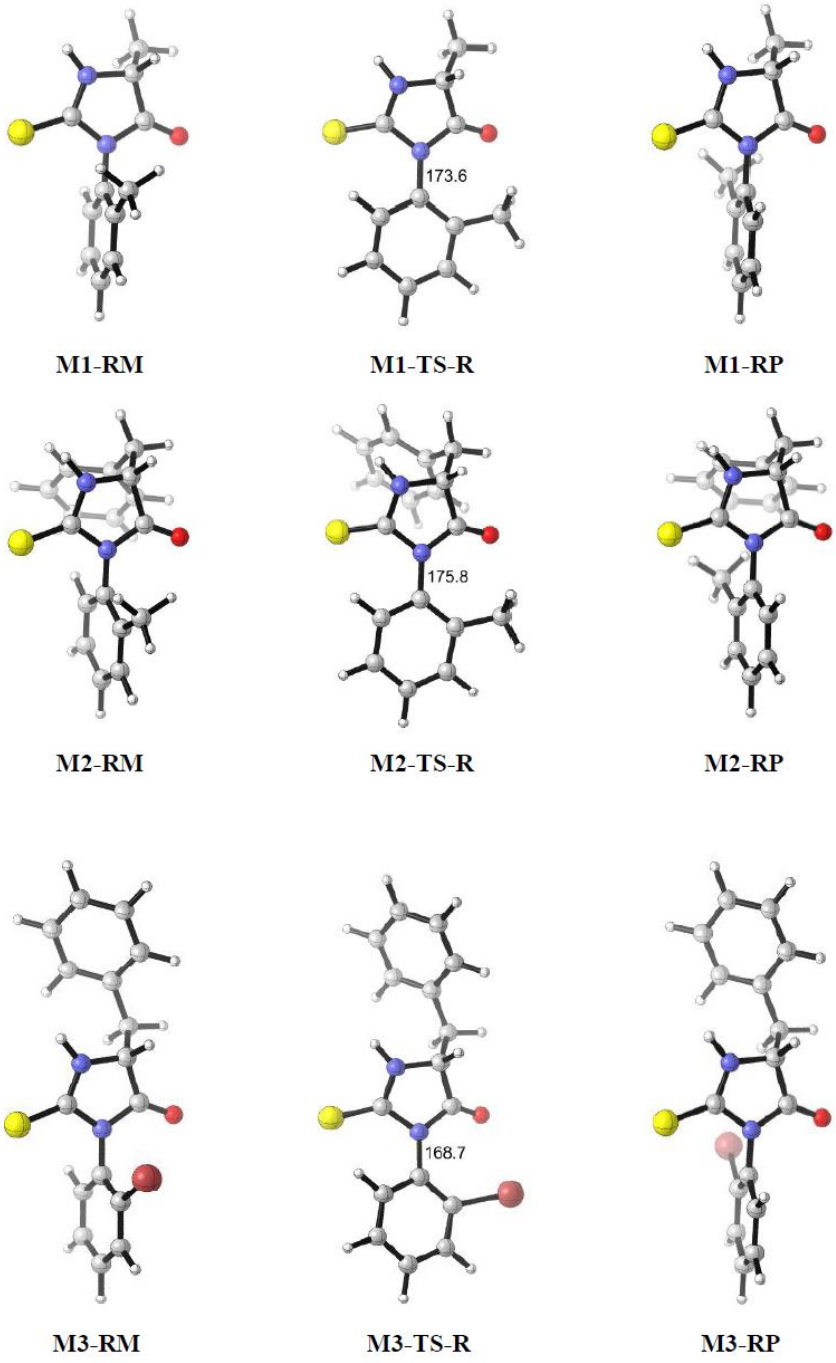

Figure A.1. 3D structures of RM, RP and transition state structures of the molecules of interest.

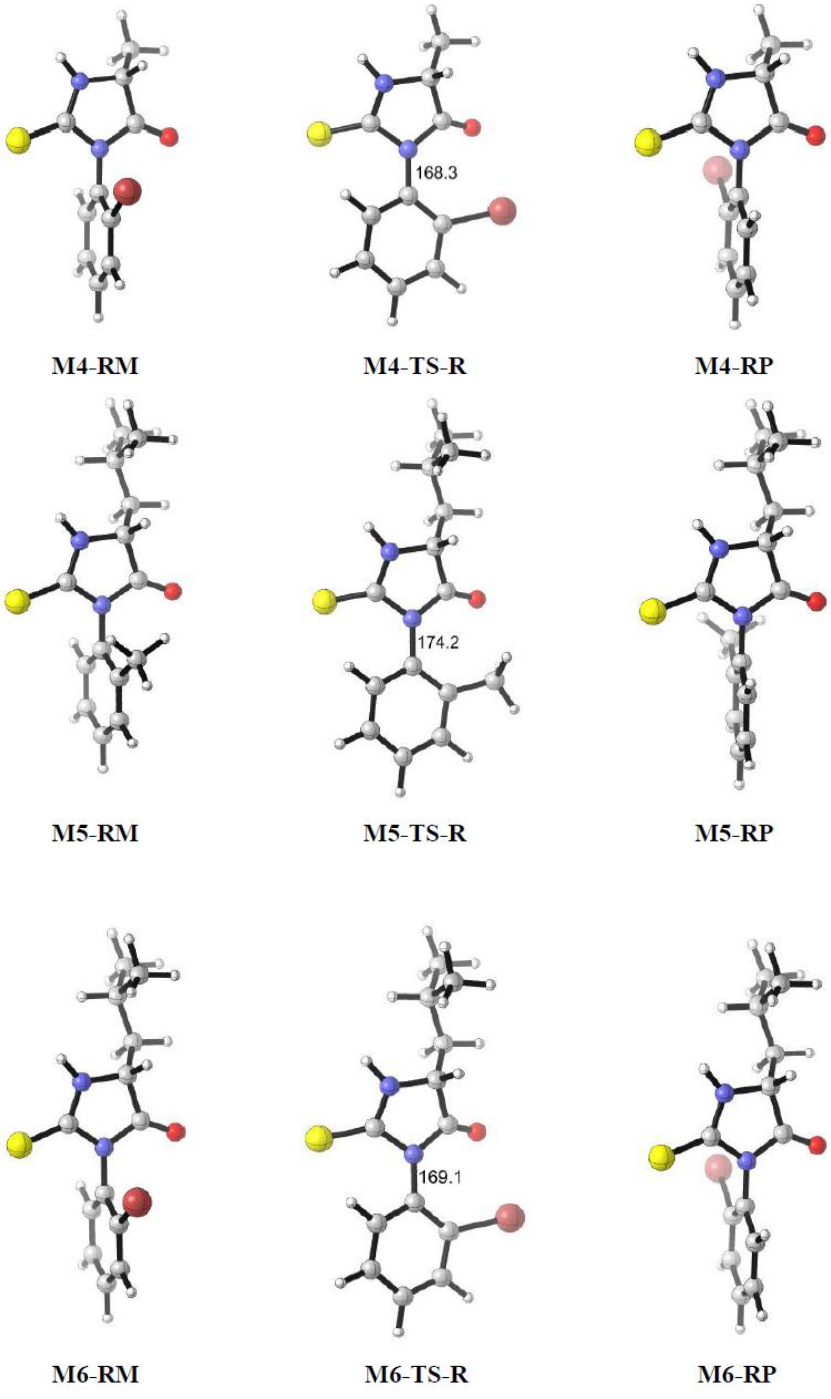

Figure A.1. 3D structures of RM, RP and transition state structures of the molecules of interest. (cont.)

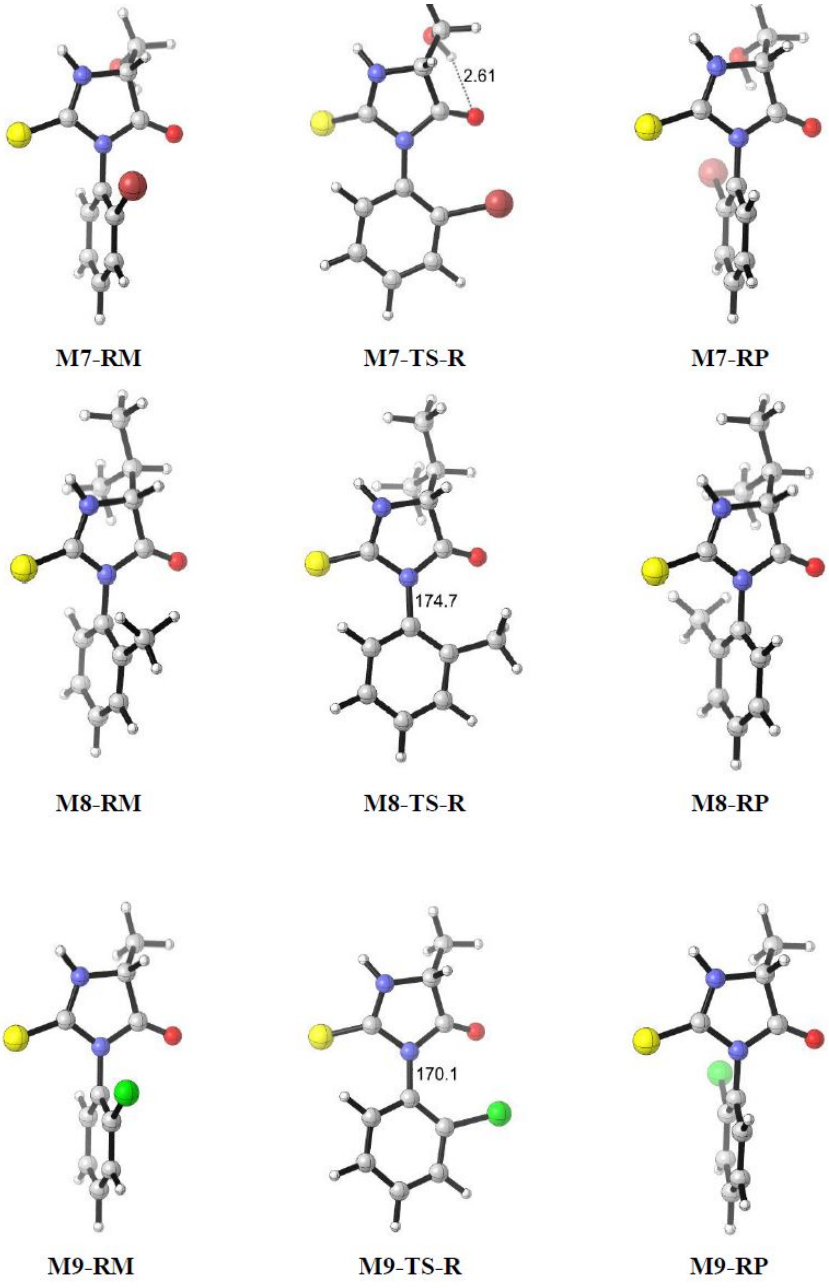

Figure A.1. 3D structures of RM, RP and transition state structures of the molecules of interest. (cont.)

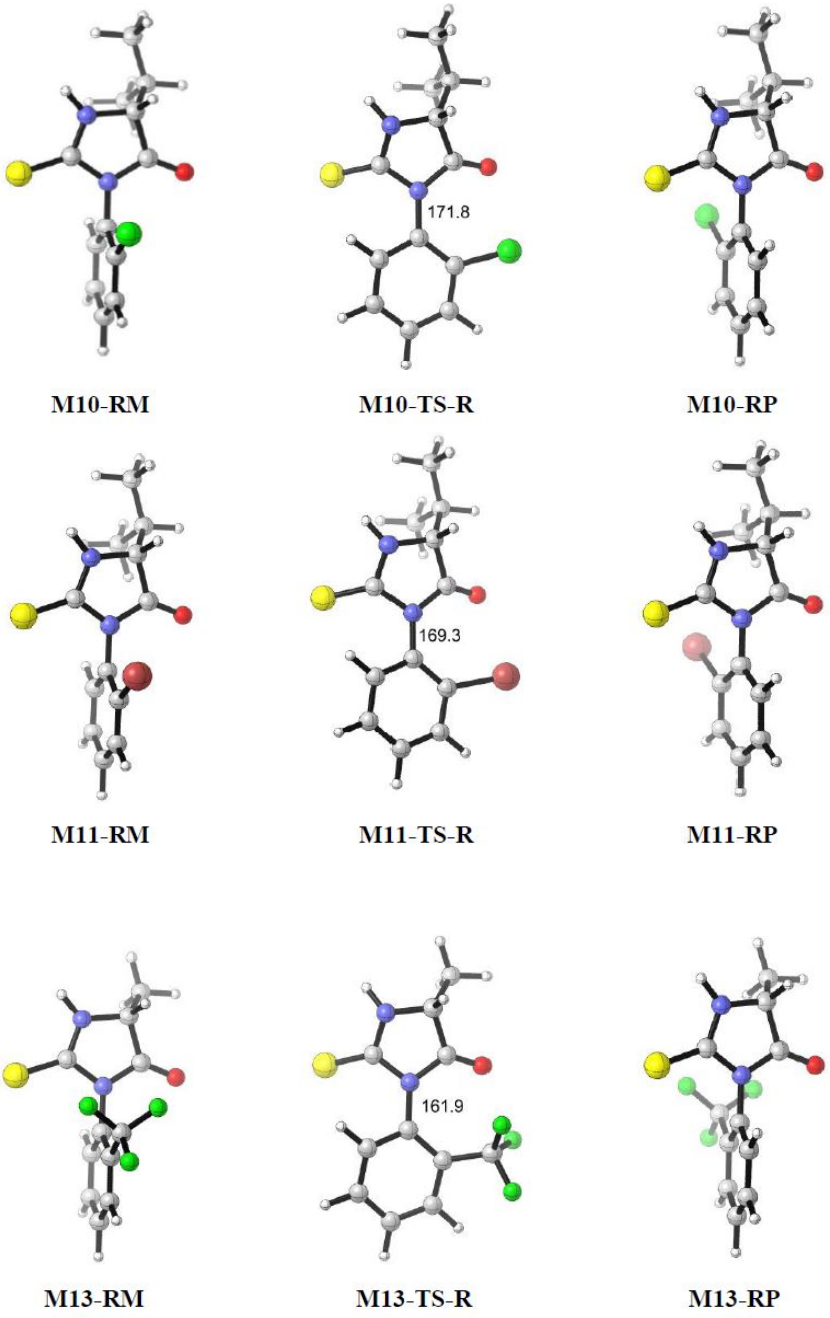

Figure A.1. 3D structures of RM, RP and transition state structures of the molecules of interest. (cont.)

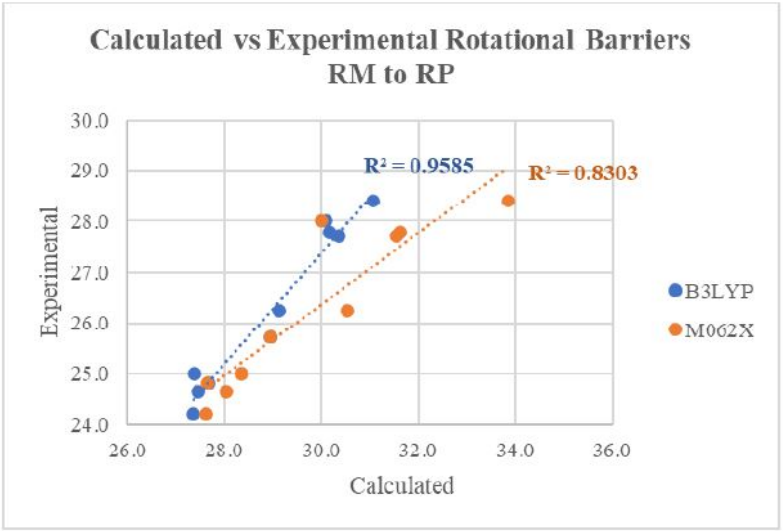

Figure A.2. Calculated vs Experimental Rotational Barriers (kcal/mol) of thiohydantoin derivatives. (RM to RP)

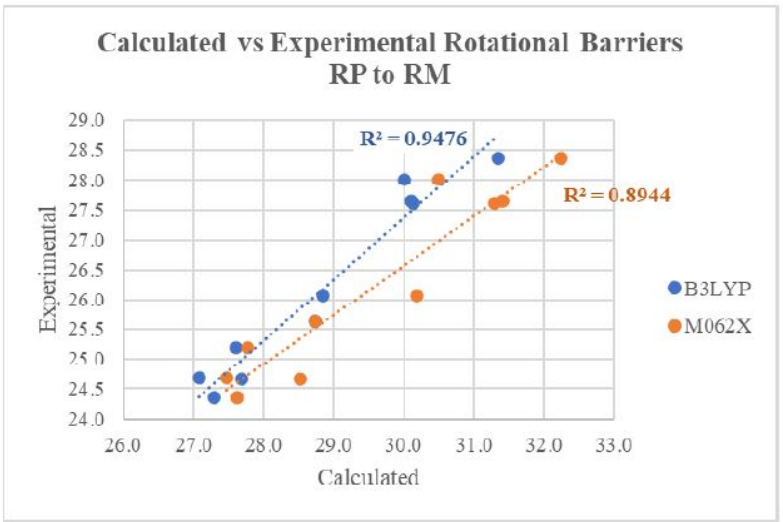

Figure A.3. Calculated vs Experimental Rotational Barriers (kcal/mol) of thiohydantoin derivatives. (RP to RM)

A.2. Rotational Barriers of M13-M in Aldol Reaction Conditions

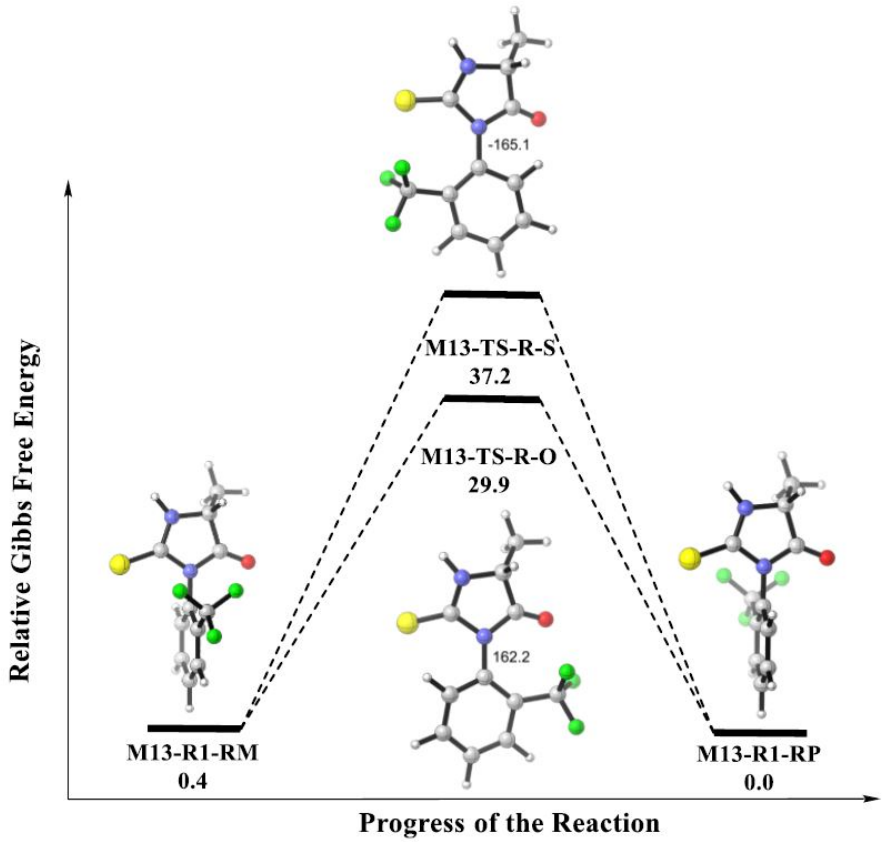

Figure A.4. Rotational energy profile (kcal/mol) of RM to RP rotation of M13. (M06-2X/6-311+G**, iefpcm, Solvent = THF, Temperature = 195 K)

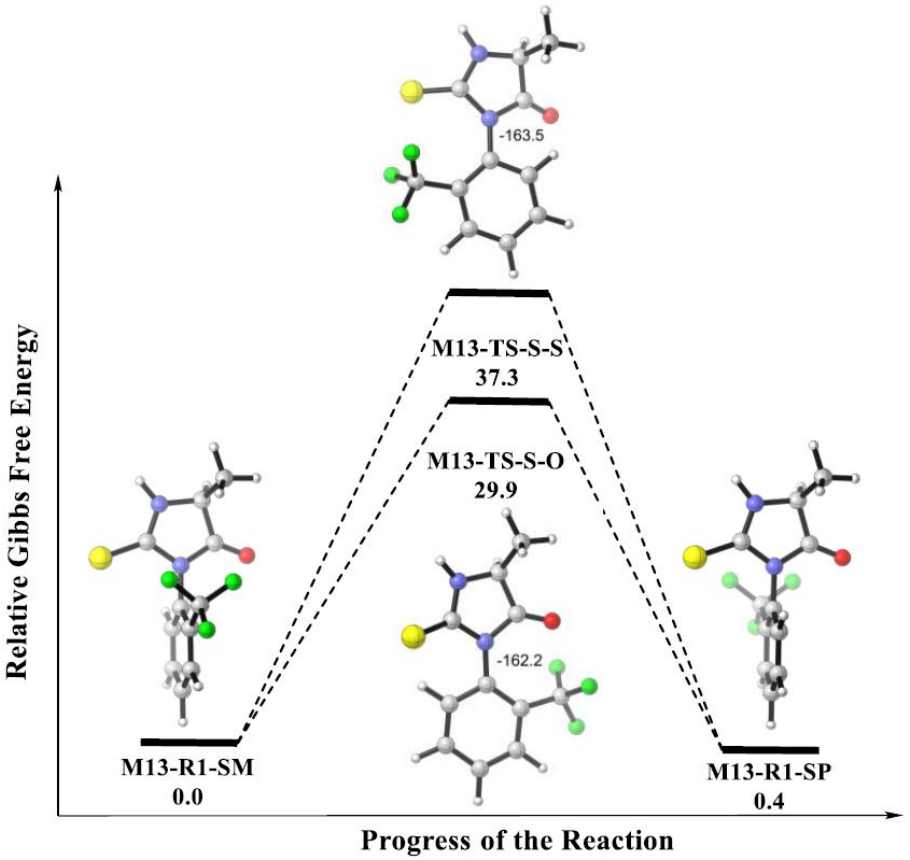

Figure A.5. Rotational energy profile (kcal/mol) of SM to SP rotation of M13. (M06-2X/6-311+G**, iefpcm, Solvent = THF, Temperature = 195 K)

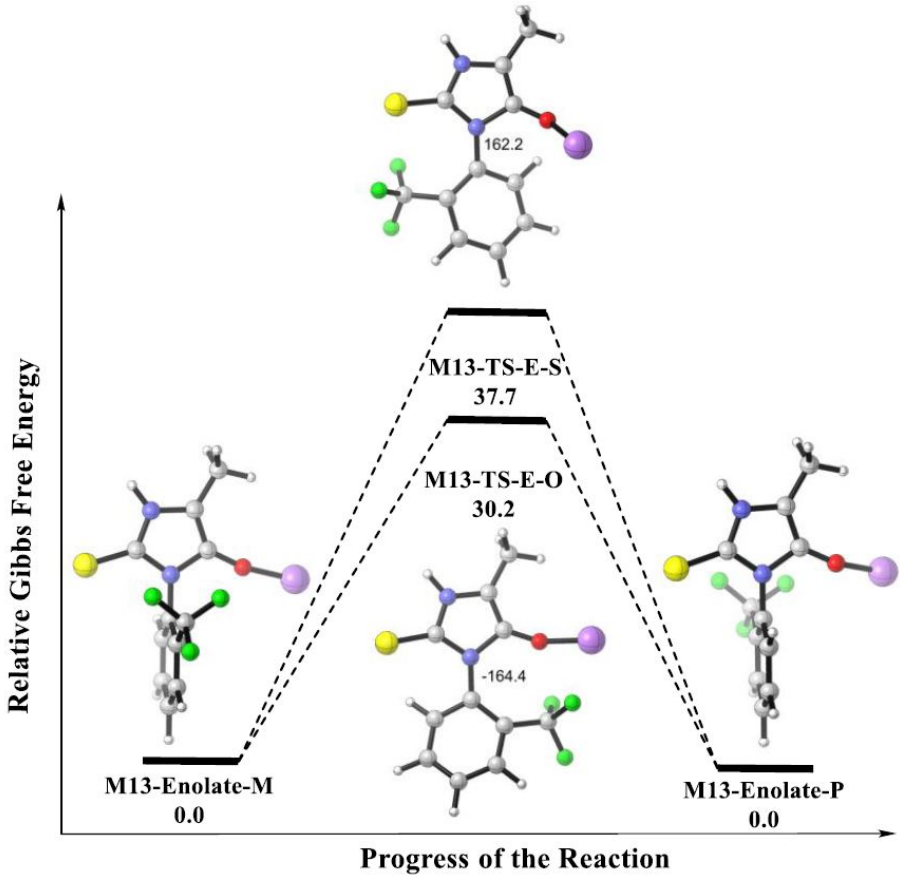

Figure A.6. Rotational energy profile (kcal/mol) of enol rotation M to P for M13. (M06-2X/6-311+G**, iefpcm, Solvent = THF, Temperature = 195 K)

A.3. Approval Licence for the Usage of Figures from Academic Articles

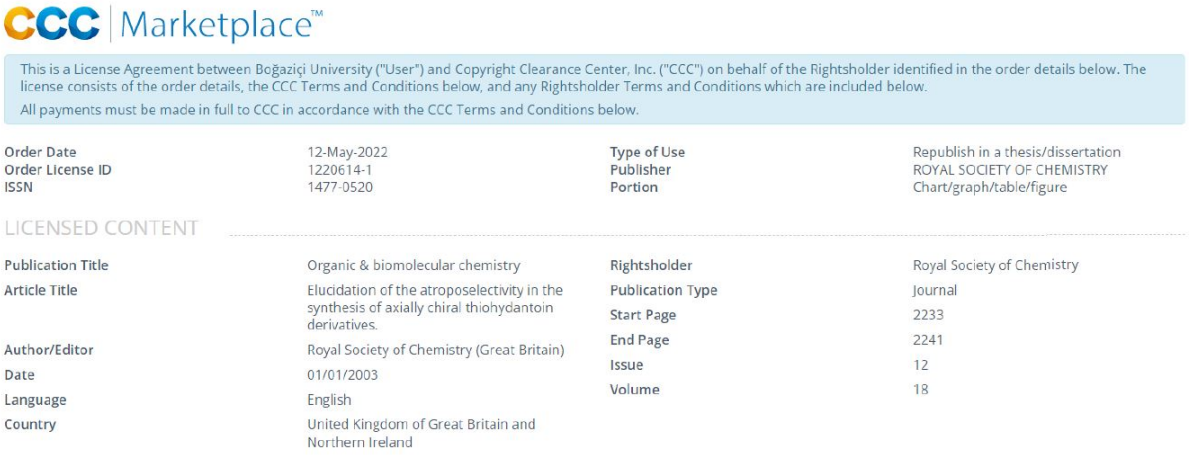

CCC Marketplace™

This is a License Agreement between Boğaziçi University ("User") and Copyright Clearance Center, Inc. ("CCC") on behalf of the Rightsholder identified in the order details below. The license consists of the order details, the CCC Terms and Conditions below, and any Rightsholder Terms and Conditions which are included below.

All payments must be made in full to CCC in accordance with the CCC Terms and Conditions below.

Order Date	12-May-2022	Type of Use	Republish in a thesis/dissertation
Order License ID	1220614-1	Publisher	ROYAL SOCIETY OF CHEMISTRY
ISSN	1477-0520	Portion	Chart/graph/table/figure

LICENSED CONTENT

Publication Title	Organic & biomolecular chemistry	Rightsholder	Royal Society of Chemistry
Article Title	Elucidation of the atroposelectivity in the synthesis of axially chiral thiohydantoin derivatives.	Publication Type	Journal
		Start Page	2233
Author/Editor	Royal Society of Chemistry (Great Britain)	End Page	2241
Date	01/01/2003	Issue	12
Language	English	Volume	18
Country	United Kingdom of Great Britain and Northern Ireland		

Figure A.7. Licence agreement with the CCC (Copyright Clearance Center) for the usage of figures from academic article.